Fatigue Analysis of Unconfined Concrete Columns

by

John B. Mander, Anindya Dutta and Jang Hoon Kim
University at Buffalo, State University of New York
Department of Civil, Structural and Environmental Engineering
Buffalo, New York 14260

NOTICE

Fatigue Analysis of Unconfined
Concrete Columns

by

J.B. Mander[1], A. Dutta[2] and J.H. Kim[3]

1   Associate Professor, Department of Civil, Structural and Environmental Engineering, University at Buffalo, State University of New York
2   Research Assistant, Department of Civil, Structural and Environmental Engineering, University at Buffalo, State University of New York
3   Assistant Professor, Department of Architecture, Ajou University, Suwon, Korea; former Post Doctoral Research Associate, Department of Civil, Structural and Environmental Engineering, University at Buffalo, State University of New York

Preface

The Multidisciplinary Center for Earthquake Engineering Research (MCEER) is a national center of excellence in advanced technology applications that is dedicated to the reduction of earthquake losses nationwide. Headquartered at the University at Buffalo, State University of New York, the Center was originally established by the National Science Foundation in 1986, as the National Center for Earthquake Engineering Research (NCEER).

Comprising a consortium of researchers from numerous disciplines and institutions throughout the United States, the Center's mission is to reduce earthquake losses through research and the application of advanced technologies that improve engineering, pre-earthquake planning and post-earthquake recovery strategies. Toward this end, the Center coordinates a nationwide program of multidisciplinary team research, education and outreach activities.

MCEER's research is conducted under the sponsorship of two major federal agencies, the National Science Foundation (NSF) and the Federal Highway Administration (FHWA), and the State of New York. Significant support is also derived from the Federal Emergency Management Agency (FEMA), other state governments, academic institutions, foreign governments and private industry.

The Center's FHWA-sponsored Highway Project develops retrofit and evaluation methodologies for existing bridges and other highway structures (including tunnels, retaining structures, slopes, culverts, and pavements), and improved seismic design criteria and procedures for bridges and other highway structures. Specifically, tasks are being conducted to:
* assess the vulnerability of highway systems, structures and components;
* develop concepts for retrofitting vulnerable highway structures and components;
* develop improved design and analysis methodologies for bridges, tunnels, and retaining structures, which include consideration of soil-structure interaction mechanisms and their influence on structural response;
* review and recommend improved seismic design and performance criteria for new highway systems and structures.

Highway Project research focuses on two distinct areas: the development of improved design criteria and philosophies for new or future highway construction, and the development of improved analysis and retrofitting methodologies for existing highway systems and structures. The research discussed in this report is a result of work conducted under the existing highway structures project, and was performed within Task 106-E-5.2, "Dependable Strength and Ductility of Eastern U.S. Bridge Columns" and Task 106-F-2.1, "Seismic Retrofit of Shear Critical Bridge Columns" of that project as shown in the flowchart on the following page.

The overall objectives of these tasks were to develop analytical procedures, verified by experimental testing, which could be used to determine the flexure-shear force-deformation behavior of bridge columns, and to develop retrofit procedures for reinforced concrete bridge columns and

their connections, respectively. This report describes the development of a seismic evaluation methodology for bridges which can be used to determine structural deficiencies prior to retrofit or rehabilitation. The authors describe an energy-based method to explore possible failure mechanisms in bridges not designed to withstand seismic loads. Specific failure mechanisms examined include unconfined concrete fatigue, bond failure in anchorages and lap splices, compression buckling of the longitudinal reinforcement steel, fracture and fatigue of the longitudinal reinforcement, and shear failure in the columns. The seismic evaluation methodology was applied to a bridge pier with multiple failure modes including that of fatigue damage and, when compared to experimental results, yielded good agreement.

SEISMIC VULNERABILITY OF EXISTING HIGHWAY CONSTRUCTION
FHWA Contract DTFH61-92-C-00106

TASK A: PROJECT ADMINISTRATION & HIGHWAY SEISMIC RESEARCH COUNCIL

TASK B

State-of-the-art Review

TASK C

Bridge Retrofit Guidelines (Interim)

TASK D

Performance Criteria

TASKS E1, E2

Vulnerability Assessment:

Seismic Hazard, Ground Motion, Spatial Variation

TASKS E3 to E7

Vulnerability Assessment:

Soils & Foundations, Components, Structures, Systems

TASKS F1 to F4

Retrofit Technologies:

Soils & Foundations, Components, Structures, Systems

TASK F5

Special Studies

TASK G

Retrofit Manuals

Vol I   Seismic Vulnerability Assessment of Highway Systems
Vol II   Retrofitting Manual for Highway Bridges
Vol III Retrofitting Manual for Highway Tunnels, Retaining
         Structures, Embankments, Culverts, and Pavements

TASK F6

Demonstration Projects

TASK H: COST IMPACT STUDIES

TASK I: TECHNOLOGY TRANSFER

ABSTRACT

Current seismic design codes which aim at maximizing the overall ductility of a structural system are a result of extensive experimental and analytical research over the past three decades. In seismic bridge engineering, the state-of-the-practice has lagged by some two decades the state-of-the-knowledge. Thus the vast majority of the bridge structures in most countries, including the United States, have been built to non-seismic codes. Since it is not economically feasible to abandon all of these existing structures, it is necessary to evaluate their expected seismic performance and then retrofit those structures that are deemed to be seismically deficient. This report is concerned with the first step in the seismic retrofit process — seismic evaluation. Using an energy based methodology it explores the various possible failure in non-seismically designed structures including: unconfined concrete fatigue; bond failure in anchorages and lap splices; compression buckling of the longitudinal reinforcement; fracture and fatigue of the longitudinal reinforcement; and shear failure of the columns. Theoretical models capable of predicting strength degradation over the cycles of loading that lead to failure are developed and verified by comparing with experimental results. Numerical examples are presented at the end of each section to explain the working procedure of the proposed evaluation methodology. The individual fatigue theories are generalized so that mixed failure modes in reinforced concrete pier bents can be tracked during cyclic loading. Progressive failure modes can therefore be explained. This generalized fatigue theory is validated against experimental results on a model pier bent which was tested at the SUNY testing facility. Good agreement between the theoretically predicted behavior and observed performance is obtained.

ACKNOWLEDGEMENTS

This research was carried out at the Department of Civil, Structural and Environmental Engineering, State University of New York at Buffalo.

TABLE OF CONTENTS

LIST OF ILLUSTRATIONS

LIST OF TABLES

SECTION 1
INTRODUCTION

1.1 BACKGROUND

In the seismic design of reinforced concrete structures, the concept of damage and damageability play a central role. The economy of construction requires that the accepted level of damage be tied to the expected risk of earthquake exposure. Thus, for minor earthquakes of relatively frequent occurrence, no damage except possibly that of minor cosmetic nature is acceptable. For earthquakes of moderate strength, and correspondingly larger return intervals, a limited amount of permanent structural damage is generally considered acceptable. However, for large earthquakes with a very low probability of occurrence (this is often referred to as the "maximum credible event" and has a return period in excess of some 2000 to 3000 years) a considerable amount of damage is acceptable. But in any case the prevention of collapse should be the supreme design objective.

The current seismic design philosophy for reinforced concrete structures started evolving only over the past decade. Thus majority of the structures built before the modern codes came into existence are potentially at risk in the event of a strong ground motion. Since it is economically not feasible to demolish these existing structures, an alternative approach would be to elevate their performance up to the level envisaged by the present codal provisions. However, before any such step is undertaken it is an absolute must to properly diagnose the deficiencies of the structure and their specific locations.

Following the principles of capacity design where a hierarchy of failure modes is chosen by the designer himself, it is possible to suppress undesirable failure modes such as shear, loss of bond and anchorage and joint failure. Energy is dissipated in the plastic hinge zones that should be specially detailed for seismic resistance. Therefore, a proper understanding of all the different potential failure modes is necessary in order to correctly design and detail a retrofitting

1

strategy and to provide "capacity protection" to the remainder of the structure. Thus a systematic study of the different failure modes including that of confined and unconfined concrete, along with longitudinal bar buckling is considered an important step in preventing catastrophic structural failure through premature failure of column hinge regions.

1.2 PREVIOUS RESEARCH

The historical evolution of the present seismic design philosophy for reinforced concrete structures subjected to strong earthquake ground motions necessitated the development of reliable mathematical models to analyze non-linear response. The last two decades has brought considerable progress in the development of non-linear (hysteretic) force-deformation and/or moment-curvature models for reinforced concrete elements. Special mention may be made of Chung et al. (1987), Gosain et al. (1977) and Banon et al. (1981). With the advent of sophisticated computer programs to predict the non-linear dynamic time history response of structures such as DRAIN 2D (Kannan and Powell, 1973), DRAIN 2DX (Allahabadi and Powell, 1988) and IDARC (Park, Reinhorn and Kunnath, 1987) an obvious question is raised: How much inelastic response will lead to failure or collapse? Thus the notion of damage was born. Different concepts related to structural damageability are described in what follows.

1.2.1 Ductility Damage

Early damage models were based on displacement ductility and a simple damage index that related ductility demand (μ_Δ^d) to capacity (μ_Δ^c) could be defined such that

$$D_\mu = \frac{\mu_\Delta^d}{\mu_\Delta^c} \tag{1-1}$$

where the ductility factor is defined as the ratio of total displacements to the yield displacement $\mu_\Delta = \Delta_u / \Delta_y$. Note that if $D_\mu \geq 1$ collapse is implied. Present seismic evaluation recommendations use an inverse form of this damage model (Capacity/Demand) that may be thought of as a factor of safety against collapse. Thus in accordance with the original ATC 6-2 (1983)

2

recommendations which have recently been incorporated into the revised Federal Highway Administrative Retrofitting Manual (Buckle and Friedland, 1995), a ductility based Capacity/Demand (C/D) ratio (r) for ductility is computed as follows:

$$r = \frac{R_C - \Sigma Q_i}{Q_{EQ}} \tag{1-2}$$

where R_C = nominal ultimate displacement or force capacity for the structural component being tested, ΣQ_i = the sum of the displacement or force demands for loads other than earthquake, and Q_{EQ} = the displacement or force demand for the design earthquake loading at the site.

1.2.2 Fatigue Damage

Investigators have realized there are shortcomings of this monotonic displacement ductility approach as it is unable to account for energy absorption or cyclic loading effects of structural elements. Cyclic loading can often be related to low cycle fatigue. An early contribution to the fatigue modeling in earthquake engineering was made by Krawinkler and Zohrei (1983) who proposed an accumulated damage model for structural steel components based on experimental data.

$$D_e = C \sum_{i=1}^{n} (\Delta \delta_{pi})^{\alpha_i} \tag{1-3}$$

where D_e = damage index of the member, C = calibration constant, α_i = fatigue damage parameter, n = number of load cycles and $\Delta \delta_{pi}$ = plastic deformation during the i-th cycle. The concept of this model was very attractive since when modified appropriately it was possible to apply it to predict the damaged state of reinforced concrete structures.

1.2.3 Combined Ductility and Fatigue Damage

Subsequently it was also realized that neither displacement ductility nor fatigue alone would suffice in describing damage to structural concrete members. The establishment of the

importance of hysteretic energy dissipated by concrete members as an index of damage sustained prompted many researchers to propose damage models which were based on the combined principles of fatigue (energy) and ductility. Special mention may be made of the models proposed by Park et al. (1985), Darwin et al. (1986). Unfortunately, these models generally do not consider the effect of loading sequence which may play an important role in assessing a residual strength capacity. The model proposed by Chung, Meyer and Shinozuka (1987) has sought to overcome this deficiency and tends to give reasonable albeit conservative estimates of sustained damage.

1.2.4 Modeling Global Damage

The overall damage state of a structure depends, however, both on the distribution and severity of localized damage. A global damage index which represents the damage on the structure in its entirety is thus obtained by combining local damage indices of its constituent elements with suitable weighting functions. Although there seems to be no consensus as to how this is best done, the most widely used approach is to take an average of the local indices weighted by the local energy absorptions (Park, Ang and Wen 1985, 1987; Chung et al. 1989a, 1989b, 1990; Kunnath et al. 1990, 1992).

An alternative, highly computational method of global damage assessment involves investigating changes in modal parameters during an earthquake. Using flexibility as a damage indicator Raghavendrachar and Atkan (1992) proposed a method by which the severity and location of damage in a structure can be assessed merely by observation of changes in the flexibility matrix. This is also the approach advocated by DiPasquale and Cakmak (1987,1988) who proposed a range of softening indices that are functions of the change in the fundamental period of the structure. Unfortunately, these methods require very full and accurate structural modal data, and current techniques appear better suited to locating localized minor damage than to quantifying widespread damage.

4

1.2.5 Modeling Local Damage

The aforementioned methods of damage analysis that examine either individual structural elements or global damage rely heavily on empirical formulations that require calibration with damage observed in either laboratory experiments, post earthquake reconnaissance observations, or both. It is considered that better progress in damage analysis techniques could be made if one was able to focus on an improved understanding of structural damage at the constituent material level using established principles of limit analysis, continuum mechanics, as well as fatigue and fracture mechanics. Once fundamental failure modes can be identified, established principles of non-linear structural analysis can be utilized to predict their effect on global behavior.

Progress to this end was first made when Mander et al. (1984, 1988a,b) established that the useful limit of confined concrete columns was related to the first fracture of the transverse hoop reinforcement. This failure mode was based on equating the inelastic work done on a concrete column with the energy absorption capacity of the transverse reinforcing steel. The energy absorption and fatigue capacity of longitudinal reinforcement was further quantified for ordinary mild and high strength high alloy steels by Mander et al. (1994). An energy-based analysis of reinforced concrete bridge columns was further advanced by Chang and Mander (1994a,b). They used a computational mechanics approach to assess and compare energy absorption capacity and energy absorption demand. Mander and his co workers have continued these studies and examined the energy absorption capacity of shear-critical square concrete bridge columns (Mander et al. 1993) and modified circular columns with weak connection details (Mander et al. 1995 and Mahmoodzadegan, 1995).

The present research seeks to examine the aforementioned work by systematically identifying possible failure modes and analyzing the energy absorption capacity to failure.

1.3 SIGNIFICANCE OF CURRENT RESEARCH

The importance of ductility as a principal design parameter cannot be overlooked despite its limitations. The assessment of the damageability of a structural concrete components require the quantification of number of inelastic cycles that can be sustained at a particular plastic drift (or plastic rotation or curvature) amplitude. By limiting this research to the study of reinforced concrete bridge columns and their connections it may be observed that failure of such components can occur by either one or a combination of the following modes.

i)   Flexural failure of concrete in unconfined columns.

ii) Flexural failure of concrete resulting from the transverse hoop fracture. This is particularly significant for columns that rely on a confined concrete core to resist applied moments at large plastic curvature.

iii) Failure of the connections by either:
     a) bond failure of the lap-splice zone at the ends of columns
     b) anchorage-bond failure within the connection
     c) joint shear failure adjacent to the column

iv) Failure of confined core concrete due to compression buckling of the longitudinal reinforcing bars.

v)   Failure of longitudinal reinforcement due to low cycle fatigue.

vi) Shear or flexure-shear failure of the column outside the potential plastic hinge zone.

An evaluation of the ultimate plastic drift capacity for each of the individual failure modes is considered to be an important step both from an analysis and design point of view. The present work looks into the whole problem from a new perspective of energy balance to come up with a rational approach that assesses the energy absorption or cyclic *capacity* for a given column. This can then be compared with energy absorption or cyclic *demand* for design earthquakes (Chang and Mander, 1994b).

6

1.4 SCOPE OF THIS STUDY

This study is made up of two portions: theory and validation. In the initial theoretical portion various failure modes of unconfined column sections are studied using an energy approach. These include: (i) flexural failure of concrete in unconfined columns; (ii) failure due to loss of bond in anchorages; (iii) failure due to loss of bond in lap splices and (iv) failure of core concrete due to compression bucking of the longitudinal reinforcing bars, (v) failure of longitudinal reinforcement due to low cycle fatigue and (vi) shear failure. Each section first derives the underlying theory for the respective failure modes and then goes to present a numerical example to illustrate how this may be used in practice. For this purpose, a bridge system, as illustrated in figure 1-1, is chosen. A typical pier bent shown in the same figure which is a part of a multispan concrete slab on steel girder bridge is utilized for the numerical example. Each span of the bridge is 20m in length and the deck is 12.5m wide. For simplicity it is assumed that the effective deck weight (girders + concrete + guard rails) to be 7 kPa. The pier is typically $915\,mm$ ($36\,in.$) in diameter, reinforced with $16 - 28\,mm$ (#9) diameter bars. The assumed specified (design) material strengths are $276\,MPa\,(40\,ksi)$ for steel and $24\,MPa\,(3500\,psi)$ for concrete. However, a seismic evaluation should be based on the probable material properties. Therefore, a yield strength of $330\,MPa$ for steel and $f_c' = 45\,MPa$ for concrete is assumed. The lateral reinforcement in the columns consist of $10\,mm$ (#3) circular hoops with a spacing of $305\,mm$ ($12\,in.$). The clear cover is $51\,mm$ ($2\,in.$). The axial load ratio ($P_e/f_c'A_g$) in the central column is assumed to be 0.04. Depending on the failure modes to be illustrated, the height of the column is varied. Note that this is a typical example of a non-seismically designed bridge pier found in abundance in the central and eastern United States.

The latter portion of this report deals with the validation of the theory. For this purpose experimental results reported previously by a number of different investigators are utilized. It should be emphasized here that there is a paucity of experimental results where a distinct mode of failure for a given specimen has been defined and documented by previous investigators. Every effort has been made to identify such well documented data and utilize it herein. More often than not, however, investigators conduct their experiments and terminate testing just prior

to a decisive failure. For such tests it is necessary to compare the overall results with envelopes of the theoretical failure modes identified in this study. Finally, conclusions drawn from the study are presented in Section 11.
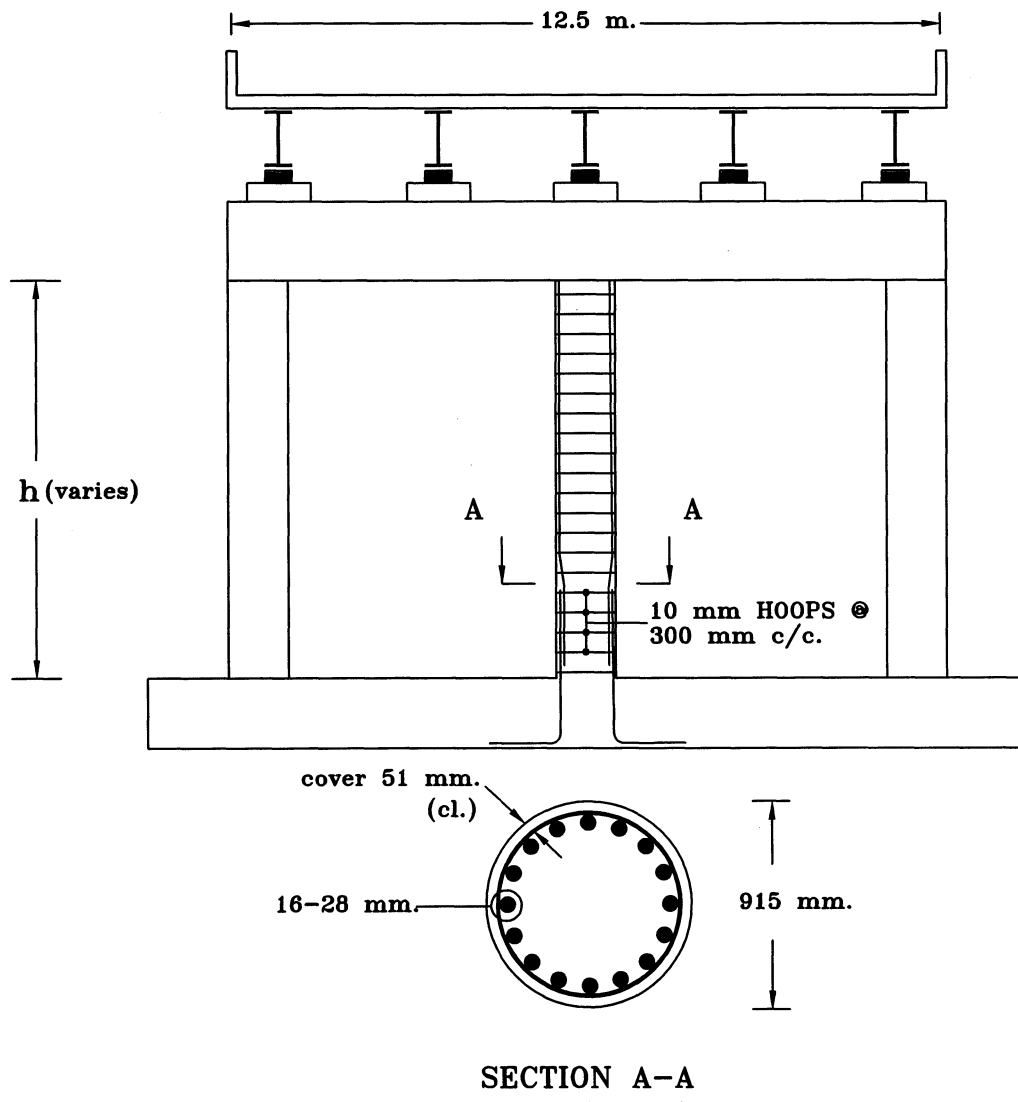
Figure 1-1 Illustrative Bridge Pier used in Numerical Example.

SECTION 2

FATIGUE FAILURE THEORIES FOR UNCONFINED CONCRETE COLUMNS

2.1 INTRODUCTION

Fatigue may be thought of as the progressive accumulation of physical deterioration of a material under repeated load applications, which eventually leads to failure. Each load or displacement cycle inflicts a certain amount of irreversible damage. The number of cycles necessary to cause a failure at some stress (or strain) level is referred to as the "fatigue life" of the material. A generalized strain-life (S-N) plot is shown for 1 to 10 million cycles in figure 2-1. If stresses are kept below a certain threshold, the material life may be indefinite. The stress threshold at which this limit is attained is referred to as the "fatigue limit", and for most materials is considered to be in excess of 2 million cycles. If the material does not yield the fatigue life may be substantial, this is commonly referred to as the high cycle fatigue. Low cycle fatigue failure occurs when inelastic material behavior is encountered. Earthquake loading is characterized by only a few large amplitude cycles, thus low cycle fatigue failure modes are of specific interest for earthquake engineering applications.

When cyclic loading is imposed, the behavior of structural concrete members is somewhat different than when monotonic loading is applied. Previous experimental observations indicate that the strength capacity of a structural concrete member decays as the number of inelastic loading cycles increases. This phenomenon can be explained and even quantified by considering energy concepts where the external work applied to the member (EWD) is equated with the structural elements' internal energy absorption capacity (IWD). At failure, this can also be expressed as:

$$EWD = IWD \tag{2-1}$$

Energy-based seismic evaluation procedures were first introduced by Mander et al. (1984) for columns under concentric axial compression. Computational modeling using fiber elements
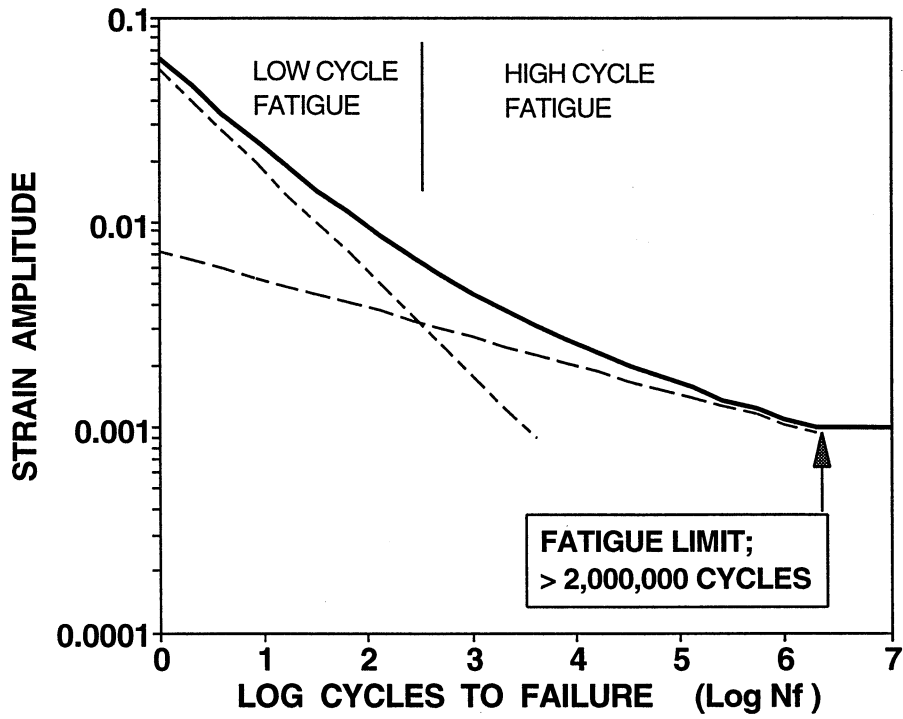
Figure 2-1 Typical Fatigue Plot for Steel.
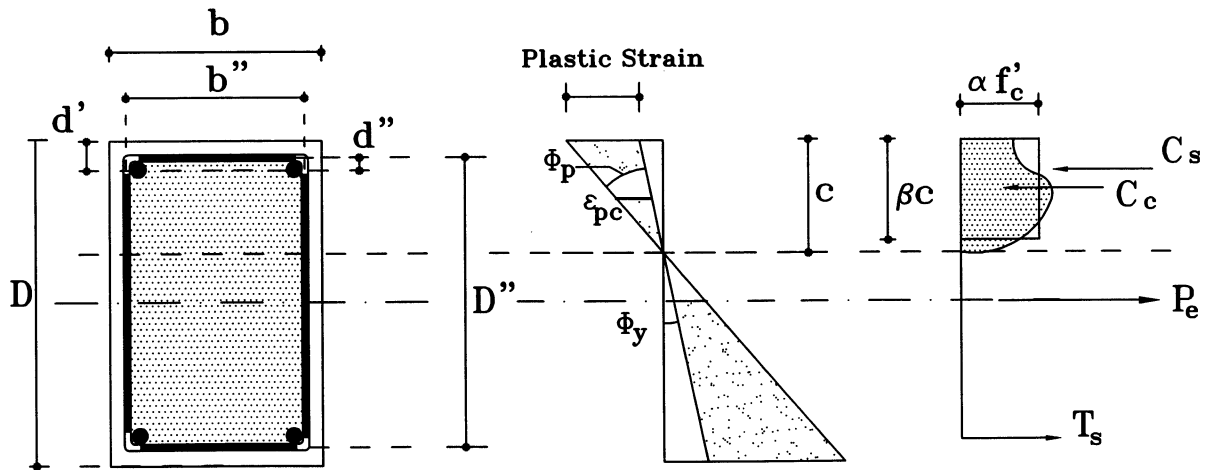
Figure 2-2 Equilibrium of Forces in a Column Section.

10

also enabled the prediction of first hoop fracture of columns under combined axial load and reversed cyclic flexure.

In a recent study a new energy-based approach was proposed by Mander et al. (1993) to determine the fatigue capacity of structural concrete sections. This method, which is based on using energy considerations assess the rate of strength loss due to repetitive cyclic loading from the initial flexural strength capacity to the final residual strength which is based on rocking or sliding of the column.

The initial lateral strength capacity is taken as the one corresponding to the nominal flexural strength. If the initial shear strength is less than the nominal flexural strength, then the member is shear-brittle and failure will generally occur by diagonal shear cracking. This analysis procedure has not yet been advanced to the point where it may be utilized for brittle shear deterioration assessment.

Damage analysis of unconfined concrete beam columns can be performed from first principles at the section level. An energy approach similar to the one adopted by Mander et al. (1988a,b) may be used to assess the cyclic capacity (cumulative drift) of concrete. The basis of the damage analysis assumes that the external work done (*EWD*) on the compressed concrete is equal to the internal work or energy absorption capacity (*IWD*) of the entire concrete section.

2.2 THEORETICAL DEVELOPMENT

2.2.1 External Work Done on Section

Consider the concrete cross-section shown in figure 2-2. The external moment applied to the section may be considered as a series of force components acting at various localities on the section. The applied concrete compression force C_c is what consumes the available energy absorption capacity. In terms of the familiar stress block parameters $C_c = \alpha f_c' \beta c b$, where f_c' = unconfined compression strength of concrete, b = section width, α = average concrete stress ratio, β = stress block depth factor and c = neutral axis depth from the extreme

11

compression fiber.

If N_c is the number of completely reversed cycles, then the external work done on the section is given by:

$$EWD = C_c \times \varepsilon_{pc} \times 2N_c \qquad (2\text{-}2)$$

where ε_{pc} = plastic strain amplitude at the location of the concrete compression force and $2N_c$ denotes the work done on each forward and reverse half-cycle. From the compression strain triangle shown in figure 2-2, the plastic strain at the center of the triangle is $\varepsilon_{pc} = 0.5\phi_p c$. This location may be approximated as the center of the force C_c (implying $\beta = 1$), thus

$$EWD = C_c \times \left(\phi_p \, \frac{c}{2}\right) \times 2N_c \qquad (2\text{-}3)$$

Therefore, the applied external work that causes deterioration of the section capacity is.

$$EWD = N_c C_c \phi_p c \qquad (2\text{-}4)$$

2.2.2 Internal Work or Energy Absorption Capacity of the Section

The internal work capacity of the unconfined concrete at the critical section is given by

$$IWD = A_g \int_0^{\varepsilon_{cu}} f_c \, d\varepsilon \qquad (2\text{-}5)$$

where the integral is actually the area beneath the unconfined concrete stress-strain curve and A_g = the gross area of the concrete cross section. In absence of a more precise analysis, the integral can be approximated as $0.008f_c'$. Note that this is the amount of energy required to cause compression failure of an unconfined concrete section.

2.2.3 Damage Analysis Using Energy

Equating the total external work done on a concrete section to the internal energy absorption capacity $EWD = IWD$. Thus setting equation (2-4) equal to equation (2-5)

12

$$N_c C_c \phi_p\ c\ =\ A_g \int\limits_0^{\varepsilon_{cu}} f_c\,d\varepsilon \qquad (2\text{-}6)$$

Dividing both sides of equation (2-6) by $f_c'A_g$ and rearranging the terms, a classical (S-N) fatigue-like relationship can be derived in terms of dimensionless plastic curvature ($\phi_p D$) and reversals to failure ($2N_c$):

$$(\phi_p D)\ =\ \frac{0.016}{\left(\dfrac{C_c}{f_c'A_g}\right)\!\left(\dfrac{c}{D}\right)}\cdot (2N_c)^{-1} \qquad (2\text{-}7)$$

where D = the overall depth or diameter of the section.

The plastic rotation can be determined from an equivalent plastic hinge length given by

$$\theta_p\ =\ \phi_p L_p\ =\ (\phi_p D)\,(L_p/D) \qquad (2\text{-}8)$$

where the equivalent plastic hinge length can be obtained from the equation suggested by Priestley and Paulay (1987)

$$L_p\ =\ 0.08L\ +\ 4400\,\varepsilon_y d_b \qquad (2\text{-}9)$$

where L = length of the column (from the maximum moment to the inflection point), ε_y and d_b are the yield strain and diameter of the longitudinal reinforcement.

Cumulative plastic drift capacity may be defined as $\Sigma\,\theta_{PC} = \theta_p\,(2N_c)$, therefore from equation (2-7) it follows:

$$\Sigma\theta_{PC}\ =\ \frac{0.016\,(L_p/D)}{\left(\dfrac{C_c}{f_c'A_g}\right)\!\left(\dfrac{c}{D}\right)} \qquad (2\text{-}10)$$

Note that the cumulative plastic drift is defined as the sum of all the positive and negative plastic drift amplitudes to a given stage of testing. For example, if a specimen with a yield drift of 0.25% (0.0025 *radians*) is cycled five times to a drift of $\pm 3\%$ then the cumulative plastic drift is $5 \times 2 \times (0.03 - 0.0025) = 0.275$ radians.

The level of damage to a structural member can be determined by comparing the amount of strain energy dissipated to the total strain energy stored in the undamaged structural member. When inelastic cyclic loading is applied, the strain energy dissipation is considered to be accumulated. Expressed in terms of column end to end plastic rotation, the cumulative damage index is defined by

$$\Sigma D_{ci} = \frac{\Sigma \theta_{pi}}{\Sigma \theta_{PC}} \qquad (2\text{-}11)$$

where $\Sigma \theta_{pi}$ is the current cumulative plastic drift up to the i-th half cycle.

Assuming the moment capacity contributed by the concrete is gradually consumed by the propagating level of damage, then at the end of the i-th cycle, the modified ideal capacity M_i can be evaluated through

$$\frac{M_i}{M_n} = 1 - \frac{M_c}{M_n} \Sigma D_{ci} = 1 - \frac{M_c}{M_n} \frac{\Sigma \theta_{pi}}{\Sigma \theta_{PC}} \qquad (2\text{-}12)$$

in which ΣD_{ci} = accumulated damage, $\Sigma \theta_{pi}$ = cumulative plastic drift, M_n = nominal moment capacity which is assumed to be the sum of the steel moment capacity M_s and the concrete moment capacity M_c generated by the eccentric concrete stress block and expressed as
(a) for a rectangular column

$$M_c = 0.5 C_c D \left(1 - \beta \frac{c}{D} \right) \qquad (2\text{-}13)$$

(b) for circular column

$$M_c = 0.5 C_c D \left(1 - 1.2 \beta \frac{c}{D} \right) \qquad (2\text{-}14)$$

where C_c = concrete compression force c/D = neutral axis depth ratio and β = stress block depth factor.

Equation (2-12) can be suitably modified to suit rectangular and circular column sections. The case of a rectangular section is examined first.

14

(a) **Rectangular Section**: C_c for a rectangular section can be expanded as follows:

$$C_c = \alpha \beta f_c'(bD)\left(\frac{c}{D}\right) = \alpha \beta f_c' A_g \left(\frac{c}{D}\right) \tag{2-15}$$

Thus, in terms of a neutral axis depth ratio

$$\left(\frac{C_c}{f_c' A_g}\right) = \alpha \beta \left(\frac{c}{D}\right) \tag{2-16}$$

Substituting into equation (2-7) gives

$$(\phi_p D) = \frac{0.016\,\alpha\beta}{\left(\dfrac{C_c}{f_c' A_g}\right)^2}\,(2N_c)^{-1} = \frac{0.016}{\alpha\beta\left(\dfrac{c}{D}\right)^2}\,(2N_c)^{-1} \tag{2-17}$$

neutral axis depth ratio (c/D) in equation (2-17) can be found from force equilibrium on the column section which requires

$$P_e = C_c + C_s - T_s \tag{2-18}$$

where P_e = the applied axial load and C_s and T_s are the forces provided by the longitudinal compression and tension reinforcement, respectively.

Consider the column sections shown in figure 2-3a. Let η denote the proportion of longitudinal steel arranged in the topmost and lowermost layer of the section. Thus for a symmetrical four bar column as in figure 2-3a(i) $\eta = 1$ and the column section in figure 2-3a(ii) with the longitudinal steel equally arranged in at the four sides, $\eta = 0.5$. However, for the wall section shown in figure 2-3a(iii) assuming bending about X-X, $\eta \approx 0$ and for bending about Y-Y axis $\eta = 1$. Assuming that under large curvature all the steel yields (such an assumption is commonly made in plastic analysis), from figure 2-3b it can be seen that the tension and compression forces due to ηA_{st} on the top and bottom layer equilibrate each other, and hence the remaining steel $(1 - \eta)A_{st}$ distributed along the sides over a depth $D - 2d'$ of the section with a total thickness t given by

$$t = \frac{(1 - \eta)A_{st}}{(D - 2d')} = \frac{\gamma A_{st}}{(D - 2d')} \tag{2-19}$$

15

(i) $\gamma = 0.5$ (ii) $\gamma = 0.0$ (iii) $\gamma = 1.0$
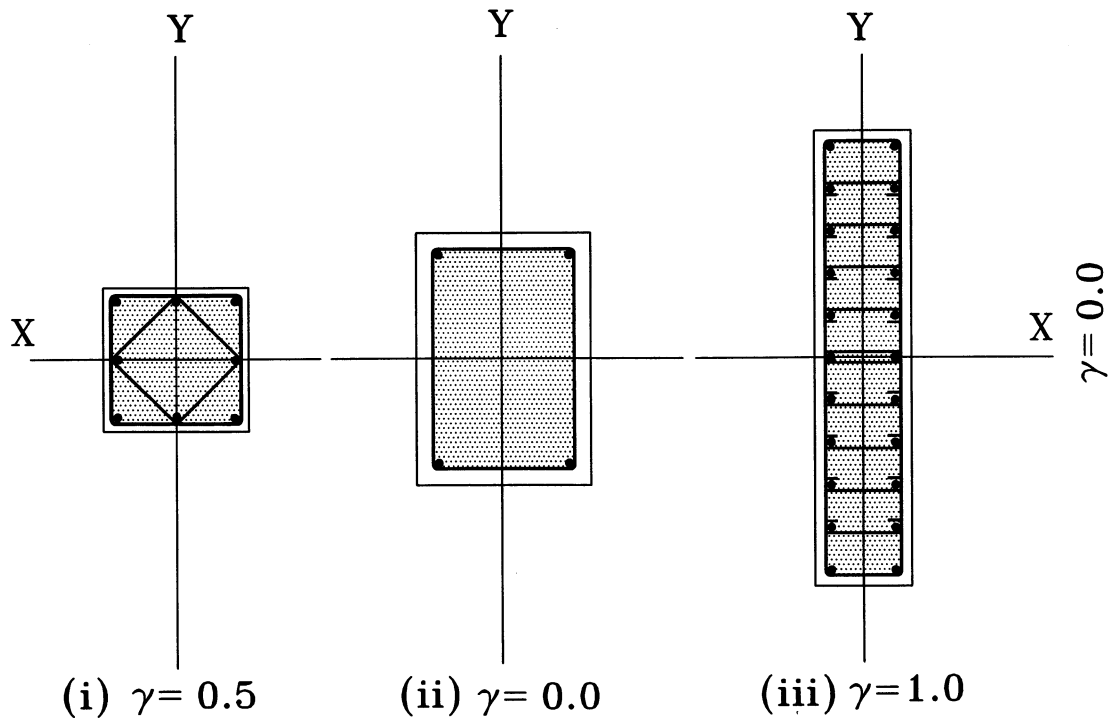
(a) Reinforcing Steel Configuration Factor
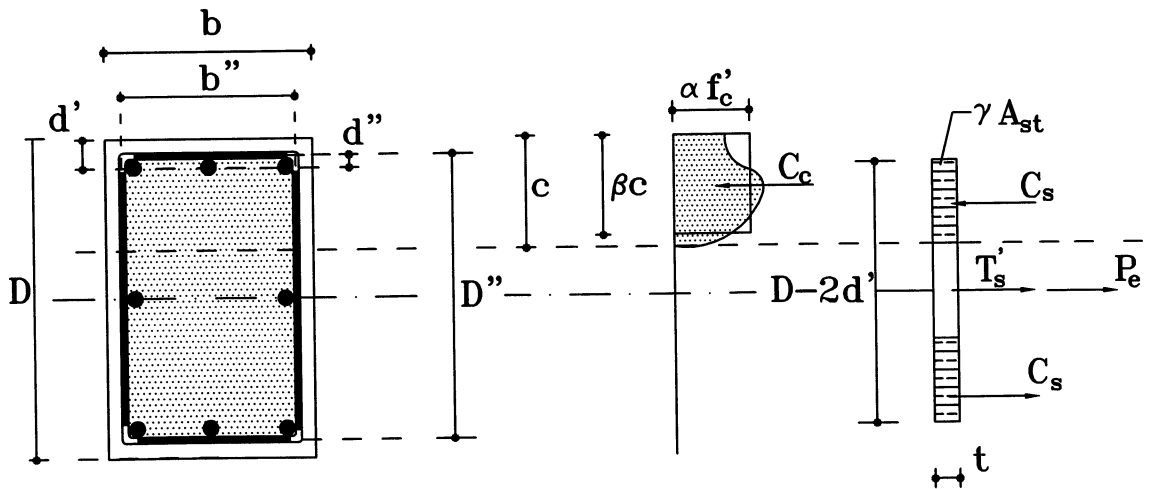
(b) Equivalent Reinforcement Strip

Figure 2-3 Showing Reinforcing Steel Configuration Factor and Equivalent Reinforcement Strip.

where $\gamma = (1 - \eta)$, d' = the effective cover from the extreme fiber to the center of outer layer of longitudinal bars. Out of this γA_{st} a part will be in tension and the rest in compression. Assuming the compressive force in a steel strip of thickness t and depths $c - d'$ equal to a tensile force in a strip of same dimension below the neutral axis, the net tensile force in steel can be assumed to be concentrated in a strip of thickness t and depth $(D - 2c)$ arranged symmetrically about the neutral axis. Thus equation (2-18) can be revised as

$$P_e = C_c - T'_s \tag{2-20}$$

where T'_s is the tensile force in the strip of depth $(D - 2c)$, thus

$$T'_s = t(D - 2c)f_y = \gamma \, \rho_t f_y A_g \, \frac{(1 - 2c/D)}{(1 - 2d'/D)} \tag{2-21}$$

Putting the values of C_c and T'_s in equation (2-20)

$$P_e = \alpha \beta f'_c A_g \left(\frac{c}{D}\right) - \gamma \, \rho_t f_y A_g \, \frac{(1 - 2c/D)}{(1 - 2d'/D)} \tag{2-22}$$

Solving for the neutral axis depth ratio gives:

$$\left(\frac{c}{D}\right) = \frac{\left(\dfrac{P_e}{f'_c A_g}\right) + \left(\dfrac{\gamma \, \rho_t f_y/f'_c}{1 - 2\,d'/D}\right)}{\left(\alpha \beta + \dfrac{2\gamma \, \rho_t f_y/f'_c}{1 - 2\,d'/D}\right)} \tag{2-23}$$

where ρ_t = volumetric ratio of the longitudinal reinforcement (A_{st}/A_g), f_y = yield strength of the longitudinal reinforcement, γ = reinforcing steel configuration factor (refer to figure 2-3a). For the general case of rectangular column γ is the proportion of the total reinforcing steel area that exists in each of the two sides of the member. Specific cases are as follows:

- for *square sections* with reinforcing steel placed symmetrically around the perimeter $\gamma = 0.5$

- for *rectangular sections* (beams) with the steel lumped at the outer faces (top and bottom reinforcement in case of beams) $\gamma = 0.0$

- for *wall sections* with two layers of steel running parallel to the long sides; when bending is about the strong axis $\gamma = 1.0$ and when bending is about weak axis $\gamma = 0.0$

17

The stress block parameters $(\alpha\beta)$ appropriate for large curvatures should be used. For ultimate limit state conditions it may be assumed that $\alpha = 0.66$ and $\beta = 1.3 - 0.01 f_c' \, (MPa)$ but $0.75 \le \beta \le 1.00$. Equation (2-23) can be substituted into equation (2-17) wherein it is possible to obtain classical S-N like fatigue relationship for a rectangular section. Also by taking moments about the reference axis (centroid) of the section the steel moment capacity for rectangular sections (see figure 2-3b) can be expressed as

$$M_s = 0.25 A_{st} f_y D \left(1 - 2\frac{d'}{D} \right) + 0.5 A_{st} f_y D \left(1 - \frac{c}{D} - \frac{d'}{D} \right) \frac{\left(\frac{c}{D} - \frac{d'}{D} \right)}{\left(1 - 2\frac{d'}{D} \right)} \tag{2-24}$$

where the symbols are the same as explained previously.

(b) *Circular Column:* Analysis of a circular column section can be carried out in a manner similar to a rectangular section. However, it should be noted that the concrete compression force is more difficult to derive. To determine the concrete compression force (C_c) consider a circle of diameter D having a chord bisected by a diameter as shown in figure 2-4a. The ratio of the area in compression A_c to the gross area A_g can be written as

$$\left(\frac{A_c}{A_g} \right)_{exact} = \frac{1}{2\pi} (\psi - \sin\psi) \tag{2-25}$$

where ψ = angle subtended at the center by the chord $= 2\cos^{-1}(1 - 2c/D)$. Using a regression analysis, Kim (1996) showed that the equation (2-25) can be approximated to

$$\left(\frac{A_{c-eff}}{A_g} \right) = 1.32 \left(\beta \, \frac{c}{D} \right)^{1.38} \tag{2-26}$$

which is valid for $c/D < 0.5$ as demonstrated by figure 2-4b. Thus concrete compression force for a circular column can be approximated as

$$C_c = 1.32 \, \alpha f_c' A_g \left(\beta \, \frac{c}{D} \right)^{1.38} \tag{2-27}$$

where α = average concrete stress ratio, β = depth ratio of the concrete stressed in compression, A_g = gross concrete area, and D = outside diameter of the section. Normalizing equation (2-26)
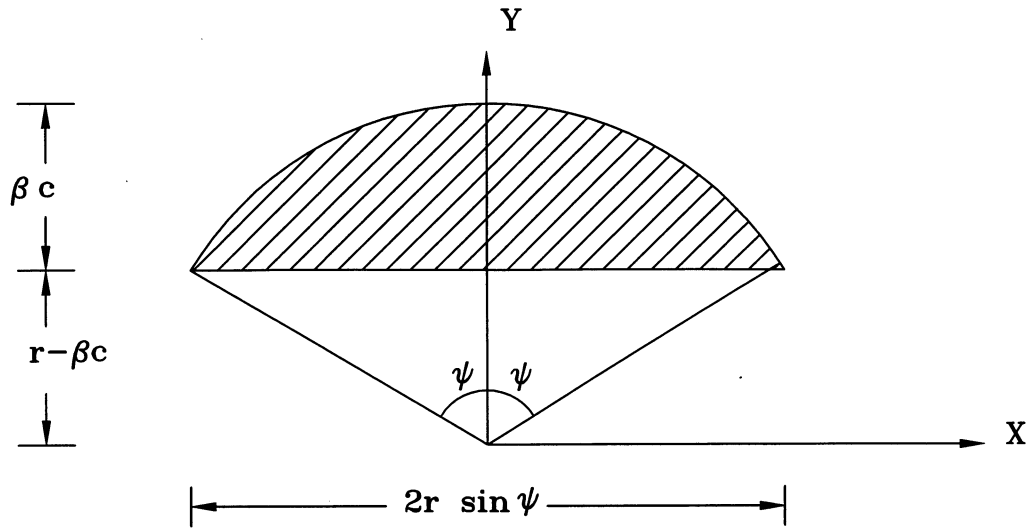
(a) Area of Compressed Concrete.
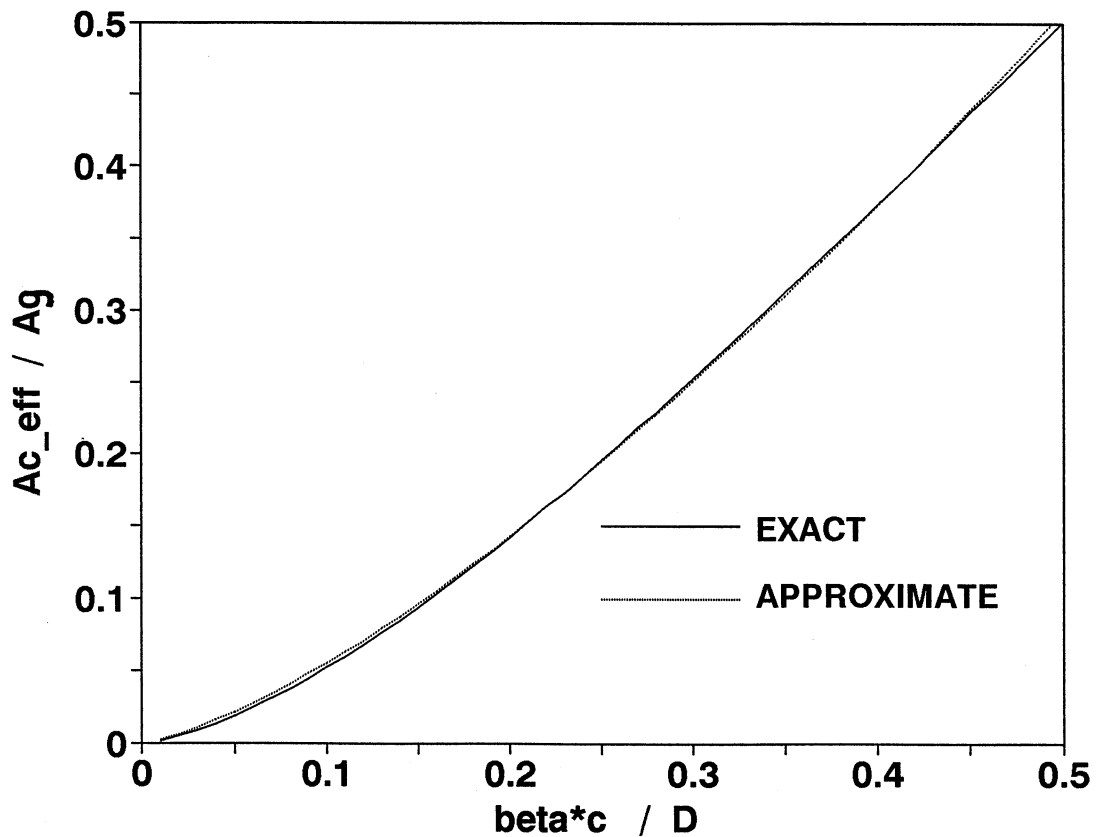
(b) Relationship between Stress Block Depth and Compression Area.

Figure 2-4 Determination of Area of Compressed Concrete in a Circular Column Section.

$$\frac{C_c}{f_c' A_g} = 1.32\, \alpha \left(\beta\, \frac{c}{D}\right)^{1.38} \qquad (2\text{-}28)$$

Substituting into equation (2-7) gives

$$(\phi_p D) = \frac{0.012}{\alpha(\beta)^{1.38} \left(\frac{c}{D}\right)^{2.38}} \cdot (2\,N_c)^{-1} \qquad (2\text{-}29)$$

The neutral axis depth for circular sections can be computed from force equilibrium requirements. Considering that in a circular section, the total area of longitudinal reinforcement is evenly distributed all along the periphery of the column all of which yields under large curvatures, it can be shown in similar way as a rectangular column that force equilibrium of the column section requires

$$P_e = C_c - 0.5\, A_{st} f_y \left(\frac{1 - 2c/D}{1 - 2d'/D}\right) \qquad (2\text{-}30)$$

where all the symbols are easily identifiable.

Using equations (2-28) and (2-30), the neutral axis depth can be expressed as:

$$\frac{c}{D} = \frac{1}{\beta}\left[\frac{\dfrac{P_e}{f_c' A_g} + 0.5\, \rho_t\, \dfrac{f_y}{f_c'}\left(\dfrac{1 - 2c/D}{1 - 2d'/D}\right)}{1.32\, \alpha}\right]^{0.725} \qquad (2\text{-}31)$$

This non-linear equation may be solved easily by fixed-point iteration.

The steel component of the moment for circular sections is also given by

$$M_s = 0.25\, A_{st} f_y D\left(1 - 2\frac{d'}{D}\right) + 0.5\, A_{st} f_y D\left(1 - \frac{c}{D} - \frac{d'}{D}\right)\frac{\left(\dfrac{c}{D} - \dfrac{d'}{D}\right)}{\left(1 - 2\dfrac{d'}{D}\right)} \qquad (2\text{-}32)$$

with the symbols as explained previously.

20
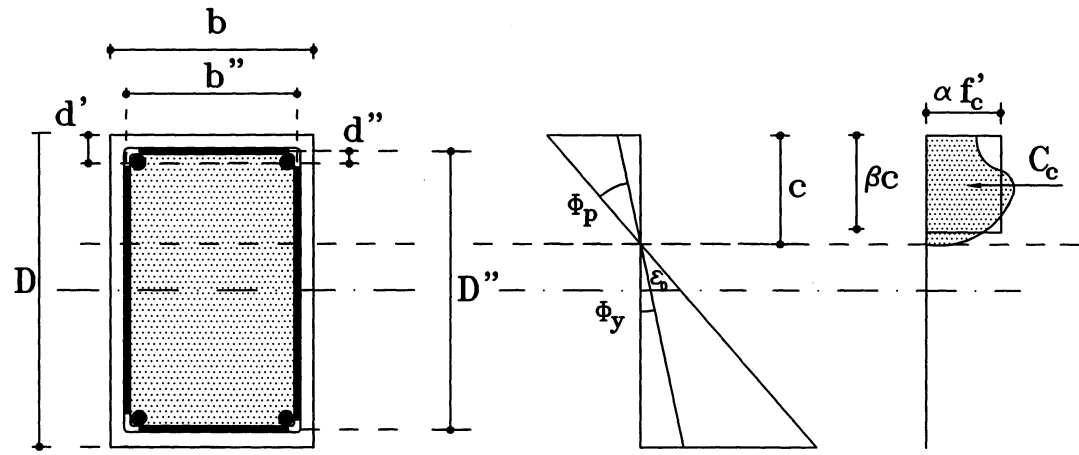
Rectangular Column
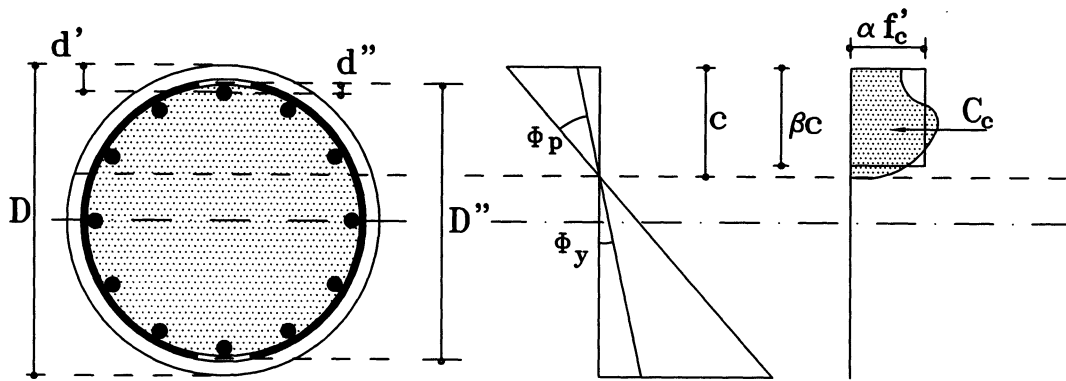
Circular Column

Figure 2-5 Sectional Parameters in Rectangular and Circular Columns.

21

2.2.4 Summary of Damage Evaluation Procedure

Step 1.   Determine the neutral axis depth c/D. For rectangular sections, use equation (2-23):

$$\left(\frac{c}{D}\right) = \frac{\left(\dfrac{P_e}{f_c' A_g}\right) + \left(\dfrac{\gamma\, \rho_t f_y/f_c'}{1 - 2\, d'/D}\right)}{\left(\alpha\beta + \dfrac{2\gamma\, \rho_t f_y/f_c'}{1 - 2\, d'/D}\right)} \qquad\text{(UC-1a)}$$

and for circular sections, use equation (2-31):

$$\frac{c}{D} = \frac{1}{\beta}\left[\frac{\dfrac{P_e}{f_c' A_g} + 0.5\, \rho_t\, \dfrac{f_y}{f_c'}\left(\dfrac{1 - 2c/D}{1 - 2\, d'/D}\right)}{1.32\,\alpha}\right]^{0.725} \qquad\text{(UC-1b)}$$

Step 2.   Determine the concrete compression force ratio $C_c/f_c' A_g$. For rectangular sections use equation (2-16):

$$\left(\frac{C_c}{f_c' A_g}\right) = \alpha\beta\left(\frac{c}{D}\right) \qquad\text{(UC-2a)}$$

and for circular sections use equation (2-28)

$$\frac{C_c}{f_c' A_g} = 1.32\,\alpha\left(\beta\,\frac{c}{D}\right)^{1.38} \qquad\text{(UC-2b)}$$

Step 3.   Determine the equivalent plastic hinge length L_p using equation (2-9):

$$L_p = 0.08L + 4400\,\varepsilon_y d_b \qquad\text{(UC-3)}$$

Step 4.   Determine the cumulative plastic drift capacity $\Sigma\theta_{pc}$ using equation (2-10):

$$\Sigma\theta_{PC} = \frac{0.016\,(L_p/D)}{\left(\dfrac{C_c}{f_c'A_g}\right)\left(\dfrac{c}{D}\right)}$$

(UC-4)

Step 5.   Determine the proportion of the moment capacity that is contributed by the concentric concrete stress block, M_c/M_n.

For rectangular sections, use equation (2-13):

$$M_c = 0.5C_cD\left(1 - \beta\,\frac{c}{D}\right)$$

(UC-5a)

and for circular sections, use equation (2-14):

$$M_c = 0.5C_cD\left(1 - 1.2\,\beta\,\frac{c}{D}\right)$$

(UC-5b)

Step 6.   Finally, applying the damage model given by equation (2-11):

$$\Sigma D_{ci} = \frac{\Sigma\theta_{pi}}{\Sigma\theta_{PC}}$$

(UC-6a)

and the model for strength degradation, model given by equation (2-12):

$$\frac{M_i}{M_n} = 1 - \frac{M_c}{M_n}\Sigma D_{ci} = 1 - \frac{M_c}{M_n}\frac{\Sigma\theta_{pi}}{\Sigma\theta_{PC}}$$

(UC-6b)

the modified theoretical strength capacity may be determined as a function of the actual (experimental) cumulative plastic drift history.

2.3 Numerical Example

The fatigue evaluation procedure described so far is explained with the aid of a numerical example in the following. A circular column illustrated in figure 1-1 is chosen for the purpose. The height of the central column in the pier bent is chosen to be 6100 *mm* (250 *in.*). This analysis is carried out in the transverse direction where the column is restrained completely at the top and bottom by relatively stocky cap beam and foundation. As a result, only half of the column (i.e., 3050 *mm*), which is the height of the equivalent cantilever will be used for the analysis. This is illustrated in the following.
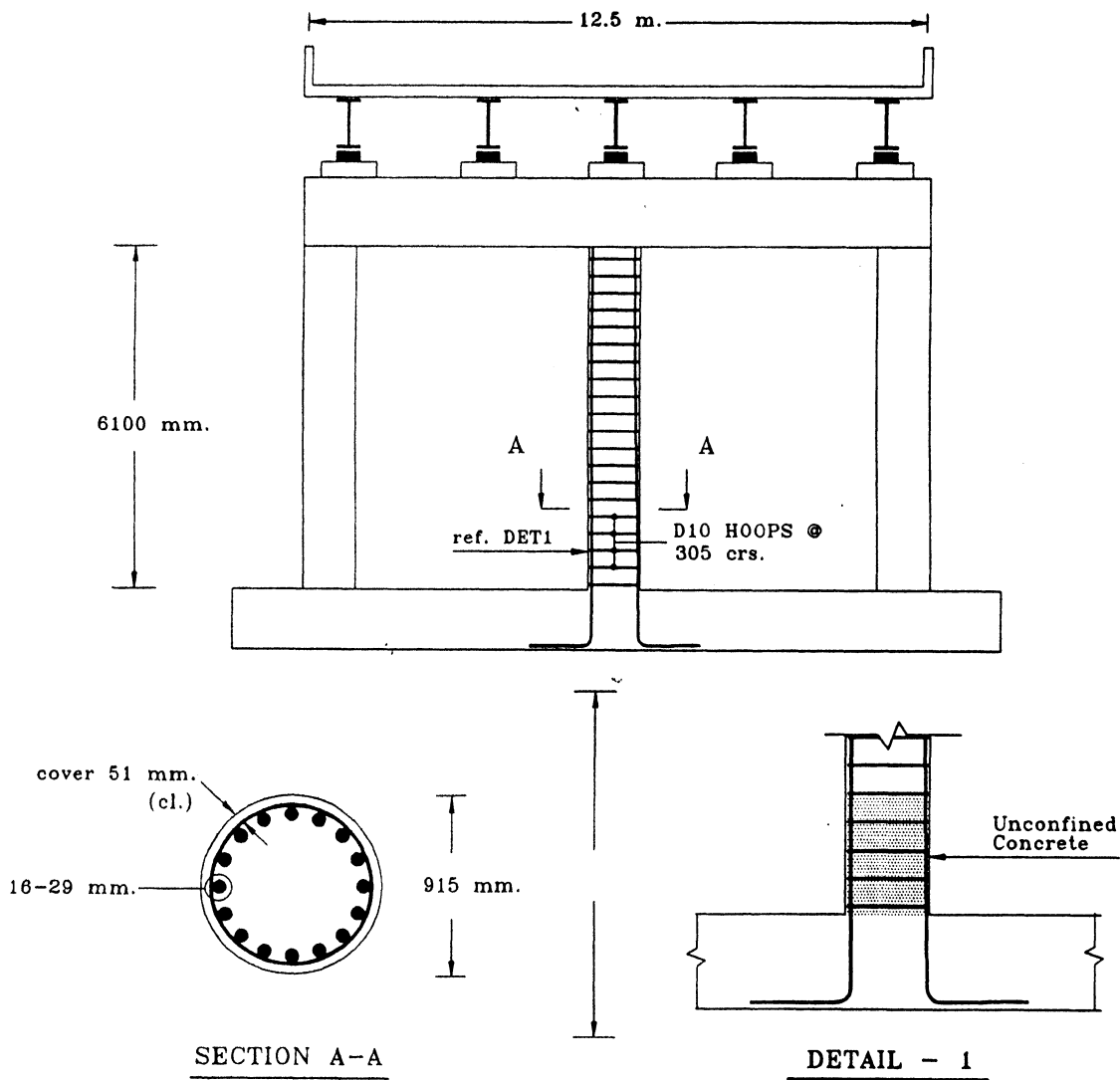
Figure 2-6 Illustrative Bridge Pier used in the Numerical Example.

<u>Given Data</u>

Diameter of the column $D = 915$ mm.

Height of the column $H = 6100$ mm.

Number of longitudinal bars $n = 16$ of diameter $d_b = 28$ mm.

Diameter of horizontal bars $d_{bh} = 10$ mm and spacing $s = 305$ mm.

Clear cover in the column $cov = 51$ mm.

Unconfined compression strength of concrete $f'_c = 45$ MPa

Yield strength of longitudinal reinforcement $f_y = 330$ MPa

Yield strength of horizontal reinforcement $f_{yh} = 330$ MPa

Axial load ratio in the column ($P_e/f'_c A_g$) denoted by $P_{rat} = 0.04$

1. <u>Neutral axis depth ratio:</u>

Longitudinal reinforcement ratio $\rho_t = \dfrac{n \cdot d_b^{\,2}}{D^2}$ -----> $\qquad \rho_t = 0.015$

Effective cover $d' = cov + d_{bh} + 0.5 \cdot d_b$ -----> $d' = 75$ mm.

Core diameter $D'' = D - 2 \cdot cov - d_{bh}$ -----> $D'' = 803$ mm.

Stress block parameters $\alpha = 0.66$ and $\beta = 1.3 - 0.01015 \cdot f'_c$ ----> $\beta = 0.8433$

Let the c/D ratio be denoted by cD_{rat}. As an initial value of this quadratic assume

$cD_{rat} = 0.2$

$$cD_{rat} = \text{root}\left[\left[\frac{P_{rat} + 0.5 \cdot \rho_t \cdot \dfrac{f_y}{f_c} \cdot \dfrac{1 - 2 \cdot cD_{rat}}{1 - 2 \cdot \dfrac{d'}{D}}}{1.32 \cdot \alpha \cdot \beta^{1.38}} \right]^{0.725} - cD_{rat}, cD_{rat} \right]$$

$cD_{rat} = 0.2071$

2. Concrete compression force ratio

Gross cross sectional area $\quad A_g := 0.25 \cdot \pi \cdot D^2 \quad \text{-----> } \quad A_g = 6.5755 \cdot 10^5 \quad mm^2$

Core cross sectional area $\quad A_{cc} := 0.25 \cdot \pi \cdot D"^2 \quad \text{-----> } \quad A_{cc} = 5.0643 \cdot 10^5 \quad mm^2$

Concrete compression force $\quad C_c := 1.32 \cdot \alpha \cdot \left(\beta \cdot cD_{rat} \right)^{1.38} \cdot f_c \cdot A_g$

Concrete compression force ratio $\quad \dfrac{C_c}{f_c \cdot A_g} = 0.0784$

3. Equivalent plastic hinge length

Young's Modulus of longitudinal steel $\quad E_s := 200000 \quad MPa$

Yield strain of longitudinal steel $\quad \varepsilon_y := \dfrac{f_y}{E_s} \quad \text{------> } \quad \varepsilon_y = 0.0017$

Equivalent plastic hinge length

$L_p := 0.08 \cdot \dfrac{H}{2} + 4400 \cdot \varepsilon_y \cdot d_b \quad \text{-------> } \quad L_p = 447.28 \quad mm.$

4. Cumulative plastic drift assuming concrete damage alone

$\Sigma \theta_{PC} := \dfrac{0.016 \cdot \dfrac{L_p}{D}}{\left(\dfrac{C_c}{f_c \cdot A_g} \right) \cdot cD_{rat}} \quad \text{-------> } \quad \Sigma \theta_{PC} = 0.4816$

5. Moment capacity generated by the eccentric concrete stress block

$M_c := 0.5 \cdot C_c \cdot D \cdot \left(1 - 1.2 \cdot \beta \cdot cD_{rat} \right) \quad \text{------> } \quad \dfrac{M_c}{f_c \cdot A_g \cdot D} = 0.031$

From ACI type analysis, nominal moment $\quad M_n := 1.65 \cdot 10^9 \quad N\text{-}mm.$

Therefore, $\quad \dfrac{M_c}{M_n} = 0.5084$

26

7. Application of the damage model

$$M_i / M_n = 1 - M_c / M_n \, (\Sigma\theta_{pi} / \Sigma\theta_{PC})$$

Above equation is plotted i figure 2-7. note that beyond $\Sigma\theta_{pi} := \Sigma\theta_{PC}$, M_i / M_n

becomes horizontal at $1 - \dfrac{M_c}{M_n} = 0.4916$ At this point the concrete damage is complete and the damage index value is $\Sigma D_{ci} = 1.0$. this ordinate also denotes the ratio of the moment contributed by the longitudinal steel to the nominal moment (M_s / M_n) as pointed out in the same figure.

Unconfined concrete fatigue analysis

$$N_c := 1$$

$$\Phi pD := \frac{0.016}{\left(\dfrac{C_c}{f_c \cdot A_g}\right) \cdot cD_{rat}} \cdot \left(2 \cdot N_c\right)^{-1}$$

This equation is plotted in figute 2-8 for N_c values ranging betweem 1 and 100.
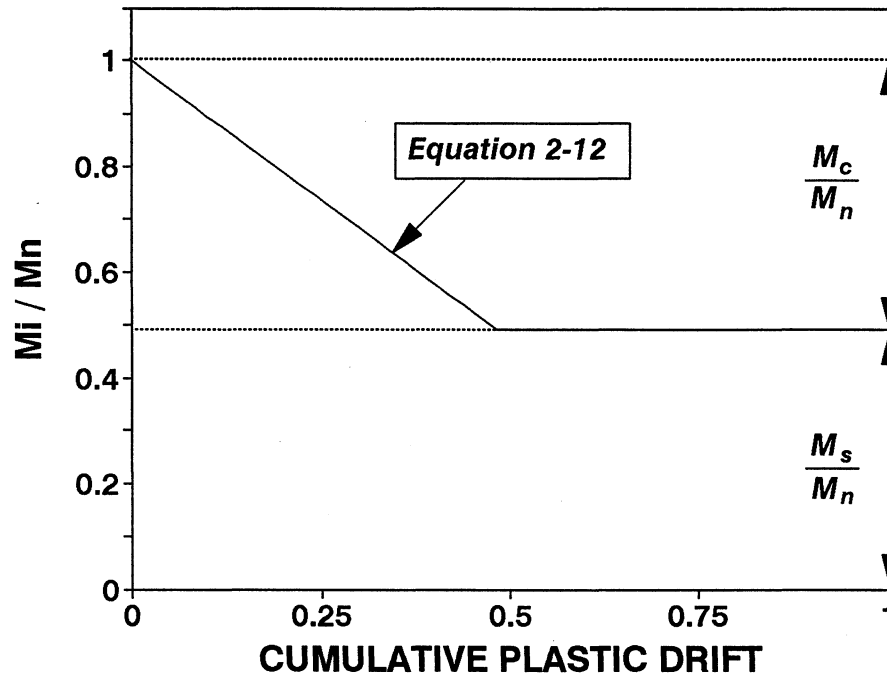
Figure 2-7 Showing the Unconfined Concrete Damage Model.
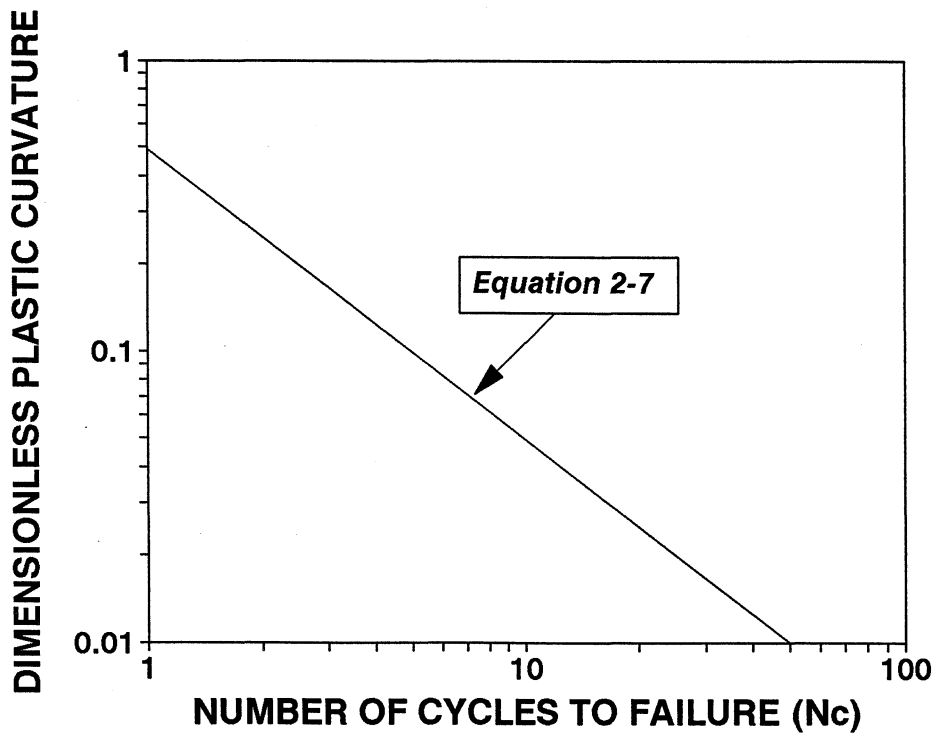
Figure 2-8 Showing the Unconfined Concrete Fatigue Model.

28

SECTION 3
ANCHORAGE ZONE FAILURE

3.1 INTRODUCTION

Failure of a column due to loss of bond and anchorage is yet another failure mode which, ideally needs to be prevented. This can be perceived using the principles of capacity design. Based on full-size prototype and one-quarter scale bridge pier experiments, Mander et al. (1993) proposed an energy based strength deterioration model to explain failure unconfined concrete bridge piers. However, the above-mentioned theory implicitly assumes that the concrete is well anchored in the cap and in the foundation, thereby eliminating any chances of anchorage failure. This section seeks to advance Mander's energy-based methodology and tries to explain the phenomenon of bond failure.

3.2 STRENGTH DETERIORATION THEORY DUE TO LOSS OF BOND IN ANCHORAGES

The degradation of strength of unconfined concrete is progressive. The process starts with the onset of plastic displacements. The strength deterioration model described in the previous section and restated here can therefore be used for this purpose.

$$\frac{F_i}{F_n} = 1 - \frac{M_c}{M_n} \Sigma D_{ci} = 1 - \frac{M_c}{M_n} \frac{\Sigma \theta_{pi}}{\Sigma \theta_{PC}} \tag{3-1}$$

in which F_n and M_n are the nominal lateral flexural strength and moment capacities, M_c = moment in the column resisted by the eccentric concrete stress block and ΣD_{ci} = cumulative damage to the unconfined concrete up to the ith cycle of loading.

The adhesive bond within the embedment zone of a longitudinal rebar anchorage is assumed to be progressively destroyed by the propagating yield stresses from the end zone of the column. The yield force can be sustained, but as soon as all the adhesive bond is destroyed, there will be a sudden drop in the moment capacity (ΔM_s). The remaining moment that can still be sustained by the column will be governed by the residual bond force which is primarily

dependant of friction.

Assuming that the total moment capacity is made up of steel and concrete components

$$M_n = M_s + M_c \tag{3-2}$$

the loss in the steel component of the moment capacity (ΔM_s) is given by

$$\Delta M_s = \left(1 - \frac{f_{rb}}{f_y}\right) M_s \tag{3-3}$$

or

$$\frac{\Delta M_s}{M_n} = \left(1 - \frac{f_{rb}}{f_y}\right)\left(1 - \frac{M_c}{M_n}\right) \tag{3-4}$$

where f_{rb} = residual bond stress in the rebar, f_y = yield stress of the longitudinal reinforcement, and M_s = moment capacity of the longitudinal steel.

By determining the cumulative plastic drift $\Sigma\theta_{PB}$ at which all the <u>adhesive bond</u> is consumed, it is possible to compute the strength prior to anchorage failure, thus

$$\frac{F_1}{F_n} = 1 - \frac{M_c}{M_n} \frac{\Sigma\theta_{PB}}{\Sigma\theta_{PC}} \tag{3-5}$$

And the strength immediately following the anchorage failure (which occurs over one cycle with a plastic drift change of $2\theta_p$)

$$\frac{F_2}{F_n} = \frac{F_1}{F_n} - \frac{\Delta M_s}{M_n} \tag{3-6}$$

Substituting equations (3-4) and (3-5) into (3-6), one obtains

$$\frac{F_2}{F_n} = \frac{f_{rb}}{f_y} + \frac{M_c}{M_n}\left[1 - \frac{\Sigma\theta_{PB}}{\Sigma\theta_{PC}} - \frac{f_{rb}}{f_y}\right] \tag{3-7}$$

Following the anchorage failure the concrete continues to decay as per

30

$$\frac{F_i}{F_n} = \frac{F_2}{F_n} - \frac{M_c}{M_n} \frac{\left(\Sigma\,\theta_{pi} - \overline{\Sigma\,\theta_{PB}} + 2\theta_p \right)}{\Sigma\,\theta_{PC}} \tag{3-8}$$

until the residual rocking strength (F_r) is obtained which is given by the lesser of the rocking strength ($F_{rocking}$) or the sliding strength given by

$$F_{sliding} = \mu_s\,W \tag{3-9}$$

where μ_s = coefficient of friction assumed to be 0.7 according to the recommendations of Paulay and Priestley (1992) and W = gravity weight.

At the final stage after column strength is lost, the resistance of the column is entirely governed by the axial compression force on the column with or without the contribution from the reinforcement. The ability of the reinforcement to resist the lateral load will solely depend upon the level of residual stresses left in the bars after bond failure. Thus the simplified sectional analysis introduced in Section 2 can be used to evaluate the moment of rocking resistance (M_r). However, it will be assumed that considerable crushing takes place at this stage and thus a reduced section excluding the cover up to the centerline of the hoops will be considered. Using the same equations from the neutral axis depth modified to account for the reduced section, the moment of rocking resistance (M_r) can be obtained as a combination of the modified steel moment (M_s') and concrete moment (M_c'). Thus for a rectangular section

$$M_c' = 0.5\,C_{cc}\,D''\left(1 - \frac{c''}{D''} \right) \tag{3-10}$$

and

$$M_s' = 0.25\,A_{st}f_{rb}\,D''\left(1 - 2\frac{d''}{D''} \right) + 0.5\,A_{st}f_{rb}\,D''\left(1 - \frac{c''}{D''} - \frac{d''}{D''} \right)\left(\frac{c''}{D''} - \frac{d''}{D''} \right) \tag{3-11}$$

with

31

$$\frac{c''}{D''} = \frac{\left(\dfrac{P_e}{f_c' A_g}\right) + \left(\dfrac{\gamma\, \rho_t f_{rb}/f_c'}{1 - 2\,d''/D''}\right)}{\left(\alpha\,\dfrac{A_{cc}}{A_g} + \dfrac{2\gamma\, \rho_t f_{rb}/f_c'}{1 - 2\,\dfrac{d''}{D''}}\right)} \tag{3-12}$$

For circular sections

$$M_c' = 0.5\, C_{cc} D''\left(1 - 1.2\,\frac{c''}{D''}\right) \tag{3-13}$$

and

$$M_s' = 0.25\, A_{st} f_{rb} D''\left(1 - 2\,\frac{d''}{D''}\right) + 0.5\, A_{st} f_{rb} D''\left(1 - \frac{c''}{D''} - \frac{d''}{D''}\right)\left(\frac{c''}{D''} - \frac{d''}{D''}\right) \tag{3-14}$$

with

$$\frac{c''}{D''} = \left[\frac{\dfrac{P_e}{f_c' A_g} + 0.5\,\rho_t\,\dfrac{f_{rb}}{f_c'}\left(\dfrac{1 - 2c''/D''}{1 - 2d''/D''}\right)}{1.32\,\alpha\,\dfrac{A_{cc}}{A_g}}\right]^{0.725} \tag{3-15}$$

In the above equations, f_{rb} = residual bond stress in the longitudinal rebar, A_{cc}/A_g = ratio of the core to gross area and other sectional dimensions are as explained previously. Note that the stress block parameters appropriate for large strains should be used and $\alpha = 0.3$ and $\beta = 1$ are to be assumed as per Mander et al. (1997). Also, C_{cc} which denotes the compression force in the core concrete is given by $C_{cc} = 0.3\, c''/D'' f_c' A_{cc}$ and $C_{cc} = 0.396\,(c''/D'')^{1.38} f_c' A_{cc}$ for rectangular and circular sections respectively. Note that for cases where there is no residual bond stress, the rocking moment of resistance entirely consists of the concrete component M_c'. Thus the rocking strength can be expressed as:

$$F_{rocking} = \frac{\Sigma M_r}{H} = \frac{\Sigma(M_c' + M_s')}{H} \tag{3-16}$$

where ΣM_r = sum of the residual moment of rocking resistance for all columns at top and bottom and H = clear column height.

The cumulative plastic drift at which the residual rocking/sliding capacity commences is thus given by

$$\Sigma\theta_{PR} = \overline{\Sigma\theta_{PB} + 2\theta_p} + \frac{\Sigma\theta_{PC}}{M_c/M_n}\left(\frac{F_2}{F_n} - \frac{F_r}{F_n}\right) \tag{3-17}$$

where θ_p = plastic drift at the current force level. The conceptual concrete and bond deterioration model is shown graphically in figure 3-1 and discussed in what follows.

3.2.1 Concrete Deterioration

The moment capacity M_c generated by the eccentric concrete stress block is given by:
(a) for rectangular sections

$$M_c = 0.5C_c D\left(1 - \beta\frac{c}{D}\right) \tag{3-18}$$

(b) for circular sections

$$M_c = 0.5C_c\left(1 - 1.2\beta\frac{c}{D}\right) \tag{3-19}$$

in which C_c = concrete compression force, D = overall depth of the section and c = neutral axis depth from extreme compression fiber. The neutral axis depth ratio (c/D) is given by equations (2-23) and (2-31) for rectangular and circular sections, respectively.

The cumulative damage to the concrete ΣD_{ci} is given by

$$\Sigma D_{ci} = \frac{\Sigma\theta_{pi}}{\Sigma\theta_{PC}} \tag{3-20}$$

where $\Sigma\theta_{pi}$ = cumulative plastic drift and $\Sigma\theta_{PC}$ = cumulative plastic drift capacity assuming concrete damage alone. This was previously shown in section 2.2.3 from work considerations [equation (2-11)].

33
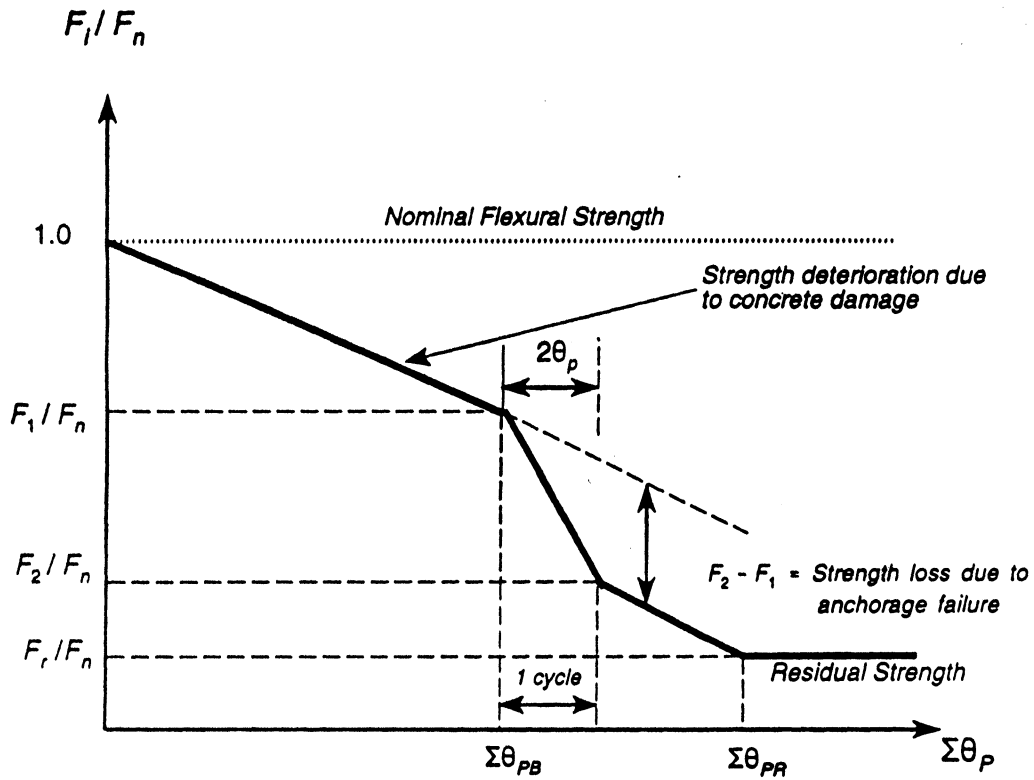
Figure 3-1 Conceptual Energy Based Lateral Force Vs. Cumulative Drift Damage Model for Piers Governed by Anchorage and Concrete Failure.

3.2.2 Deterioration of Bond in Anchorages

The cumulative damage arising from damage of bond to the anchorage zone is given by

$$\Sigma D_{bi} = \frac{\Sigma \theta_{pi}}{\Sigma \theta_{PB}} \tag{3-21}$$

where $\Sigma \theta_{pi}$ = current cumulative plastic drift and $\Sigma \theta_{PB}$ = cumulative plastic drift assuming all damage depends on bond deterioration. The cumulative plastic drift capacity of the bond is obtained using a virtual work approach:

$$EWD = IWD \tag{3-22}$$

$$(\Delta M_s)(\xi \, \Sigma \theta_{PB}) = n \, \pi \, d_b \, \ell_{em} \int u d\Delta_s \tag{3-23}$$

by rearranging one can compute the cumulative plastic drift at incipient bond failure:

$$\Sigma \theta_{PB} = \frac{n \, \pi \, d_b \, \ell_{em} \int u d\Delta_s}{\xi (\Delta M_s)} \tag{3-24}$$

in which ΔM_s = moment contribution of the longitudinal reinforcement relying on adhesive bond, n = number of longitudinal bars in the column, d_b = diameter of the longitudinal reinforcing bars, ξ = proportion of the column drift arising from bond-slip (yield penetration) to the total column rotation, and ℓ_{em} = embedment length of the longitudinal reinforcement. The product $\pi \, d_b \, \ell_{em}$ denotes the surface area of one embedded bar and the integral $\int u d\Delta_s$ is the area beneath the bond stress slip curve that relies on adhesion bond.

The determination for the cumulative plastic drift capacity $\Sigma \theta_{PB}$ and the integral $\int u d\Delta_s$ requires an appropriate bond-stress slip model. Although there is no dealt of available materials in this subject but none of the models can be used for this purpose since most of them relate to interior beam column joints with a very good amount of confining steel. For the present case a conservative bond stress slip model such as the one proposed by Malvar (1992) can be used. Based on the results of Malvar a frictional coefficient of μ_b = 0.5 can be assumed for the residual bond stress capacity that exists for slip displacements exceeding 10 *mm* (3/8 *in.*).

35

Figure 3-2 shows the proposed bond stress slip model resulting from the above-mentioned analysis. The residual frictional bond stress is given by

$$U_{rb} = \mu_b \, f_{cp} \qquad (3\text{-}25)$$

where $\mu_b = 0.5$ = friction coefficient and f_{cp} = confinement pressure. The maximum adhesion bond stress is given by

$$U_{ab} = 2\sqrt{f_c'}\,MPa = 24\sqrt{f_c'}\,psi \qquad (3\text{-}26)$$

where f_c' = concrete strength.

The integral $\int u d\Delta_s$ may thus be evaluated as

$$
\begin{aligned}
\overline{U}_{ab} = \int u d\Delta s &= \left(\tfrac{2}{3} \times U_{ab} \times 1\right) + \left(U_{ab} \times 1\right) + \left(\tfrac{1}{2} \times U_{ab} \times 8\right) \\
&= \left(\tfrac{2}{3} \times U_{ab} \times 1\right) + U_{ab}(3 - 1) + \tfrac{1}{2}(10.5 - 3)U_{ab}
\end{aligned}
\qquad (3\text{-}27)
$$

$$\overline{U}_{ab} = 6.24 \, U_{ab} \, N/mm^2\text{-}mm = 0.253 \, U_{ab} \, psi\text{-}in. \qquad (3\text{-}28)$$

where $\overline{U}_{ab}$ = work done to completely break the adhesion bond.

The residual bond stress f_{rb} for rebars passively confined by transverse hoop reinforcement that produces tri-axial confinement stress f_l from force equilibrium in figure 3-3

$$f_l(sD'') = 2A_{bh}f_{yh} \qquad (3\text{-}29)$$

and hence

$$f_l = \frac{2A_{bh}}{sD''} f_{yh} = \frac{\rho_s}{2} f_{yh} \qquad (3\text{-}30)$$

where s = spacing of the lateral hoop reinforcement with area A_{bh} and yield strength f_{yh} and D'' = core concrete diameter. Note that ρ_s denotes the volumetric ratio of transverse confinement which for rectangular and circular sections with a single perimeter hoop can be expressed as
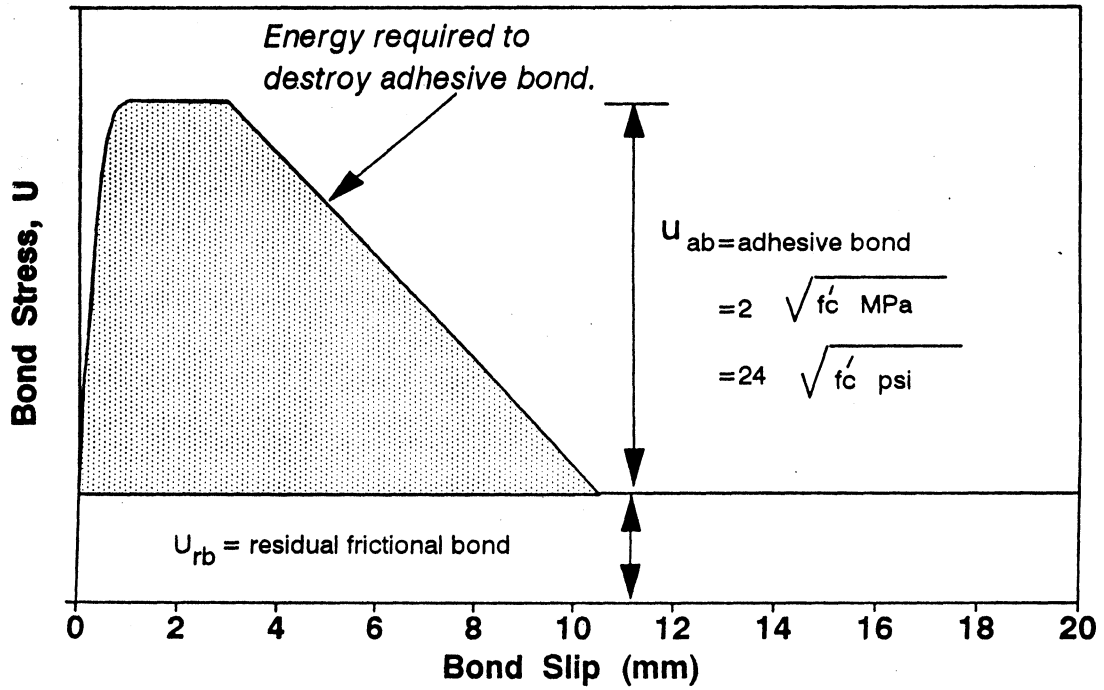
Figure 3-2 Local Bond Stress-Slip Model for the Assessment of Energy Absorption Capacity.
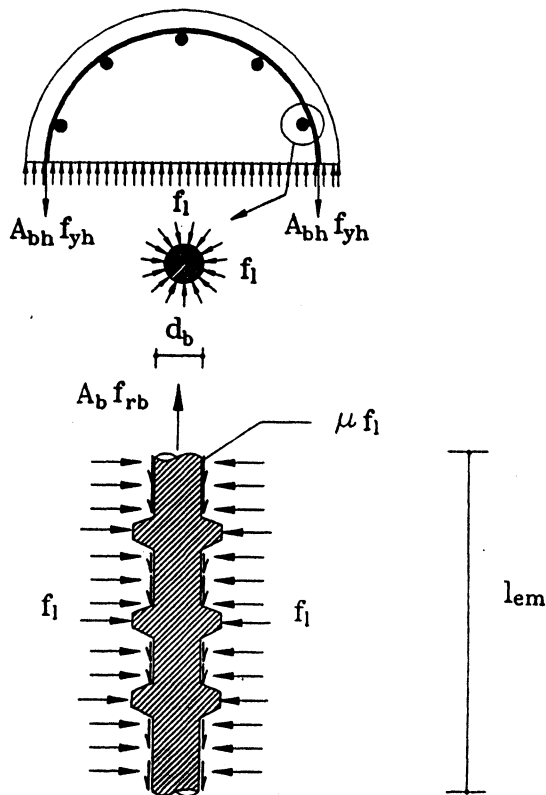
Figure 3-3 Computation of Residual Bond Stress.

$$\rho_s = \frac{4A_{bh}}{sD''} \tag{3-31}$$

Now applying vertical force equilibrium

$$f_{rb}A_b = \mu_b (\pi d_b)l_{em} \rho_s f_{yh} \tag{3-32}$$

from which

$$f_{rb} = \frac{\mu_b \pi d_b l_{em} \rho_s f_{yh}}{2A_b} = 2\mu_b \rho_s f_{yh} \frac{l_{em}}{d_b} \tag{3-33}$$

where d_b = diameter and A_b = cross-sectional area of the longitudinal bar, l_{em} = length of embedment and μ_b = coefficient of friction. Above result is also good for a rectangular section with a single perimeter hoop. Equivalent expressions can be easily derived for other complex hoop arrangements. The coefficient of friction (μ_b) may be taken as 0.5 for low levels of axial load that are typical for such members.

3.2.3 Combined Anchorage and Concrete Deterioration

As noted above, it is necessary to assess the proposition of the total plastic displacements that arise from anchorage pullout and flexure. The empirical equation for assessing the equivalent plastic hinge length gives an appropriate insight into this phenomenon. This equation takes this form

$$L_p = L_{py} + L_{pc} \tag{3-34}$$

where $L_{py} = 4400\varepsilon_y d_b$ is the effective length of yield penetration and $L_{pc} = 0.8L$ is the effective length of damaged concrete. As defined earlier, ξ is the proportion of yield penetration that also corresponds to pullout with respect to the overall plastic deformation, thus

$$\xi = \frac{4400\varepsilon_y d_b}{4400\varepsilon_y d_b + 0.8L} = \frac{4400\varepsilon_y d_b}{L_p} \tag{3-35}$$

3.2.4 Summary of Damage Evaluation Procedure

Step 1. Determine the neutral axis depth ratio c/D. For rectangular sections, use equation (2-23):

$$\left(\frac{c}{D}\right) = \frac{\left(\dfrac{P_e}{f_c' A_g}\right) + \left(\dfrac{\gamma\, \rho_t f_y/f_c'}{1 - 2\,d'/D}\right)}{\left(\alpha\beta + \dfrac{2\gamma\, \rho_t f_y/f_c'}{1 - 2\,d'/D}\right)} \qquad \text{(JA-1a)}$$

and for circular sections, use equation (2-31):

$$\frac{c}{D} = \frac{1}{\beta}\left[\frac{\dfrac{P_e}{f_c' A_g} + 0.5\,\rho_t\, \dfrac{f_y}{f_c'}\left(\dfrac{1 - 2c/D}{1 - 2\,d'/D}\right)}{1.32\,\alpha}\right]^{0.725} \qquad \text{(JA-1b)}$$

Step 2. Determine the concrete compression force ratio $C_c/f_c' A_g$. For rectangular sections, use equation (2-16):

$$\left(\frac{C_c}{f_c' A_g}\right) = \alpha\beta\left(\frac{c}{D}\right) \qquad \text{(JA-2a)}$$

and for circular sections, use equation (2-28):

$$\frac{C_c}{f_c' A_g} = 1.32\,\alpha\left(\beta\,\frac{c}{D}\right)^{1.38} \qquad \text{(JA-2b)}$$

Step 3. Determine the equivalent plastic hinge length L_p using use equation (2-9)

$$L_p = 0.08L + 4400\,\varepsilon_y d_b \qquad \text{(JA-3)}$$

Step 4. Determine the cumulative plastic drift capacity $\Sigma\theta_{PC}$ using equation (2-10):

$$\Sigma\theta_{PC} = \frac{0.016\,(L_p/D)}{\left(\dfrac{C_c}{f_c'A_g}\right)\left(\dfrac{c}{D}\right)} \tag{JA-4}$$

Step 5. Determine the component of the moment contributed by the eccentric concrete stress block M_c. For rectangular sections, use equation (2-13):

$$M_c = 0.5\,C_cD\left(1 - \beta\,\frac{c}{D}\right) \tag{JA-5a}$$

and for circular sections, use equation (2-11)

$$M_c = 0.5C_cD\left(1 - 1.2\,\beta\,\frac{c}{D}\right) \tag{JA-5b}$$

Step 6. Determine the residual bond stress f_{rb} (equation 3-33), strength loss ratio due to bond failure $\Delta M_s / M_n$ (equation 3-4) and energy required to break the adhesive bond $\overline{U}_{ab}$ (equation 3-28):

$$f_{rb} = \frac{\mu_b\,\pi d_b\,l_{em}\,\rho_s f_{yh}}{2\,A_b} = 2\mu_b\,\rho_s f_{yh}\,\frac{l_{em}}{d_b} \tag{JA-6a}$$

$$\frac{\Delta M_s}{M_n} = \left(1 - \frac{f_{rb}}{f_y}\right)\left(1 - \frac{M_c}{M_n}\right) \tag{JA-6b}$$

$$\overline{U}_{ab} = 12.48\,\sqrt{f_c'\,(MPa)}\ \ N/mm^2\text{-}mm. \tag{JA-6c}$$

Step 7. Determine the cumulative plastic drift at incipient bond failure $\Sigma\theta_{PB}$ using equation (3-24):

$$\Sigma\theta_{PB} = \frac{n\,\pi\,d_b\,\ell_{em}\int u\,d\Delta_s}{\xi\,(\Delta M_s)} \tag{JA-7}$$

Step 8. Determine the strength ratio at incipient bond failure F_1/F_n using equation (3-5):

40

$$\frac{F_1}{F_n} = 1 - \frac{M_c}{M_n} \frac{\Sigma\theta_{PB}}{\Sigma\theta_{PC}} \qquad \text{(JA-8)}$$

Step 9.   Determine the strength immediately after the bond failure F_2/F_n using equation (3-7):

$$\frac{F_2}{F_n} = \frac{f_{rb}}{f_y} + \frac{M_c}{M_n}\left[1 - \frac{\Sigma\theta_{PB}}{\Sigma\theta_{PC}} - \frac{f_{rb}}{f_y}\right] \qquad \text{(JA-9)}$$

Step 10.   Determine the rocking strength F_r using the lesser of equations (3-9) and (3-16):

$$F_{siding} = \mu_s W \qquad \text{(JA-10a)}$$

$$F_{rocking} = \frac{\Sigma M_r}{H} = \frac{\Sigma(M_c' + M_n')}{H} \qquad \text{(JA-10b)}$$

where for rectangular sections, use equations (3-10), (3-11) and (3-12)

$$M_c' = 0.5\, C_{cc} D''\left(1 - \frac{c''}{D''}\right) \qquad \text{(JA-10c)}$$

$$M_s' = 0.25\, A_{st} f_{rb} D''\left(1 - 2\frac{d''}{D''}\right) + 0.5\, A_{st} f_{rb} D''\left(1 - \frac{c''}{D''} - \frac{d''}{D''}\right)\left(\frac{c''}{D''} - \frac{d''}{D''}\right) \qquad \text{(JA-10d)}$$

$$\frac{c''}{D''} = \frac{\left(\dfrac{P_e}{f_c' A_g}\right) + \left(\dfrac{\nu\, \rho_t f_{rb}/f_c'}{1 - 2\,d''/D''}\right)}{\left(\alpha\dfrac{A_{cc}}{A_g} + \dfrac{2\nu\, \rho_t f_{rb}/f_c'}{1 - 2\dfrac{d''}{D''}}\right)} \qquad \text{(JA-10e)}$$

and for circular sections, use equations (3-13) through (3-15):

$$M_c' = 0.5\, C_{cc} D''\left(1 - 1.2\frac{c''}{D''}\right) \qquad \text{(JA-10f)}$$

41

$$M_s' = 0.25 A_{st} f_{rb} D'' \left(1 - 2\frac{d''}{D''}\right) + 0.5 A_{st} f_{rb} D'' \left(1 - \frac{c''}{D''} - \frac{d''}{D''}\right)\left(\frac{c''}{D''} - \frac{d''}{D''}\right) \qquad \text{(JA-10g)}$$

$$\frac{c''}{D''} = \left[\frac{\dfrac{P_e}{f_c' A_g} + 0.5\, \rho_t\, \dfrac{f_{rb}}{f_c'}\left(\dfrac{1 - 2c''/D''}{1 - 2d''/D''}\right)}{1.32\, \alpha\, \dfrac{A_{cc}}{A_g}}\right]^{0.725} \qquad \text{(JA-10h)}$$

Step 11.   Determine the cumulative plastic drift at which rocking commences $\Sigma\theta_{PR}$ using equation (3-17):

$$\Sigma\theta_{PR} = \overline{\Sigma\theta_{PB} + 2\theta_p} + \frac{\Sigma\,\theta_{PC}}{M_c/M_n}\left(\frac{F_2}{F_n} - \frac{F_r}{F_n}\right) \qquad \text{(JA-11)}$$

Step 12.   Determine relationship between nominal strength and cumulative plastic drift in the form

$$\frac{F_i}{F_n} = 1 - C\,\Sigma\theta_{pi} \qquad \text{(JA-12)}$$

3.3 Numerical Example

The energy-based theoretical model described in the previous section can be explained with a numerical example. The same column used in section 2.3 is chosen. However, it is presumed the failure due to the loss of bond in anchorage occurs at the junction of per cap and the central column. Relevant details are given in figure 3-4.

Figure 3-4 Illustrative Bridge Pier used in the Numerical Example.

43

Carried over parameters

Unconfined concrete compression strength $f_c = 45$ MPa.

Diameter of the section $D = 915$ mm.

Effective cover $d' = 75$ mm.

Core diameter $D'' = 803$ mm.

Plastic hinge length ratio $\dfrac{L_p}{D} = 0.4888$

Neutral axis depth ratio $cD_{rat} = 0.2071$

Concrete compression force ratio $\dfrac{C_c}{f_c \cdot A_g} = 0.0784$

Cumulative plastic drift capacity considering concrete damage $\Sigma\theta_{PC} = 0.4816$ rad.

Normalized concrete moment ratio $\dfrac{M_c}{f_c \cdot A_g \cdot D} = 0.031$

Ratio of concrete to nominal moment $\dfrac{M_c}{M_n} = 0.5084$

These values are obtained from Section 2.3 and correspond to Steps 1 through 5.

Also provided embedment length $l_{em} = 762$ mm.

6. Residual bond stress in the rebar

Volumetric ratio of lateral reinforcement $\rho_s := \dfrac{\pi \cdot d_{bh}^2}{D'' \cdot s}$ $----->$ $\rho_s = 0.0013$

Consider coefficient of friction $\mu_b = 0.5$

For rebars passively confined by transverse hoop reinforcement that produces triaxial confinement, the residual bond stress is given by

$f_{rb} := 2 \cdot \mu_b \cdot \rho_s \cdot f_{yh} \cdot \dfrac{l_{em}}{d_b}$ $------->$ $f_{rb} = 11.5198$ MPa. $------>$ $\dfrac{f_{rb}}{f_y} = 0.0349$

44

Loss in moment capacity due to anchorage failure

$$\Delta M_s := M_n \cdot \left(1 - \frac{f_{rb}}{f_y}\right) \cdot \left(1 - \frac{M_c}{M_n}\right) \quad \text{-----}> \quad \Delta M_s = 7.8275 \cdot 10^8 \quad \text{N-mm.}$$

and hence the ratio $\quad \dfrac{\Delta M_s}{M_n} = 0.4744$

Work done to completely break the adhesive bond

$$U_{ab} := 12.48 \cdot \sqrt{f'_c} \quad \text{------}> \quad U_{ab} = 83.7184 \quad \text{N/mm}^2\text{-mm}$$

7. Cumulative drift necessary to cause anchorage bond failure

Proportion of inelastic displacements caused by anchorage damage

$$\xi := \frac{4400 \cdot \varepsilon_y \cdot d_b}{L_p} \quad \text{------}> \quad \xi = 0.4545$$

Cumulative drift necessary to cause anchorage bond failure

$$\Sigma\theta_{PB} := \frac{n \cdot \pi \cdot d_b \cdot U_{ab} \cdot l_{em}}{\xi \cdot \Delta M_s} \quad \text{------}> \quad \Sigma\theta_{PB} = 0.2524 \quad \text{rad.}$$

8. Force just prior to bond failure

Nominal force capacity $\quad F_n := \dfrac{2 \cdot M_n}{H}$

$$F_1 := F_n \cdot \left(1 - \frac{M_c}{M_n} \cdot \frac{\Sigma\theta_{PB}}{\Sigma\theta_{PC}}\right) \quad \text{------}> \quad \frac{F_1}{F_n} = 0.7335$$

9. Force one cycle after anchorage-bond failure

$$F_2 := F_n \cdot \left(\frac{F_1}{F_n} - \frac{\Delta M_s}{M_n}\right) \quad \text{-------}> \quad \frac{F_2}{F_n} = 0.2592$$

45

10. Residual rocking strength

Residual rocking strength is given by the lesser of the sliding and rocking strength.
Assuming a coefficient of sliding friction

$$\mu_s := 0.7 \qquad ; \qquad W := P_{rat} \cdot f_c \cdot A_g$$

$$F_{sliding} := \mu_s \cdot W \qquad ------> \qquad F_{sliding} = 8.2852 \cdot 10^5 \qquad N.$$

<u>Calculation of rocking strength:</u>

Let the c''/D'' ratio be denoted by c''_{rat}. As an initial value of this quadratic assume

$$c''_{rat} := 0.2 \quad \text{Also} \quad \alpha := 0.3 \quad \text{and} \quad d'' := 0.5 \cdot \left(d_{bh} + d_b \right)$$

$$c''D''_{rat} := root\left[\left[\frac{P_{rat} + 0.5 \cdot \rho_t \cdot \dfrac{f_{rb}}{f_c} \cdot \dfrac{1 - 2 \cdot c''_{rat}}{1 - 2 \cdot \dfrac{d''}{D''}}}{1.32 \cdot \alpha \cdot \dfrac{D''^2}{D^2}} \right]^{0.725} - c''_{rat}, c''_{rat} \right]$$

$$c''D''_{rat} = 0.1329$$

Modified concrete compression force $\qquad C_{cc} := 1.32 \cdot \alpha \cdot \left(c''D''_{rat} \right)^{1.38} \cdot f_c \cdot A_{cc}$

Hence, $\qquad M'_c := 0.5 \cdot C_{cc} \cdot D'' \cdot \left(1 - 1.2 \cdot c''D''_{rat} \right) \quad ----> \quad M'_c = 4.1361 \cdot 10^8 \qquad$ N-mm.

Also for $\qquad A_{st} := \rho_t \cdot A_g \qquad -----> \qquad A_{st} = 9.852 \cdot 10^3 \qquad mm^2$

$$M'_{s1} := 0.25 \cdot A_{st} \cdot f_{rb} \cdot D'' \cdot \left(1 - 2 \cdot \frac{d''}{D''} \right) \qquad \text{and}$$

$$M'_{s2} := 0.5 \cdot A_{st} \cdot f_{rb} \cdot D'' \cdot \left(1 - c''D''_{rat} - \frac{d''}{D''} \right) \cdot \frac{c''D''_{rat} - \dfrac{d''}{D''}}{1 - 2 \cdot \dfrac{d''}{D''}}$$

Thus, $M'_s := M'_{s1} + M'_{s2}$ --------> $M'_s = 2.6113 \cdot 10^7$ N-mm.

Hence, $F_{rocking} := \left(\dfrac{M'_c + M'_s}{0.5 \cdot H} \right)$ -----> $F_{rocking} = 1.4417 \cdot 10^5$ N.

Normalized rocking strength $\dfrac{F_{rocking}}{F_n} = 0.2665$

These values are plotted in figure 3-5.
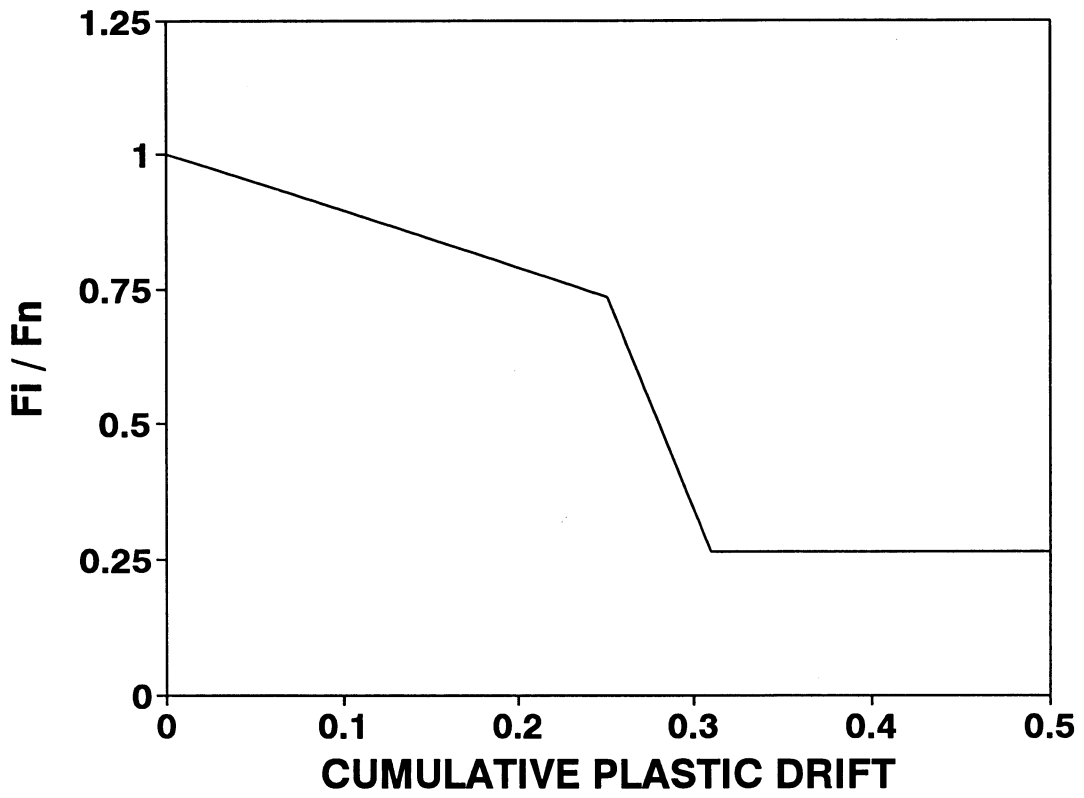
Figure 3-5 Energy Based Strength Deterioration Model Applied to the Illustrative Bridge
Pier Example.

SECTION 4
LAP SPLICE ZONE BOND FAILURE

4.1 INTRODUCTION

A lapped splice transfers force from one bar to another through the concrete surrounding both the bars. At any point in the splice, forces are transferred by bond from the bar to the concrete and simultaneously from the concrete to the bar also by bond. Figure 4-1 shows such splitting cracks for circular and rectangular sections. This section presents a theory that analyses the failure of bond in the lap splice zone and goes on to give a numerical example.

4.2 THEORETICAL DEVELOPMENT

The theoretical model developed for failure due to loss of bond in the anchorages can be adapted for failures dictated by the loss of bond in lapped splices as well. However realizing that for failures in the lapped splice zone, the longitudinal reinforcement shears a portion of the concrete during pull-out, an appropriate model is required for determination of $\Sigma\theta_{PB}$. An energy based formulation as before can be used where the external work done is equated to the internal energy absorption capacity of the sheared concrete surface. Thus,

$$EWD = IWD \tag{4-1}$$

$$\Delta M_s \, \xi \, \Sigma\theta_{PB} = \left[\pi(D'-d_b) + 2n\left(d' + \frac{d_b}{2}\right) \right] L_{sp} G_f \tag{4-2}$$

in which ΔM_s = moment contribution of the longitudinal reinforcement relying on adhesive bond, n = Number of longitudinal bars in the column, d' = effective cover (as shown in figure 4-1), d_b = diameter of the longitudinal reinforcing bars, ξ = proportion of the column drift arising from loss of bond in the lapped splice to the total column rotation = 1.0 , D' = pitch circle diameter, L_{sp} = length of the lapped splice and G_f = energy per unit area of the cracked surface. Note that the term in the right hand side of the equation 4-2 in square brackets denote the total surface length of the crack.

49
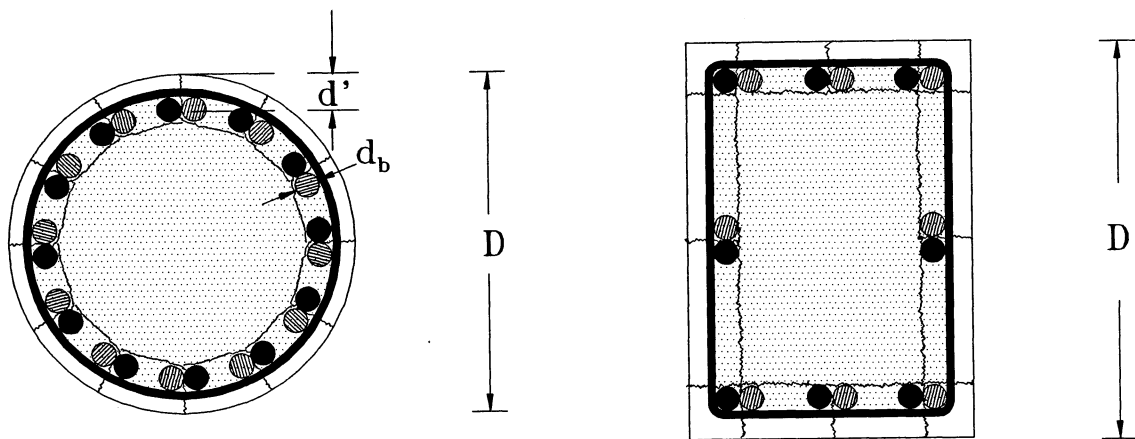
Figure 4-1 Splitting Cracks in Circular and Rectangular Column Sections.

The evaluation of the energy per unit area of the cracked surface (G_f) requires an appropriate model. According to Morcos and Bjorhovde (1995), G_f can be expressed as

$$G_f = 0.23664 \, \varepsilon_0 \, h f_t \qquad (4-3)$$

where ε_0 = ultimate strain in the tensile softening curve for concrete ≈ 0.002, f_t = tensile strength of concrete $\approx 0.1 f'_c$ and h was determined by Bazant and Oh (1983) as three times the maximum aggregate size. Thus,

$$G_f = (0.23664)(0.002)(3a_g)(0.1f'_c) \approx 0.00014 f'_c a_g \qquad (4-4)$$

where f'_c = unconfined compression strength of concrete and a_g = maximum aggregate size. Combining equations (4-3) and (4-4) the cumulative plastic drift at incipient lap splice failure $\Sigma \theta_{PB}$ can be expressed as

$$\Sigma \theta_{PB} = \frac{\left[\pi (D' - d_b) + 2n \left(d' + \frac{d_b}{2} \right) \right] L_{sp} (0.00014 f'_c a_g)}{\Delta M_s} \qquad (4-5)$$

Using the same convention as for anchorage zone failure, the strength just prior to lap splice failure is given by

$$\frac{F_1}{F_n} = 1 - \frac{M_c}{M_n} \frac{\Sigma \theta_{PB}}{\Sigma \theta_{PC}} \qquad (4-6)$$

and the force one cycle after the lap splice failure

$$\frac{F_2}{F_n} = \frac{F_1}{F_n} - \frac{\Delta M_s}{M_n} \qquad (4-7)$$

Following the lap splice failure, the concrete continues to decay as per

$$\frac{F_i}{F_n} = \frac{F_2}{F_n} - \frac{M_c}{M_n} \frac{\left(\Sigma \theta_{pi} - \overline{\Sigma \theta_{PB} + 2 \theta_p} \right)}{\Sigma \theta_{PC}} \qquad (4-8)$$

until the rocking strength F_r (refer section 3.2) is obtained at cumulative plastic drift given by

$$\Sigma \theta_{PR} = \overline{\Sigma \theta_{PB} + 2 \theta_p} + \frac{\Sigma \theta_{PC}}{M_c / M_n} \left(\frac{F_2}{F_n} - \frac{F_r}{F_n} \right) \qquad (4-9)$$

4.2.1 Summary of Damage Evaluation Procedure

Step 1.   Determine the neutral axis depth ratio c/D. For rectangular sections, use equation (2-23):

$$\left(\frac{c}{D}\right) = \frac{\left(\frac{P_e}{f_c' A_g}\right) + \left(\frac{\gamma\, \rho_t f_y/f_c'}{1-2d'/D}\right)}{\left(\alpha\beta + \frac{2\gamma\, \rho_t f_y/f_c'}{1-2d'/D}\right)} \tag{LS-1a}$$

and for circular sections, use equation (2-31):

$$\frac{c}{D} = \frac{1}{\beta}\left[\frac{\dfrac{P_e}{f_c' A_g} + 0.5\,\rho_t \dfrac{f_y}{f_c'}\left(\dfrac{1-2c/D}{1-2d'/D}\right)}{1.32\,\alpha}\right]^{0.725} \tag{LS-1b}$$

Step 2.   Determine the concrete compression force ratio $C_c/f_c' A_g$. For rectangular sections, equation (2-16):

$$\left(\frac{C_c}{f_c' A_g}\right) = \alpha\beta\left(\frac{c}{D}\right) \tag{LS-2a}$$

and for circular sections, use equation (2-23):

$$\frac{C_c}{f_c' A_g} = 1.32\,\alpha\left(\beta\ \frac{c}{D}\right)^{1.38} \tag{LS-2b}$$

Step 3.   Determine the equivalent plastic hinge length L_p using equation (2-9):

$$L_p = 0.08L + 4400\,\varepsilon_y d_b \tag{LS-3}$$

Step 4.   Determine the cumulative plastic drift capacity $\Sigma\theta_{PC}$ using equation (2-10):

$$\Sigma\theta_{PC} = \frac{0.016\,(L_p/D)}{\left(\dfrac{C_c}{f_c'\,A_g}\right)\!\left(\dfrac{c}{D}\right)}$$ (LS-4)

Step 5.   Determine the component of the moment contributed by the eccentric concrete stress block M_c. For rectangular sections use equation (2-13):

$$M_c = 0.5C_c D\left(1 - \frac{\beta c}{D}\right)$$ (LS-5a)

and for circular sections, use equation (2-14):

$$M_c = 0.5C_c D\left(1 - 1.2\,\beta\,\frac{c}{D}\right)$$ (LS-5b)

Step 6.   Determine the residual bond stress f_{rb} (equation 3-33), strength loss ratio after lap splice failure $\Delta M_s/M_n$ (equation 3-4) and the energy per unit area of cracked surface G_f using equation (4-4)

$$f_{rb} = \frac{\mu_b\,\pi d_b\,l_{em}\,\rho_s f_{yh}}{2A_b} = 2\mu_b\,\rho_s f_{yh}\,\frac{l_{em}}{d_b}$$ (LS-6a)

$$\frac{\Delta M_s}{M_n} = \left(1 - \frac{f_{rb}}{f_y}\right)\!\left(1 - \frac{M_c}{M_n}\right)$$ (LS-6b)

$$G_f = 0.00014 f_c'\,a_g$$ (LS-6c)

Step 7.   Determine the cumulative plastic drift at incipient lap splice failure $\Sigma\theta_{PB}$ using equation (4-5):

$$\Sigma\theta_{PB} = \frac{\left[\pi(D'-d_b) + 2n\left(d' + \dfrac{d_b}{2}\right)\right]L_{sp}(0.00014f_c'a_g)}{\Delta M_s}$$ (LS-7)

Step 8.   Determine the strength ratio at incipient lap splice failure F_1/F_n using equation (4-6):

$$\frac{F_1}{F_n} = 1 - \frac{M_c}{M_n} \frac{\Sigma\theta_{PB}}{\Sigma\theta_{PC}} \tag{LS-8}$$

Step 9.   Determine the strength ratio immediately after lap splice failure F_2/F_n using equation (4-7):

$$\frac{F_2}{F_n} = \frac{F_1}{F_n} - \frac{\Delta M_s}{M_n} \tag{LS-9}$$

Step 10.   Determine rocking strength F_r using the lesser of

$$F_{sliding} = \mu_s W \tag{LS-10a}$$

or

$$F_{rocking} = \frac{\Sigma M_r}{H} = \frac{\Sigma (M_c' + M_s')}{H} \tag{LS-10b}$$

Step 11.   Determine the cumulative plastic drift capacity at which rocking commences $\Sigma\theta_{PR}$ using equation (4-9):

$$\Sigma\theta_{PR} = \overline{\Sigma\theta_{PB} + 2\theta_p} + \frac{\Sigma\theta_{PC}}{M_c/M_n}\left(\frac{F_2}{F_n} - \frac{F_r}{F_n}\right) \tag{LS-11}$$

Step 12.   Determine relationship between nominal strength and cumulative plastic drift in the form

$$\frac{F_i}{F_n} = 1 - C\Sigma\theta_{pi} \tag{LS-12}$$

The conceptual damage analysis model is shown graphically in figure 4-2.
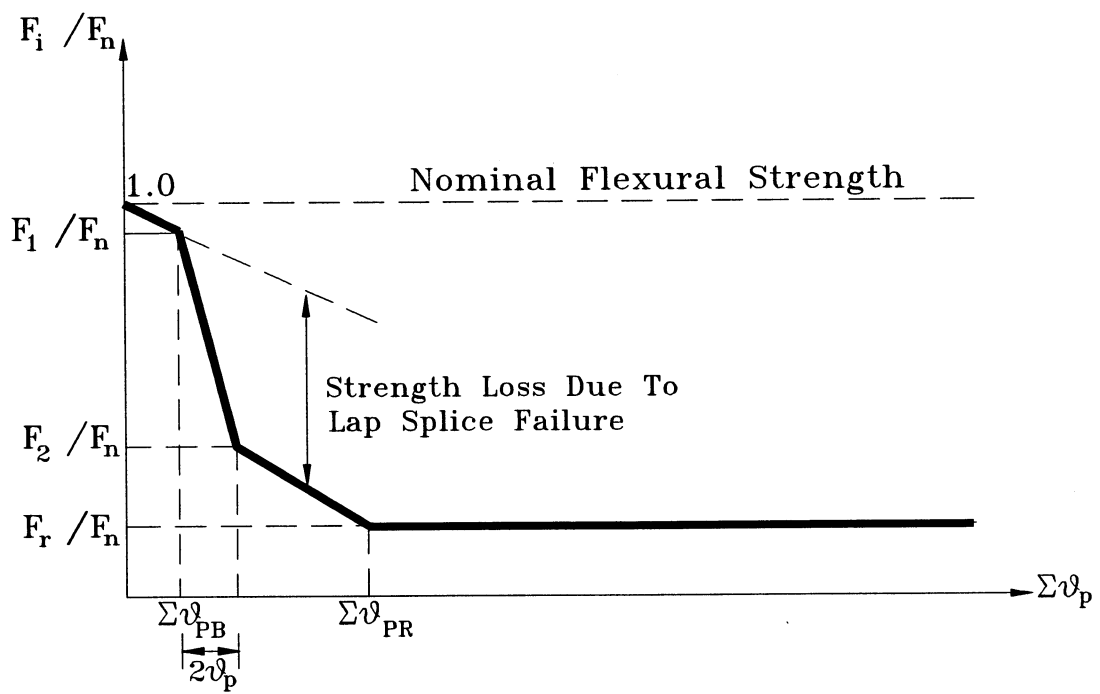
Figure 4-2 Conceptual Energy Based Lateral Force Vs. Cumulative Drift Damage Model for Piers Governed by Lap Splice and Concrete Failure.

55

4.3 NUMERICAL EXAMPLE

As before, a numerical example can be used to illustrate the energy-based fatigue model. The same column as Section 2.3 is chosen for the purpose. However, a lap spliced length of 580 mm ($\approx 20d_b$) is provided at the junction of the column and foundation. Failure is assumed to occur at this location. Relevant details are shown in figure 4-3.
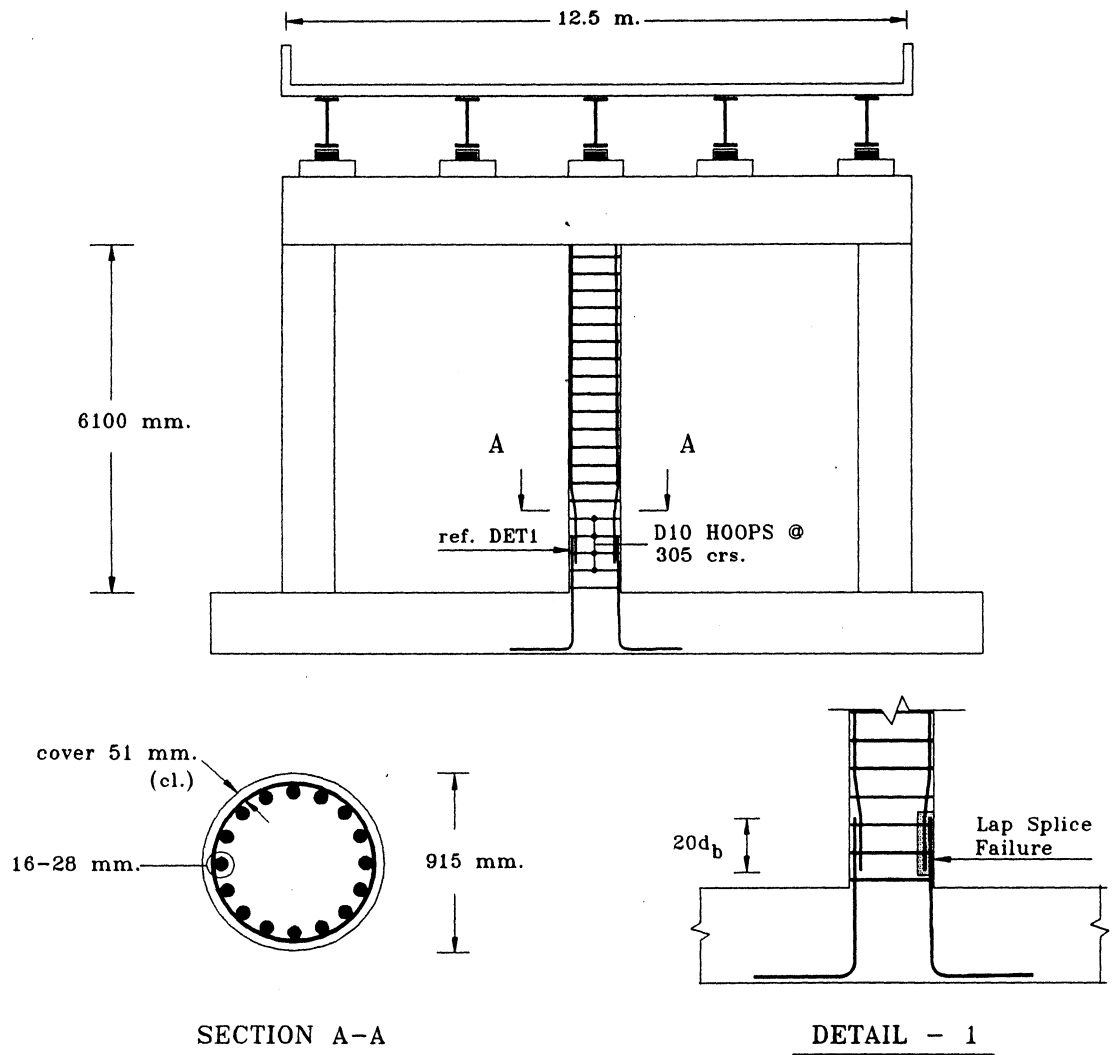
Figure 4-3 Illustrative Bridge Pier used in the Numerical Example.

<u>Carried over parameters</u>

Unconfined concrete compression strength $f_c = 45$ MPa.

Diameter of the section $D = 915$ mm.

Effective cover $d' = 75$ mm.

Core diameter $D'' = 803$ mm.

Plastic hinge length ratio $\dfrac{L_p}{D} = 0.4888$

Neutral axis depth ratio $cD_{rat} = 0.2071$

Concrete compression force ratio $\dfrac{C_c}{f_c \cdot A_g} = 0.0784$

Cumulative plastic drift capacity considering concrete damage $\Sigma\theta_{PC} = 0.4816$ rad.

Normalized concrete moment ratio $\dfrac{M_c}{f_c \cdot A_g \cdot D} = 0.031$

Ratio of concrete to nominal moment $\dfrac{M_c}{M_n} = 0.5084$

These values are obtained from Section 2.3 and correspond to Steps 1 through 5.

Also provided lap length $l_{sp} := 560$ mm.

6. <u>Residual bond stress in the rebar</u>

Volumetric ratio of lateral reinforcement $\rho_s := \dfrac{\pi \cdot d_{bh}^2}{D'' \cdot s}$ -----> $\rho_s = 0.0013$

Consider coefficient of friction $\mu_b := 0.5$

For rebars passively confined by transverse hoop reinforcement that produces triaxial confinement, the residual bond stress is given by

$$f_{rb} := 2 \cdot \mu_b \cdot \rho_s \cdot f_{yh} \cdot \dfrac{l_{sp}}{d_b} \quad \text{-------} \quad f_{rb} = 8.466 \quad \text{MPa.} \text{-------} \quad \dfrac{f_{rb}}{f_y} = 0.0257$$

Loss in moment capacity due to lap splice failure

$$\Delta M_s := M_n \cdot \left(1 - \frac{f_{rb}}{f_y}\right) \cdot \left(1 - \frac{M_c}{M_n}\right) \quad ----\!> \quad \Delta M_s = 7.9025 \cdot 10^8 \qquad \text{N-mm.}$$

and hence the ratio $\quad \dfrac{\Delta M_s}{M_n} = 0.4789$

Work done to completely break the adhesive bond

Assuming maximum aggregrate size $\quad a_g := 25.4 \quad$ mm.

$$G_f := 0.00014 \cdot f'_c \cdot a_g \qquad\qquad ------\!> \quad G_f = 0.16 \qquad\qquad \text{N/mm}^2\text{-mm}$$

7. Cumulative drift necessary to cause anchorage bond failure

Pitch circle diameter $\quad D' := D - 2 \cdot \left(cov + d_{bh} + 0.5 \cdot d_b\right) \quad ---\!> \quad D' = 765 \qquad$ mm

Cumulative drift necessary to cause anchorage bond failure

$$\Sigma\theta_{PB} := \frac{\left[\pi \cdot \left(D' - d_b\right) + 2 \cdot n \cdot \left(d' + 0.5 \cdot d_b\right)\right] \cdot l_{sp} \cdot G_f}{\Delta M_s}$$

$$------\!> \quad \Sigma\theta_{PB} = 5.855 \cdot 10^{-4} \quad \text{rad.}$$

8. Force just prior to bond failure

Nominal force capacity $\quad F_n := \dfrac{2 \cdot M_n}{H}$

$$F_1 := F_n \cdot \left(1 - \frac{M_c}{M_n} \cdot \frac{\Sigma\theta_{PB}}{\Sigma\theta_{PC}}\right) \qquad ------\!> \qquad \frac{F_1}{F_n} = 0.9994$$

9. Force one cycle after anchorage-bond failure

$$F_2 := F_n \cdot \left(\frac{F_1}{F_n} - \frac{\Delta M_s}{M_n}\right) \qquad -------\!> \qquad \frac{F_2}{F_n} = 0.5204$$

58

10. Residual rocking strength

Residual rocking strength is given by the lesser of the sliding and rocking strength. Assuming a coefficient of sliding friction

$$\mu_s := 0.7 \qquad ; \qquad W := P_{rat} \cdot f_c \cdot A_g$$

$$F_{sliding} := \mu_s \cdot W \qquad \text{------>} \qquad F_{sliding} = 8.2852 \cdot 10^5 \quad \text{N.}$$

Calculation of rocking strength:

Let the c"/D" ratio be denoted by $c"_{rat}$. As an initial value of this quadratic assume

$$c"_{rat} := 0.2 \qquad \text{Also} \quad \alpha := 0.3 \quad \text{and} \quad d" := 0.5 \cdot \left(d_{bh} + d_b \right)$$

$$c"D"_{rat} := \text{root} \left[\left[\frac{P_{rat} + 0.5 \cdot \rho_t \cdot \dfrac{f_{rb}}{f_c} \cdot \dfrac{1 - 2 \cdot c"_{rat}}{1 - 2 \cdot \dfrac{d"}{D"}}}{1.32 \cdot \alpha \cdot \dfrac{D"^2}{D^2}} \right]^{0.725} - c"_{rat}, c"_{rat} \right]$$

$$c"D"_{rat} = 0.132$$

Modified concrete compression force $\qquad C_{cc} := 1.32 \cdot \alpha \cdot \left(c"D"_{rat} \right)^{1.38} \cdot f_c \cdot A_{cc}$

Hence, $\qquad M'_c := 0.5 \cdot C_{cc} \cdot D" \cdot \left(1 - 1.2 \cdot c"D"_{rat} \right) \quad \text{---->} \quad M'_c = 4.1025 \cdot 10^8 \qquad \text{N-mm.}$

Also for $\qquad A_{st} := \rho_t \cdot A_g \qquad \text{----->} \qquad A_{st} = 9.852 \cdot 10^3 \qquad \text{mm}^2$

$$M'_{s1} := 0.25 \cdot A_{st} \cdot f_{rb} \cdot D" \cdot \left(1 - 2 \cdot \frac{d"}{D"} \right) \qquad \text{and}$$

$$M'_{s2} := 0.5 \cdot A_{st} \cdot f_{rb} \cdot D" \cdot \left(1 - c"D"_{rat} - \frac{d"}{D"} \right) \cdot \frac{c"D"_{rat} - \dfrac{d"}{D"}}{1 - 2 \cdot \dfrac{d"}{D"}}$$

Thus, $M'_s := M'_{s1} + M'_{s2}$ --------> $M'_s = 1.9167 \cdot 10^7$ N-mm.

Hence, $F_{rocking} := \left(\dfrac{M'_c + M'_s}{0.5 \cdot H} \right)$ -----> $F_{rocking} = 1.4079 \cdot 10^5$ N.

Normalized rocking strength $\dfrac{F_{rocking}}{F_n} = 0.2603$

11. <u>Cumulative plastic drift at the onset of residual rocking</u>

Assume the lap splice failure is complete at a plastic drift level of $\theta_p := 0.02$ rad.

$$\Sigma\theta_{PR} := \left(\Sigma\theta_{PB} + 2 \cdot \theta_p \right) + \dfrac{\Sigma\theta_{PC}}{\left(\dfrac{M_c}{M_n} \right)} \cdot \left(\dfrac{F_2}{F_n} - \dfrac{F_{rocking}}{F_n} \right)$$ ------> $\Sigma\theta_{PR} = 0.287$ rad.

These values are plotted in figure 4-4.
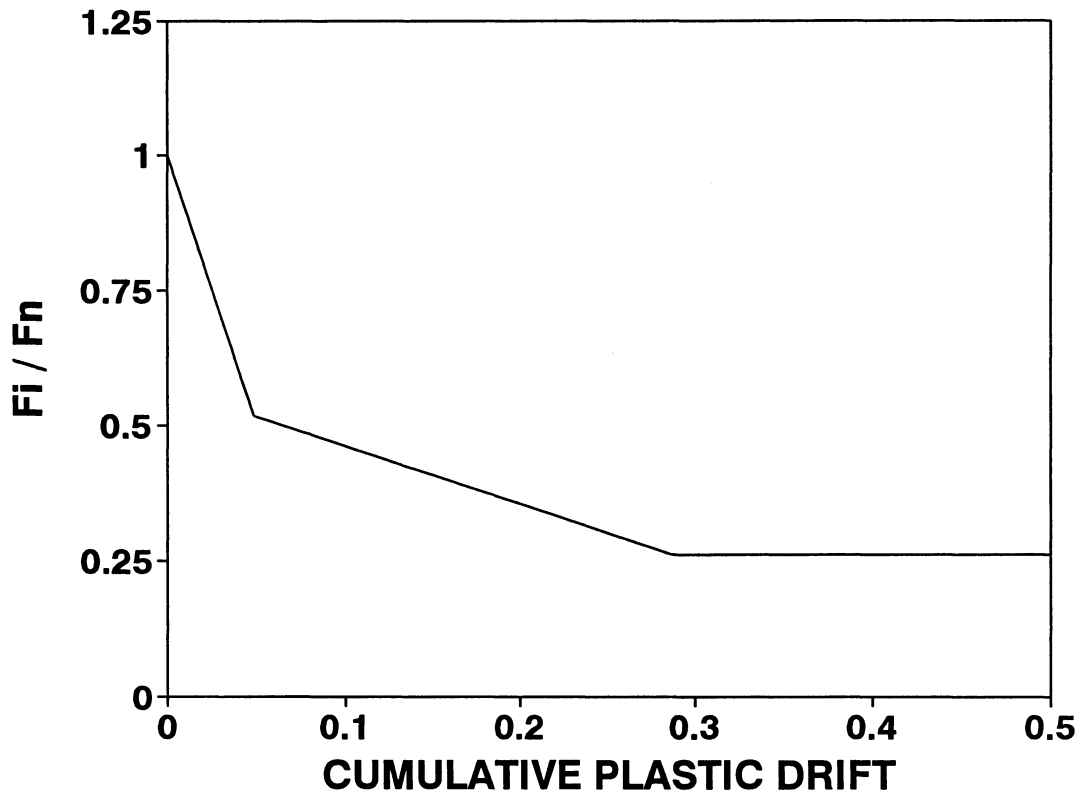
Figure 4-4 Energy Based Strength Deterioration Model Applied to the Illustrative Bridge Pier Example.

SECTION 5
COMPRESSION BUCKLING FAILURE OF LONGITUDINAL REINFORCING STEEL

5.1 BACKGROUND

Buckling of longitudinal reinforcement is a commonly reported mode of failure. If the spacing of the transverse hoops is not too large, then the compression steel may buckle inelastically under high compressive strains eventually leading to column instability. Bucking of the longitudinal reinforcement may either be a local or global phenomena. Local buckling is defined as double curvature buckling between two successive hoops. Global buckling may occur when there are many closely spaced hoops consisting of small diameter steel. One of these small transverse hoops has insufficient strength to restrain local buckling deformations, thus the longitudinal reinforcing bar is restrained by several hoops that traverse the longitudinal buckled bar. The former case is common for poorly detailed non-seismically designed columns, whereas the latter is possible in the seismic design of large diameter columns. Although a detailed analysis of both the buckling modes had been performed by Dutta and Mander (1997), this section restricts itself to analyzing the former case using excerpts from that research.

5.2 PLASTIC ANALYSIS APPROACH FOR SOLVING THE LOCAL BUCKLING PROBLEM

Consider a flexural reinforcement bar as shown in figure 5-1 fixed at the two ends. End reactions may consist of a moment, a horizontal shear force, and the applied axial load. However, shear force aids the buckling and hence the critical buckling condition is attained when $V = 0$. Focussing on the equilibrium of the quarter-length of the buckled bar, it can be stated that the lateral plastic displacement Δ_p will increase up to a point when the full plastic moment capacity will be mobilized at the base of the buckled bar. At this instant, the plastic moment capacity M_p corresponding to the critical ultimate load P_{cr} will equal the P-Δ moment at the base of the buckled bar which is distributed as shown in figure 5-1b. The plastic moment M_p has an associated plastic curvature Φ_p which is conceivably distributed in the form of a n-th degree parabolic curve as shown in figure 5-1c. Details of the derivation of the curvature shape is

(a) Local Buckling   (b) Moment   (c) Curvature
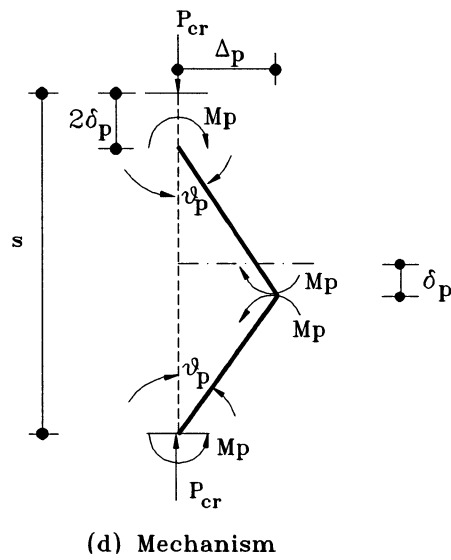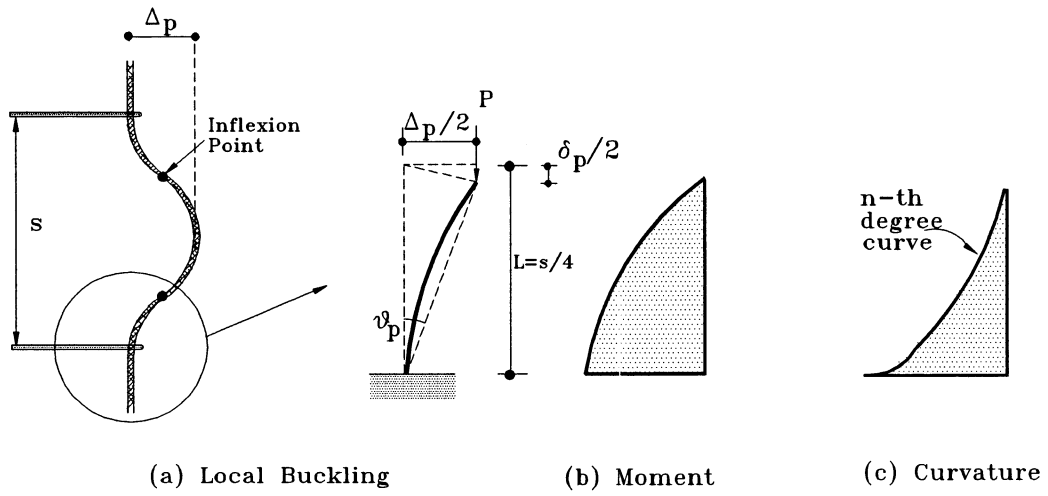
(d) Mechanism

Figure 5-1 Plastic Analysis of Local Buckling of Longitudinal Reinforcement.

given elsewhere (see Dutta and Mander, 1997). Postulating a rigid plastic mechanism whereby it is assumed that the resistance to the vertical load is entirely provided by the plastic moments that develop at the extremities a virtual work equation can be written as

$$EWD = IWD \qquad (5\text{-}1)$$

$$P_{cr} \cdot 2\,\delta_p = 4\,M_p\,\theta_{pb} \qquad (5\text{-}2)$$

$2\,\delta_p$ being the total downward movement of the axial load due to buckling and θ_{pb}, M_p are the plastic rotations and the plastic moments as shown in figure 5-1d. From geometry however,

$$\frac{\delta_p}{\Delta_p} = \tan\left(\frac{\theta_{pb}}{2}\right) \approx \frac{\theta_{pb}}{2} \quad (\textit{for small } \theta_{pb}) \qquad (5\text{-}3)$$

and

$$\frac{\Delta_p}{s/2} = \sin(\theta_{pb}) \approx \theta_{pb} \qquad (5\text{-}4)$$

Combining equations (5-3) and (5-4)

$$\delta_p = \frac{s}{4}\,\theta_{pb}^2 \qquad (5\text{-}5)$$

Substituting the expression for δ_p in equation (5-2) and on subsequent simplification

$$P_{cr} = \frac{8\,M_p}{s\,\theta_{pb}} \qquad (5\text{-}6)$$

Dividing both sides of the above equation by the area of cross section, the same equation can be written in terms of stresses as

$$f_{cr} = \frac{32}{\pi}\,\frac{M_p}{d_b^2\,s\,\theta_{pb}} \qquad (5\text{-}7)$$

However, it was shown by Dutta and Mander (1998), that the minimum buckling stress corresponds to the peak plastic moment M_{pp}. The maximum plastic moment M_{pp} depends upon the magnitude of the axial compression. For a particular critical ultimate load P_{cr}, the associated peak plastic moment can be obtained from the interaction diagram via a complete moment

65

curvature analysis that considers the strain-hardening effect of the steel. For nominal Grade 60 reinforcing steel it can be shown that the plastic moment is related to the critical stress by a simple expression

$$M_{pp} = M_{pu}\left[1 - \left(\frac{f_{cr}}{f_{su}}\right)^2\right]$$ (5-8)

where $M_{pu} = f_{su} d_b^3 / 6 =$ fully plastic ultimate moment for a circular section without any axial load and $f_{su} =$ ultimate stress in the longitudinal reinforcement. This expression gives an almost perfect match for Grade 60 reinforcement; some slight error is introduced when applying the formula to Grade 40 reinforcing steel and prestressing threadbars, but this error is minimal.

The average strain in the buckled bar can be expressed as

$$\varepsilon_{cr} = \frac{2\,\delta_p}{s}$$ (5-9)

where the axial displacement is given by equation (5-5). Combining equations (5-5), (5-7), (5-8) and (5-9) and simplifying one obtains

$$\varepsilon_{cr} = \frac{1.44}{(s/d_b)^2}\left(\frac{f_{su}}{f_{cr}}\right)^2\left[1 - \left(\frac{f_{cr}}{f_{su}}\right)^2\right]^2$$ (5-10)

From simulated laboratory tests on steel reinforcement, Mander et al. (1984) observed that specimens with high s/d_b ratios which is very common for poorly detailed column specimens, are still able to sustain yield stress. However, there is a rapid degradtion in strength soon after the strain exceeds the yield strain. Substituting $f_{cr} = f_y$ in the above equation

$$\varepsilon_{cr} = \frac{1.44}{(s/d_b)^2}\left(\frac{f_{su}}{f_y}\right)^2\left[1 - \left(\frac{f_y}{f_{su}}\right)^2\right]^2$$ (5-11)

For typical Grade 40 and Grade 60 reinforcement with $f_{su} \approx 1.5 f_y$, equation (5-11) can be further simplified to

$$\varepsilon_{cr} = \frac{1}{(s/d_b)^2} \tag{5-12}$$

In terms of dimensionless plastic curvature, from strain diagram, one obtains

$$\phi_p D = \frac{(\varepsilon_{cr} - \varepsilon_y)}{\left(\dfrac{c}{D} - \dfrac{d'}{D}\right)} \tag{5-13}$$

where ε_{cr} and the other symbols having their usual meaning.

It is to be noted that the dimensionless plastic curvature is independent of the number of cycles to failure.

5.2.1 Summary of Fatigue Evaluation Procedure

Step 1.   Determine the neutral axis depth c/D. For rectangular sections, use equation (2-23):

$$\left(\frac{c}{D}\right) = \frac{\left(\frac{P_e}{f_c' A_g}\right) + \left(\frac{\gamma \, \rho_t f_y / f_c'}{1 - 2 \, d'/D}\right)}{\left(\alpha\beta + \frac{2\gamma \, \rho_t f_y / f_c'}{1 - 2 \, d'/D}\right)} \tag{CB-1a}$$

and for circular sections, use equation (2-31):

$$\frac{c}{D} = \frac{1}{\beta}\left[\frac{\frac{P_e}{f_c' A_g} + 0.5\,\rho_t \frac{f_y}{f_c'}\left(\frac{1-2c/D}{1-2\,d'/D}\right)}{1.32\,\alpha}\right]^{0.725} \tag{CB-1b}$$

Step 2.   Determine the critical buckling strain ε_{cr} using equation (5-12):

$$\varepsilon_{cr} = \frac{1}{(s/d_b)^2} \tag{CB-2}$$

Step 3.   Determine the maximum dimensionless plastic curvature from equation (5-13):

$$\phi_p D = \frac{(\varepsilon_{cr} - \varepsilon_y)}{\left(\frac{c}{D} - \frac{d'}{D}\right)} \tag{CB-3}$$

5.3 Numerical Example

A numerical example is also presented in this section to illustrate the working procedure. The illustrative pier bent chosen for this purpose is the same as was used in section 2.3. Hence details of the calculation are not reproduced.

The neutral axis depth ratio c/D as obtained from section 2.3 is 0.2071. For the specimen with the longitudinal bar diameter of $28\ mm$ and spacing of $s = 305\ mm$, the critical strain as given by equation (5-12) is 0.0085. Finally using equation (5-13) the dimensionless plastic curvature is 0.054. This is plotted in figure 5-2.
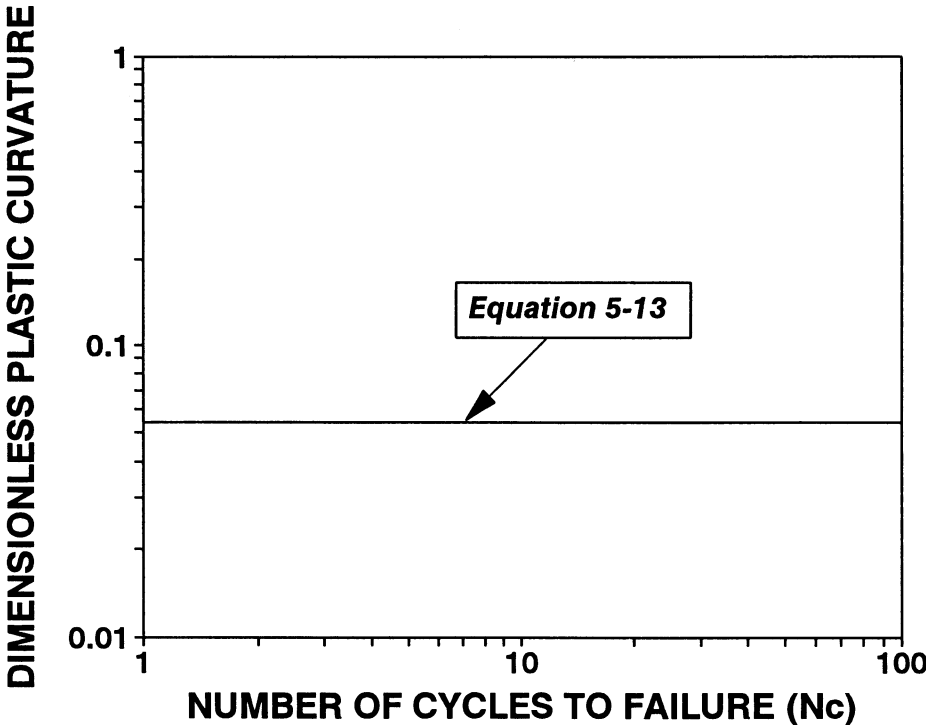
Figure 5-2   Fatigue Plot for the Illustrative Pier Example governed by Longitudinal Bar Buckling.

69

SECTION 6

LOW CYCLE FATIGUE OF
LONGITUDINAL REINFORCEMENT

6.1 BACKGROUND

Highway structures, such as pavements and bridges, generally experience several million load reversals over their normal service life. It is thus desirable that working stress reversals are kept below the fatigue limit in order to keep the structure functioning indefinitely. Under seismic loads, however, it is not economically feasible to keep steel strains below the yield strain, let alone the fatigue limit strain. Thus during earthquakes, longitudinal reinforcing steel in potential plastic hinge zones may experience large strains that could eventually lead to low cycle fatigue failure. If the duration of strong ground shaking is long enough, and/or in conjunction with strong after shocks, such a failure is inevitable.

6.2 FATIGUE FAILURE THEORY OF STEEL REINFORCEMENT

In a recent study on the low cycle fatigue behavior of reinforcing steel, Mander et al. (1994) showed that the _plastic_ strain amplitude (ε_{ap}) is given in terms of the fatigue life (N_f cycles to failure) by the relation

$$\varepsilon_{ap} = 0.08(2N_f)^{-0.5} \tag{6-1}$$

and a re-plot of the results given by Mander et al. (1994) in terms of the total strain amplitude gives a simple relation in the form

$$\varepsilon_a = 0.08(2N_f)^{-0.333} \tag{6-2}$$

where $2N_f$ = number of reversals to the appearance of first fatigue crack, ε_a = total strain and ε_{ap} = plastic strain at the level of reinforcing bar. This result is plotted with experimental results from low cycle fatigue tests on two types of reinforcing steel in figure 6-1.

71
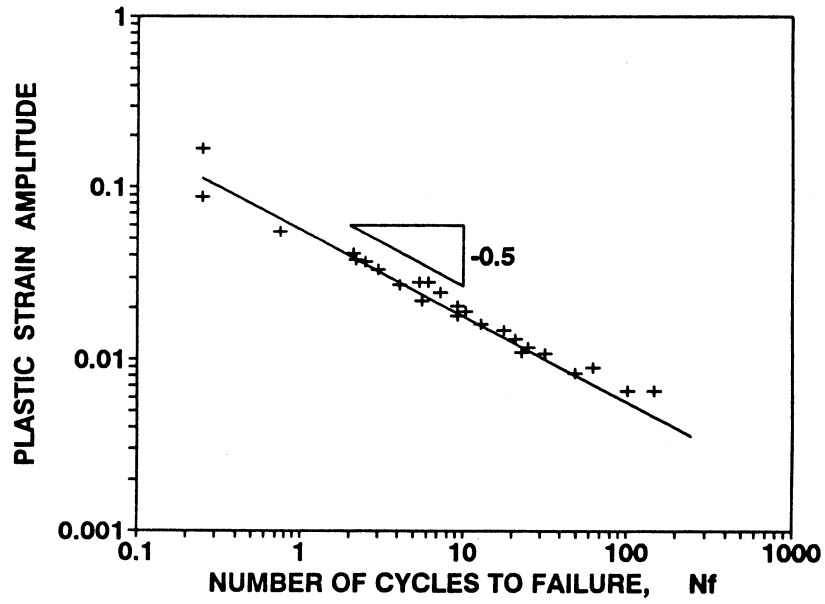
(a) Coffin-Manson Plastic Strain-Life Model
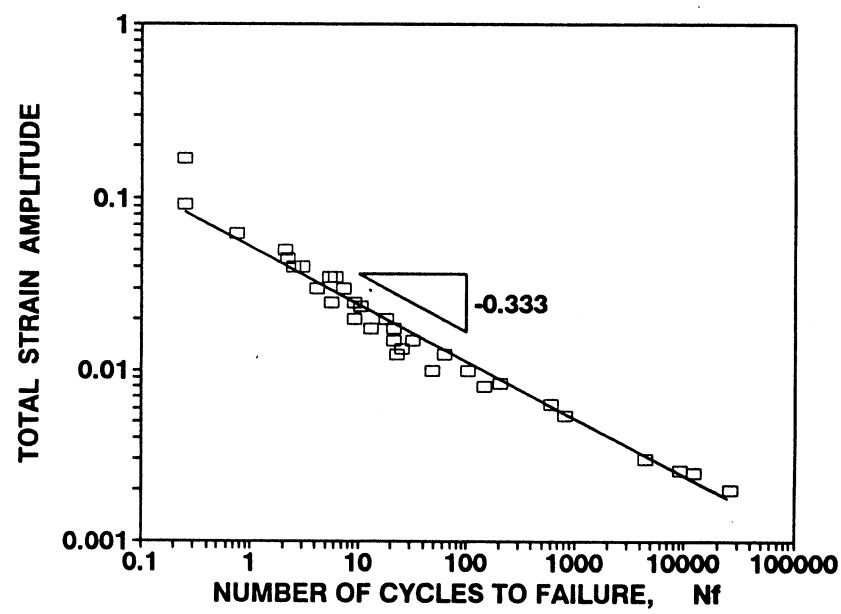
(b) Koh-Stephens Total Strain-Life Model

Figure 6-1 Fatigue Life of Reinforcing Steel based on the results of Mander et al.(1994).

It is possible to transform the low cycle fatigue behavior of individual rebars into familiar fatigue expressions for concrete columns. Consider the strain diagram shown in figure 6-2. Through geometry an equation can be derived which relates the total plastic strain range $(2\varepsilon_{ap})$ with the dimensionless plastic curvature of the section $(\phi_p D)$:

$$2\varepsilon_{ap} = \phi_p D \left(1 - \frac{2d'}{D}\right) \tag{6-3}$$

where D = overall depth (diameter) of the section and d' = distance from the top of the section to the centroid of the nearest longitudinal reinforcing bar.

Substituting equation (6-1) into (6-2) one obtains an expression relating the dimensionless plastic curvature $(\phi_p D)$ with the number of cycles (N_f):

$$\phi_p D = \frac{0.16}{1 - 2d'/D} \cdot (2N_f)^{-0.5} \tag{6-4}$$

Note that $1 - 2d'/D$ is the ratio of the pitch circle diameter of the longitudinal steel for a circular column or the ratio of the depth between outer layers of longitudinal rebars to the overall depth of a rectangular column. Alternatively, if the equivalent plastic hinge length (L_p) is known then this expression can be written relating plastic rotation (θ_p) and cycles to failure (N_f)

$$\theta_p = 0.16 \frac{L_p}{D'} \cdot (2N_f)^{-0.5} \tag{6-5}$$

where $D' = D - 2d'$ = pitch circle diameter, L_p = equivalent plastic hinge length given by equation (2-9).

However, realizing that a fracture of the longitudinal reinforcement merely causes a finite drop in the moment capacity contributed by steel (M_s), the energy-based strength deterioration model proposed in section 2 can be adapted to quantify the decay in the lateral strength capacity for failure modes governed by low cycle fatigue of the longitudinal reinforcement as well. This is discussed in what follows.

73

6.2.1 Deterioration in Steel Moment Capacity

The deterioration of the steel moment capacity depends on the geometrical shape of the section. Two specific cases — one for rectangular and the other for circular section are considered.

(a) *Rectangular Section*: The same assumptions used for the derivation of neutral axis depth (section 2.2.3) are used. Thus γA_{st} part of the longitudinal steel is assumed to be distributed in the form of a thin strip over a depth D' of thickness given by equation (2-19). When the plastic strain amplitude at a certain level exceeds the value given by equation (6-1), the portion of the longitudinal steel above that level over a depth $\Delta D'$ (henceforth referred to as the loss depth) loses it's moment capacity. This causes an instantaneous change in the pitch circle diameter and hence equation (6-5) can be modified as

$$\theta_p = 0.16 \frac{L_p}{D' - \Delta D'} \cdot (2N_f)^{-0.5} \tag{6-6}$$

Multiplying both sides by $2N_f$ gives

$$\Sigma \theta_p = 2N_f \theta_p = 0.16 \left(\frac{L_p}{D' - \Delta D'} \right)(2N_f)^{0.5} \tag{6-7}$$

from which $\Delta D'$ can be solved as

$$\frac{\Delta D'}{D'} = 0.5 - 0.08 \frac{L_p / D'}{\sqrt{\theta_p \Sigma \theta_p}} \tag{6-8}$$

The strength loss ratio can be computed in terms of the moment capacity as follows:

$$\frac{\Delta M_s}{M_n} = \frac{\Delta D'}{D'} \cdot \frac{\gamma A_{st} f_y D'}{M_n} \cdot \left(1 - \frac{\Delta D'}{D'} \right) \tag{6-9}$$

(b) *Circular Section*: Assuming that in a circular section, the total longitudinal steel is distributed in the form of a tube of diameter D' (figure 6-2), and thickness given by

74

$$t = \frac{A_{st}}{\pi D'}$$
(6-10)

the length along the arc of the steel ring in that region is found to be given by

$$Arc\ Length = 0.7\ \pi\ D'\left(\frac{\Delta D'}{D'}\right)^{0.53}$$
(6-11)

which is valid for $\Delta D'/D' \leq 0.5$ as shown in figure 6-3. As a bar fractures, there is an instantaneous drop in the steel component of the moment capacity ΔM_s. Expressing this as the ratio of the nominal moment, this is given by

$$\frac{\Delta M_s}{M_n} = 0.7\ \frac{A_{st}f_y D'}{M_n}\cdot\left(\frac{\Delta D'}{D'}\right)^{0.53}\cdot\left(1 - 0.7\frac{\Delta D'}{D'}\right)$$
(6-12)

with the assumption that the centroid of the ring of depth $\Delta D'$ is at $0.35\,\Delta D'$ from the top.

The concrete portion of the moment capacity (M_c), also decays according to equation (2-12) till the rocking strength (F_r) as given by the lesser of equation (3-9) or (3-16) is attained. However, rocking strength $F_{rocking}$ should be evaluated for $f_{rb} = 0$. Hence for rectangular sections

$$M_c' = 0.5\,P_e D''\left(1 - \frac{c''}{D''}\right)$$
(6-13)

with

$$\frac{c''}{D''} = \frac{P_e}{0.3\,f_c'A_{cc}}$$
(6-14)

and for circular sections

$$M_c' = 0.5\,P_e D''\left(1 - 1.2\,\frac{c''}{D''}\right)$$
(6-15)

with

$$\frac{c''}{D''} = \left(\frac{P_e}{0.396\,f_c'A_{cc}}\right)^{0.725}$$
(6-16)
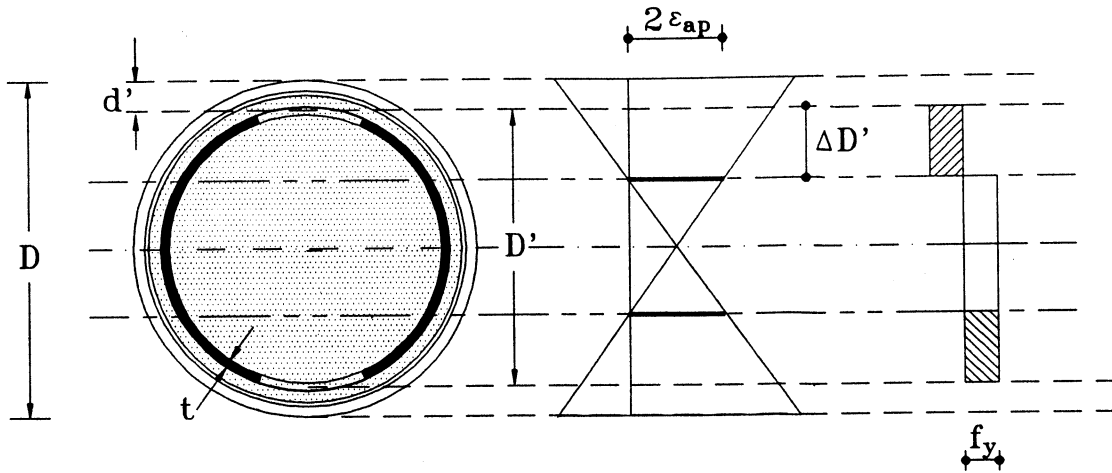
Figure 6-2 Decay in the Steel Component of the Moment Capacity.
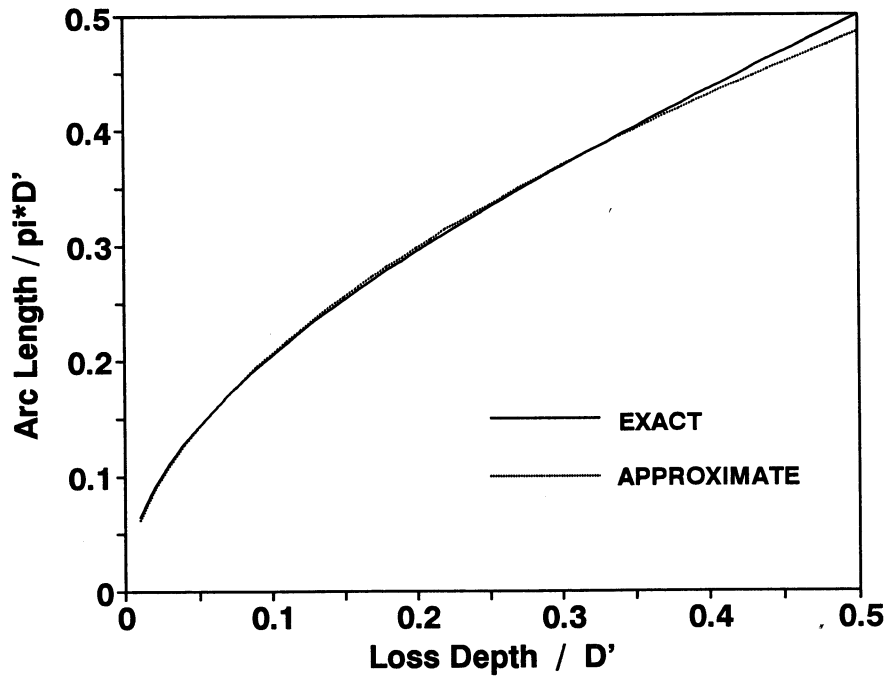
Figure 6-3 Relationship between Arc Length and Loss Depth.

6.2.2 Summary of Damage Evaluation Procedure

Step 1.   Determine the plastic hinge length L_p using equation (2-9):

$$L_p = 0.08L + 4400 \, \varepsilon_y d_b \qquad \text{(FF-1)}$$

Step 2.   Determine the current cumulative plastic drift $\Sigma \theta_{pi}$

Step 3.   Determine the loss depth ratio $\Delta D'/D'$ using equation (6-8):

$$\frac{\Delta D'}{D'} = 0.5 - 0.08 \frac{L_p/D'}{\sqrt{\theta_p \Sigma \theta_p}} \qquad \text{(FF-3)}$$

Step 4.   Determine the steel moment loss ratio $\Delta M_{si}/M_n$. For rectangular sections use equation (6-9):

$$\frac{\Delta M_s}{M_n} = \frac{\Delta D'}{D'} \cdot \frac{\gamma A_{st} f_y D'}{M_n} \cdot \left(1 - \frac{\Delta D'}{D'}\right) \qquad \text{(FF-4a)}$$

and for circular sections use equation (6-12):

$$\frac{\Delta M_s}{M_n} = 0.7 \frac{A_{st} f_y D'}{M_n} \cdot \left(\frac{\Delta D'}{D'}\right)^{0.53} \cdot \left(1 - 0.7 \frac{\Delta D'}{D'}\right) \qquad \text{(FF-4b)}$$

Step 5.   Describe the steel component of the lateral strength (F_s) in the form

$$\frac{F_{si}}{F_n} = \frac{M_s}{M_n} - \frac{\Delta M_{si}}{M_n} \qquad \text{(FF-5)}$$

Step 6.   Determine the neutral axis depth ratio c/D. For rectangular sections use equation (2-23):

$$\left(\frac{c}{D}\right) = \frac{\left(\frac{P_e}{f_c' A_g}\right) + \left(\frac{\gamma \, \rho_t f_y / f_c'}{1 - 2d'/D}\right)}{\left(\alpha \beta + \frac{2\gamma \, \rho_t f_y / f_c'}{1 - 2d'/D}\right)} \qquad \text{(FF-6a)}$$

and for circular sections use equation (2-31):

77

$$\frac{c}{D} = \frac{1}{\beta} \left[\frac{\dfrac{P_e}{f'_c A_g} + 0.5 \, \rho_t \, \dfrac{f_y}{f'_c} \left(\dfrac{1-2c/D}{1-2d'/D} \right)}{1.32 \, \alpha} \right]^{0.725}$$ (FF-6b)

Step 7.   Determine the concrete compression force ratio $C_c / f'_c A_g$. For rectangular sections use equation (2-16)

$$\left(\frac{C_c}{f'_c A_g} \right) = \alpha \beta \left(\frac{c}{D} \right)$$ (FF-7a)

and for circular sections use equation (2-28)

$$\frac{C_c}{f'_c A_g} = 1.32 \, \alpha \left(\beta \, \frac{c}{D} \right)^{1.38}$$ (FF-7b)

Step 8.   Determine the cumulative plastic drift capacity $\Sigma \theta_{PC}$ using equation (2-10)

$$\Sigma \theta_{PC} = \frac{0.016 \, (L_p / D)}{\left(\dfrac{C_c}{f'_c A_g} \right) \left(\dfrac{c}{D} \right)}$$ (FF-8)

Step 9.   Determine the component of the moment contributed by the eccentric concrete stress block M_c. For rectangular sections use equation (2-13)

$$M_c = 0.5 C_c D \left(1 - \beta \, \frac{c}{D} \right)$$ (FF-9a)

and for circular sections use equation (2-14)

$$M_c = 0.5 C_c D \left(1 - 1.2 \, \beta \, \frac{c}{D} \right)$$ (FF-9b)

Step 10.   Determine rocking strength F_r using the lesser of equations (3-9) and (3-16)

78

$$F_{sliding} = \mu_s W \qquad \text{(FF-10a)}$$

or

$$F_{rocking} = \frac{\Sigma M_c^/}{H} \qquad \text{(FF-10b)}$$

with $f_{rb} = 0$. For rectangular sections use equations (6-13) and (6-14):

$$M_c^/ = 0.5 P_e D^{//}\left(1 - \frac{c^{//}}{D^{//}}\right) \qquad \text{(FF-10c)}$$

with

$$\frac{c^{//}}{D^{//}} = \frac{P_e}{0.3 f_c^/ A_{cc}} \qquad \text{(FF-10d)}$$

and for circular sections use equations (6-15) and (6-16):

$$M_c^/ = 0.5 P_e D^{//}\left(1 - 1.2\frac{c^{//}}{D^{//}}\right) \qquad \text{(FF-10e)}$$

with

$$\frac{c^{//}}{D^{//}} = \left(\frac{P_e}{0.396 f_c^/ A_{cc}}\right)^{0.725} \qquad \text{(FF-10f)}$$

Step 11.   Describe the concrete component of the lateral strength (F_s) in the form

$$\frac{F_{ci}}{F_n} = \left(1 - \frac{M_c}{M_n}\frac{\Sigma \theta_{pi}}{\Sigma \theta_{PC}}\right) \not{*} \frac{F_r}{F_n} \qquad \text{(FF-11)}$$

Step 12.   Determine the net lateral strength given by

$$\frac{F_i}{F_n} = \frac{F_{si}}{F_n} + \frac{F_{ci}}{F_n} \qquad \text{(FF-12)}$$

79

6.3 Numerical Example

The low cycle fatigue analysis of longitudinal reinforcement explained so far can be illustrated with the aid of a numerical example. The same column used in the previous sections is analyzed for this purpose. Relevant junction details are shown in figure 6-4.
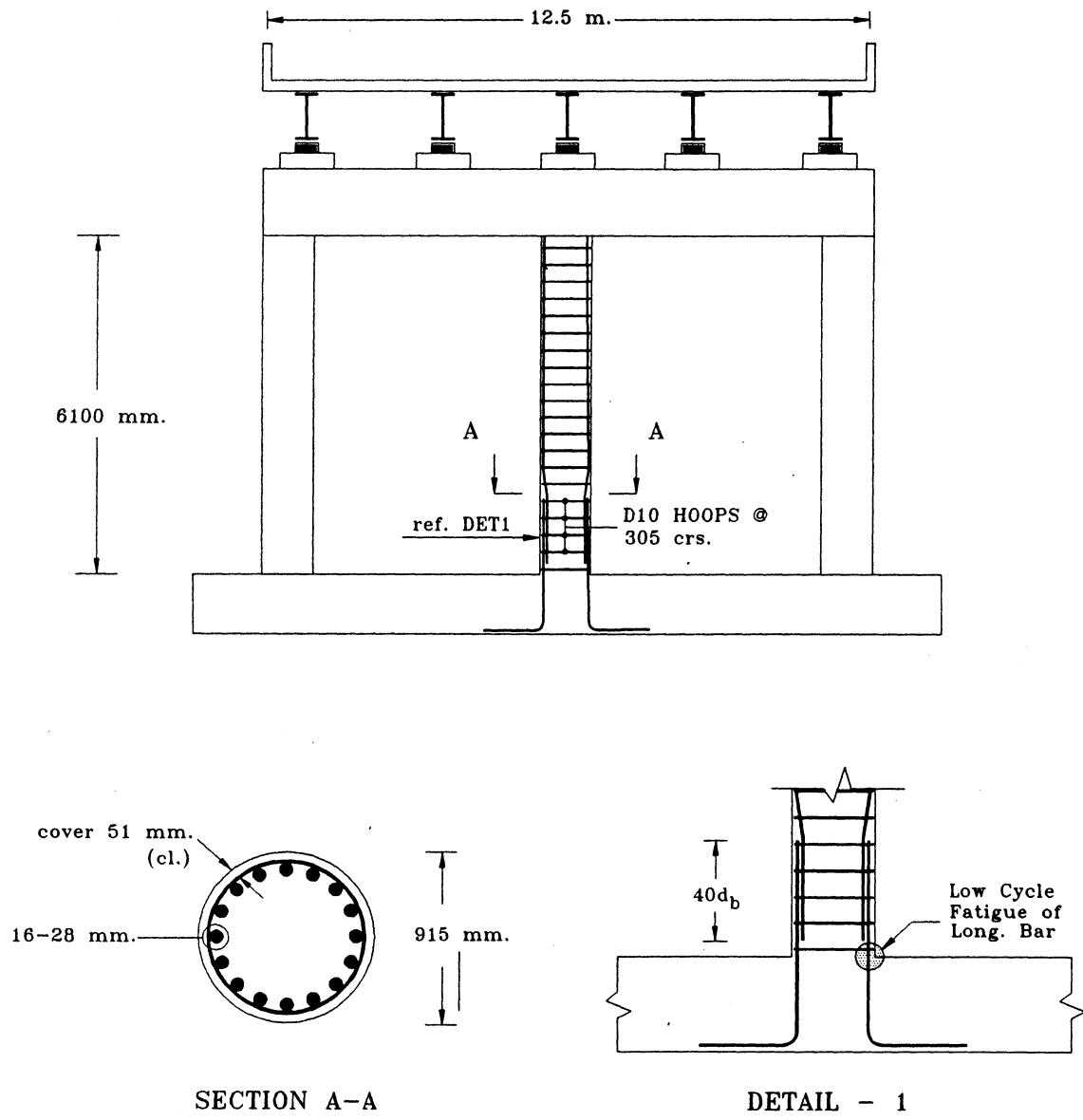
Figure 6-4 Illustrative Bridge Pier used in the Numerical Example.

Sample calculations for two data points are illustrated here. The yield rotation is assumed to be: $\theta_y = 0.0125$ rad.

1. Plastic hinge length

$$L_p = 0.08 \cdot \frac{H}{2} + 4400 \cdot \varepsilon_y \cdot d_b \quad \text{------>} \quad L_p = 447.28 \quad \text{mm.}$$

This value is same as obtained in Section 3.3

Case I: $\theta_i = 0.02$ rad. $\qquad N_f = 2$

2. Current cumulative plastic drift

$$\theta_{pi} = \theta_i - \theta_y \quad \text{------>} \quad \theta_{pi} = 0.0075 \quad \text{rad.}$$

$$\Sigma\theta_{pi} = 2 \cdot N_f \cdot \theta_{pi} \quad \text{------>} \quad \Sigma\theta_{pi} = 0.03 \quad \text{rad.}$$

3. Determine the loss depth ratio

Pitch circle diameter $\quad D' = D - 2 \cdot d' \quad \text{----->} \quad D' = 765 \quad \text{mm.}$

This value is same as obtained in Section 3.3

$$\Delta D' = 0.5 \cdot D' - \frac{0.08 \cdot L_p}{\sqrt{\theta_{pi} \cdot \Sigma\theta_{pi}}} \quad \text{------>} \quad \Delta D' = -2.003 \cdot 10^3 \quad \text{mm.}$$

Therefore, $\quad \dfrac{\Delta D'}{D'} = -2.6183$

4. Determine the steel moment loss ratio

The negative value of the loss depth ratio signifies that the longitudinal steel is yet to fracture and the steel moment capacity at the present drift level is still intact at

$$M_s = M_n \cdot \left(\frac{M_c}{M_n}\right) \quad \text{Hence,} \quad M_{si} = M_n \cdot \left(1 - \frac{M_c}{M_n}\right) \quad \text{------>} \quad \frac{M_{si}}{M_n} = 0.4916$$

Note that M_c/M_n is the same as was obtained in Section 3.3

81

5. Describe the steel component of the lateral strength

$$F_{si} := \frac{M_{si}}{M_n} \cdot F_n \qquad \text{------>} \qquad \frac{F_{si}}{F_n} = 0.4916$$

6. Carried over parameters

Neutral axis depth ratio $\quad cD_{rat} = 0.2071$

Concrete compression force ratio $\quad \dfrac{C_c}{f'_c \cdot A_g} = 0.0784$

Cumulative plastic drift capacity considering concrete damage $\quad \Sigma\theta_{PC} = 0.4816 \quad$ rad.

Normalized concrete moment ratio $\quad \dfrac{M_c}{f'_c \cdot A_g \cdot D} = 0.031$

Ratio of concrete to nominal moment $\quad \dfrac{M_c}{M_n} = 0.5084$

Rocking strength $\quad \dfrac{F_{rocking}}{F_n} = 0.2665$

These values are obtained from Section 3.3 and correspond to Steps 6 through 10.

11. Describe the concrete component of the lateral strength

$$F_{ci} := F_n \cdot \left[\frac{M_c}{M_n} \cdot \left(1 - \frac{\Sigma\theta_{pi}}{\Sigma\theta_{PC}} \right) \right] \qquad \text{------>} \qquad \frac{F_{ci}}{F_n} = 0.4768$$

12. Determine the net lateral strength

$$F_i := F_n \cdot \left(\frac{F_{si}}{F_n} + \frac{F_{ci}}{F_n} \right) \qquad \text{------>} \qquad \frac{F_i}{F_n} = 0.9683$$

Case II: Column had already beensubjected to 2 cycles at drift levels each of 2, 3, 4 and 5%.

Hence, $\theta_i := 0.05$ rad.

2. <u>Current cumulative plastic drift</u>

$\theta_{pi} := \theta_i - \theta_y$ ------> $\theta_{pi} = 0.0375$ rad.

$\Sigma\theta_{pi} := 2\cdot2\cdot(0.0075 + 0.0175 + 0.0275 + 0.0375)$ ------> $\Sigma\theta_{pi} = 0.36$ rad.

3. <u>Determine the loss depth ratio</u>

$$\Delta D' := 0.5\cdot D' - \frac{0.08\cdot L_p}{\sqrt{\theta_{pi}\cdot\Sigma\theta_{pi}}}$$ ------> $\Delta D' = 74.5341$ mm.

Therefore, $\dfrac{\Delta D'}{D'} = 0.0974$

4. <u>Determine the steel moment loss ratio</u>

Unconfined concrete compression strength $f_c = 45$ MPa.

Concrete gros sectional area $A_g = 6.5755\cdot10^5$ mm^2

Overall diameter $D = 915$ mm.

These values are obtained from Section 3.3.

$$\Delta M_{si} := 0.7\cdot\rho_t\cdot\frac{f_y}{f_c}\cdot\left(\frac{\Delta D'}{D'}\right)^{0.53}\cdot\left(1 - 0.7\cdot\frac{\Delta D'}{D'}\right)\cdot f_c\cdot A_g\cdot D'$$

Therefore, $\dfrac{\Delta M_{si}}{M_n} = 0.2862$

5. <u>Describe the steel component of the lateral strength</u>

$$F_{si} := F_n\cdot\left(\frac{M_s}{M_n} - \frac{\Delta M_{si}}{M_n}\right)$$ ------> $\dfrac{F_{si}}{F_n} = 0.2223$

Steps 6 through 10 are same as before.

10. Deterimine the rocking strength

Residual rocking strength is given by the lesser of the sliding and rocking strength.
Assuming a coefficient of sliding friction

$$\mu_s := 0.7 \qquad ; \qquad W := P_{rat} \cdot f_c \cdot A_g$$

$$F_{sliding} := \mu_s \cdot W \qquad \text{------>} \qquad F_{sliding} = 8.2852 \cdot 10^5 \qquad \text{N.}$$

Calculation of rocking strength:

$$c"D"_{rat} := \left[\frac{P_{rat}}{0.396 \cdot \dfrac{A_{cc}}{A_g}}\right]^{0.725} \qquad \text{------>} \qquad c"D"_{rat} = 0.2293$$

Modified concrete compression force $\qquad C'_c := 1.32 \cdot 0.3 \cdot \left(c"D"_{rat}\right)^{1.38} \cdot f_c \cdot A_{cc}$

$$\frac{C'_c}{f_c \cdot A_g} = 0.04 \qquad\qquad P_{rat} = 0.04$$

Hence, $\quad M'_c := 0.5 \cdot C'_c \cdot D" \cdot \left(1 - 1.2 \cdot c"D"_{rat}\right) \quad \text{---->} \quad M'_c = 3.4411 \cdot 10^8 \qquad \text{N-mm.}$

Hence, $\quad F_{rocking} := \left(\dfrac{M'_c}{0.5 \cdot H}\right) \qquad \text{----->} \qquad F_{rocking} = 1.1282 \cdot 10^5 \qquad \text{N.}$

Normalized rocking strength $\qquad \dfrac{F_{rocking}}{F_n} = 0.2086$

11. Describe the concrete component of the lateral strength

Cumulative plastic drift at which rocking commences:

$$\Sigma\theta_{PR} := \Sigma\theta_{PC} \cdot \left(1 - \frac{M_n}{M_c} \cdot \frac{F_{rocking}}{F_n}\right) \qquad \text{------>} \qquad \Sigma\theta_{PR} = 0.2841 \quad \text{rad.}$$

Since the present cumulative plastic drift $\quad \Sigma\theta_{pi} = 0.36 \qquad$ rad. is greater than the

plastic drift level at which rocking commences,

$F_{ci} := F_{rocking}$ Therefore, $\dfrac{F_{ci}}{F_n} = 0.2086$

!2. <u>Determine the net lateral strength</u>

$$F_i := F_n \cdot \left(\dfrac{F_{si}}{F_n} + \dfrac{F_{ci}}{F_n} \right)$$ -------> $\qquad$ $\dfrac{F_i}{F_n} = 0.4308$
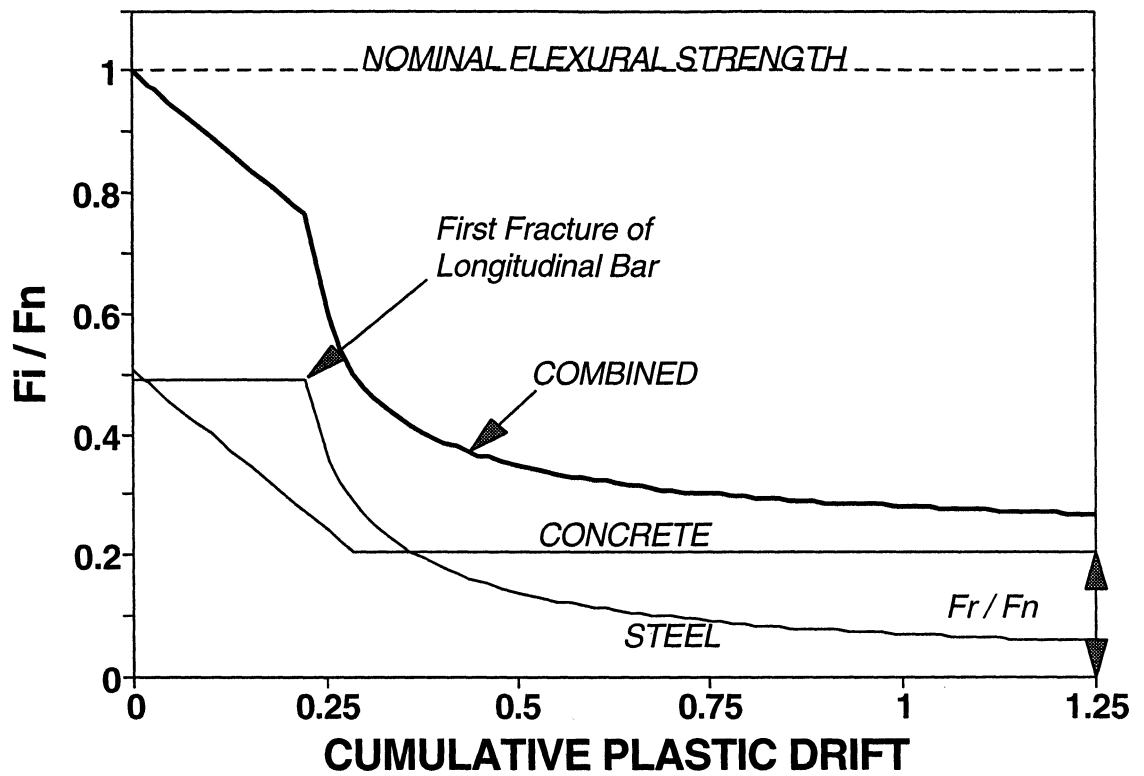
Figure 6-5   Low Cycle Fatigue Model applied to the Illustrative Bridge Pier
Example.

SECTION 7

TRANSVERSE REINFORCEMENT FAILURE IN SHEAR

7.1 BACKGROUND

The shear analysis of reinforced concrete beam-columns has been a contentious issue to researchers, as well as structural engineers, for decades. This is because there has been a general lack of comprehensive analysis tools that permit cyclic inelastic shear analysis similar to column flexural analysis (Schlaich et al., 1987; Collins and Mitchell, 1991; Hsu, 1993). As a result, analysis approaches that unify shear and flexural behavior have been difficult to achieve in a comprehensive way. Even though certain researchers have proposed some advanced analysis tools (Collins and Mitchell, 1991; Chang and Mander, 1994; Priestley et al. 1994a,b,c) to overcome some of the modelling difficulties, they are still complicated in usage and limited in applicability.

However, a valuable insight into the whole problem can be obtained using truss models for the analysis of structural concrete members. Significant amount of work in this aspect has been performed in a companion research by Kim and Mander (1997) with advanced inelastic Strut and Tie (SAT) models. This section uses excerpts from that research to compute the cumulative plastic deformation at hoop fracture using an energy balance approach. This is reported in the following.

7.2 FUNDAMENTALS OF SHEAR RESISTANCE IN REINFORCED CONCRETE MEMBERS

In the most general form, the ultimate shear resistance can be expressed as

$$V_u = V_s + V_c + V_p \tag{7-1}$$

where V_s = shear resisted by the transverse reinforcement, V_c = shear resisted by the tensile stress in the concrete, and V_p = shear carried by the axial compression. However, a concrete

87

member is considered as a structural element of combined mechanisms as shown in figure 7-1. Therefore, the resultant lateral resistance of the column should be the <u>lesser</u> of

$$V = V_u = V_s + V_c + V_p \qquad (7\text{-}2)$$

and

$$V = V_f = \frac{M_s + M_c}{L} \qquad (7\text{-}3)$$

where V_f = shear resisted by the flexural mechanism, M_s = moment contributed by the longitudinal steel, M_c = moment contributed by the eccentric concrete compression block, and L = lever arm of the cantilever column. In order to maintain the deformation compatibility and equilibrium conditions between the load transferring mechanisms, it is assumed that the column cross-section is proportional to the ratio of the component strength to the total strength. Thus

$$A_{vs} = b_{ws}jd \quad ; \quad A_{vc} = b_{wc}jd \quad ; \quad A_{vp} = b_{wp}jd \qquad (7\text{-}4)$$

where jd = internal lever arm, A_{vs}, A_{vc}, A_{vp} are respectively effective shear areas for V_s, V_c and V_p mechanisms and b_{ws}, b_{wc}, b_{wp} are respectively the effective column width for V_s, V_c and V_p mechanism which are estimated as

$$\frac{b_{ws}}{b_w} = \frac{V_s}{V_u} \quad ; \quad \frac{b_{wc}}{b_w} = \frac{V_c}{V_u} \quad ; \quad \frac{b_{wp}}{b_w} = \frac{V_p}{V_u} \qquad (7\text{-}5)$$

It is noted that $b_w = b_{ws} + b_{wc} + b_{wp}$ as shown in figure 7-2 and $A_v = A_{vs} + A_{vc} + A_{vp} = b_w jd$ in which A_v = total shear area of the concrete column.

Considering equilibrium of forces along the cracked surface of a beam-column it can be shown that the shear resisted by the transverse reinforcement is given by

$$V_s = A_{sh}f_T \frac{jd}{s} \cot \theta \qquad (7\text{-}6)$$

in which A_{sh} = section area of the transverse reinforcement at spacing s, f_T = stress in the transverse reinforcement, and θ = crack angle. Also using advanced truss models the shear
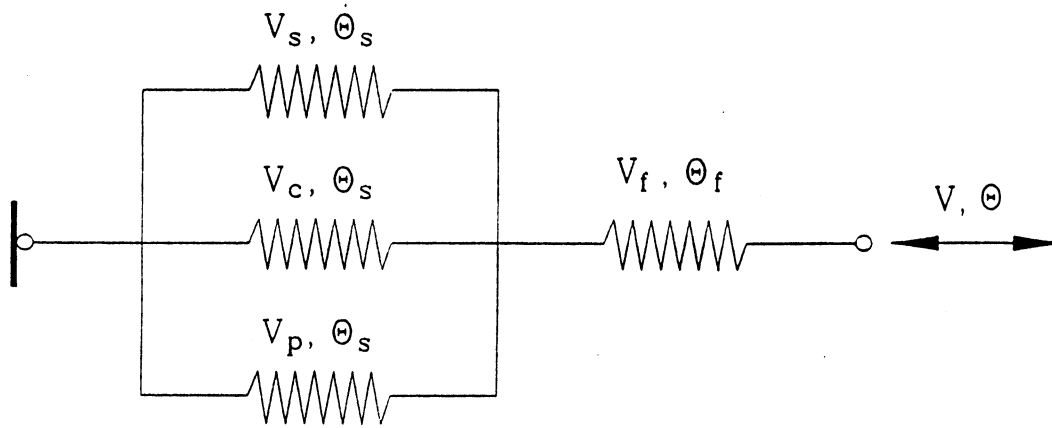
Figure 7-1 Spring Analogy for Combination of Load Transfer Mechanisms.
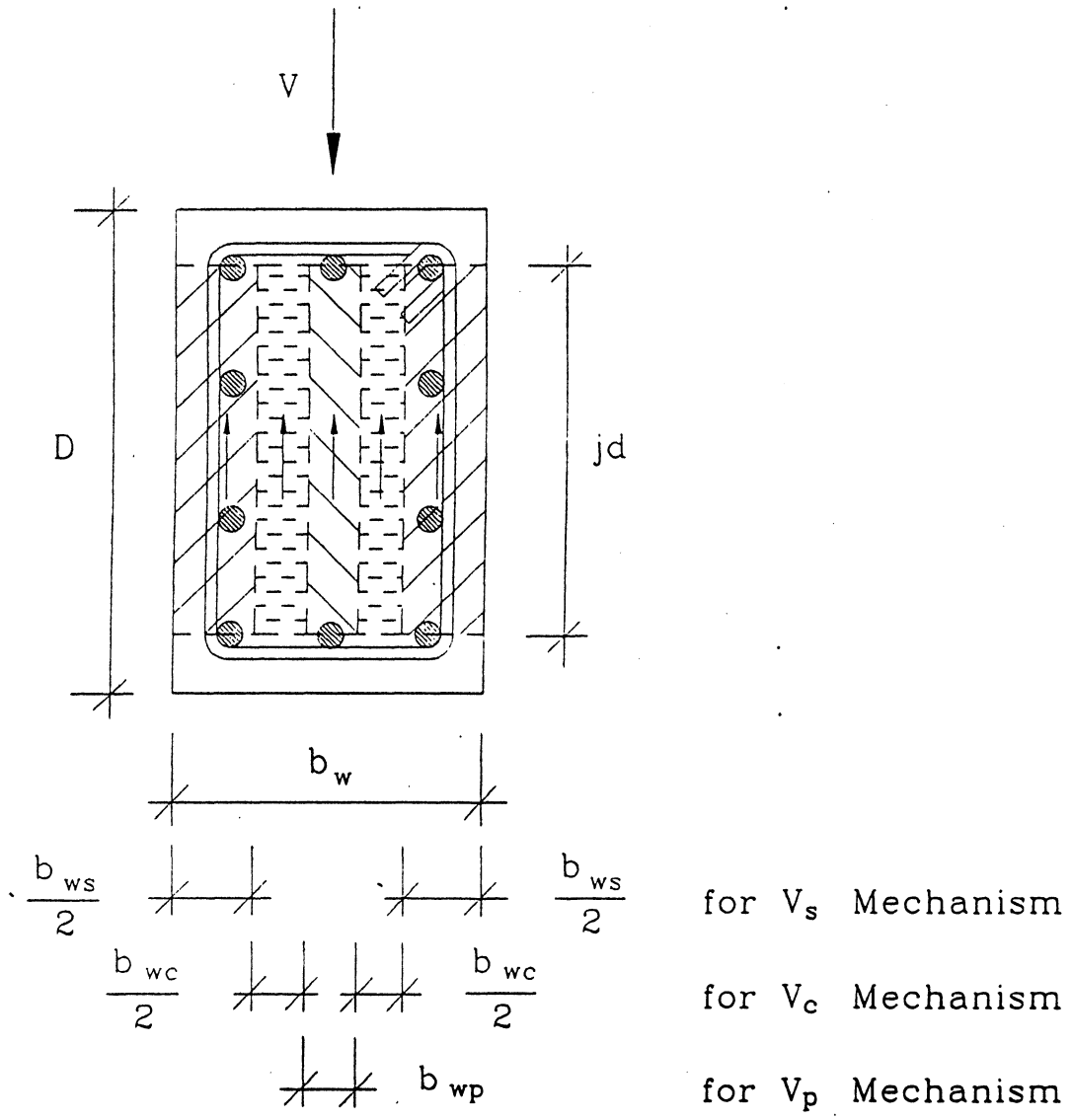
Figure 7-2 Proportioning of Column Load Transfer Mechanisms.

resisted by the concrete and axial load components can be shown to be

$$V_c = A_v f_1^{avg} \cot \theta (1 - 2 \sin^2 \theta) \qquad (7\text{-}7)$$

and

$$V_p = 0.5 E_c A_v \left(\frac{b_{wp}}{b_w}\right)\left(1.5 \frac{D}{jd} - 1\right)\sin^2\alpha \cdot \Theta_s \qquad (7\text{-}8)$$

$$V_p = \eta P (\tan \alpha - \Theta_s) \qquad (7\text{-}9)$$

where f_1^{avg} = average tensile stress in the concrete tension ties, E_c = modulus of elasticity of concrete, D = overall depth of the section, α = corner to corner diagonal angle, Θ_s = drift angle due to shear, and P = applied axial load. Note η = 1.0 for fixed-fixed ends and 0.5 for fixed-pinned ends and $\tan \alpha = jd/L$. Detailed derivation of the above expressions can be found elsewhere (Kim, 1996).

The above mentioned column shear strength components are also considered to deteriorate by inelastic cyclic loading as the flexural components are as discussed in Section 2.2, if the structural response is governed by the column shear strength. The column shear strength degradation can also be assessed by energy considerations which will be discussed in what follows. In the proposed damage analysis on shear components, it is assumed that the diagonal concrete compressive struts are within the elastic range and not considered to be a prime source of energy dissipation.

7.3 SHEAR FRACTURE OF TRANSVERSE HOOP STEEL AT MID-COLUMN HEIGHT

7.3.1 Cumulative Plastic Shear Deformation at Average Hoop Fracture

Consider the foregoing concept of energy balance. Then, the external work done (*EWD*) by the steel truss mechanism is calculated by

$$EWD = V_s \Delta_{pS} \tag{7-10}$$

which V_s is given in equation (7-6) and Δ_{pS} is the plastic portion of column shear displacement. Expanding the right hand side terms of equation (7-10) gives the total energy at fracture in terms of <u>cumulative</u> plastic shear displacement:

$$EWD = \left(A_{sh} f_T \frac{jd}{s} \cot\theta\right)\left(\Theta_{pS} jd \cot\theta \left[2 N_c\right]\right) \tag{7-11}$$

where Θ_{pS} is the plastic portion of column shear rotation and N_c is the number of loading cycles at applied drift Θ_{pS}. It is noted that the transverse hoop steel stress f_T is the <u>average</u> stress over the unit shear length defined by the crack angle which is $jd \cot\theta$. Also note that $A_{sh} = 2A_b$ for rectangular hoop steel, in which A_b is the section area of a single leg of a transverse hoop, and A_{sh} for circular hoop is given by the explicit expression derived by Kim and Mander (1997)

$$A_{sh} = 2\left(\frac{s}{jd} \tan\theta\right) \frac{\sin\left(\dfrac{\pi/2}{1 + \dfrac{s}{jd} \tan\theta}\right)}{\sin\left(\dfrac{\pi/2}{1 + \dfrac{jd}{s} \cot\theta}\right)} \tag{7-12}$$

where the symbols have their usual meaning.

The internal work done (*IWD*) by the transverse hoop steel within the unit shear length is calculated by considering the volume of the steel participating the shear resistance, that is, for rectangular hoop,

$$IWD = U_{sf}(2 A_b) jd \frac{jd}{s} \cot\theta \tag{7-13}$$

for circular hoop,

92

$$IWD = U_{sf}A_b\,jd\,\pi\,\frac{jd}{s}\cot\theta \tag{7-14}$$

where U_{sf} is the strain energy required to fracture reinforcing steel in tension and is approximately given by $110\,MJ/m^3$. Formulating the energy balance, the cumulative plastic column drift capacity due to the steel truss mechanism can be estimated.

7.3.1.1 Members with Rectangular Hoops

Equating equations (7-11) and (7-13) in the form of $EWD = IWD$ gives:

$$\left(A_{sh}\bar{f}_s\frac{jd}{s}\cot\theta\right)\!\left(\Theta_{pS}\,jd\cot\theta\,[2N_c]\right) = U_{sf}(2A_b)\,jd\,\frac{jd}{s}\cot\theta \tag{7-15}$$

in which $\bar{f}_s$ is the average yield stress in the transverse hoop steel. Rearranging equation (7-15), the cumulative plastic column shear deformation capacity for concrete members with rectangular hoops is

$$\Sigma\,\Theta_{pS}(c) = \Theta_{pS}\big[2N_c\big] = \frac{U_{sf}}{\bar{f}_s}\tan\theta \tag{7-16}$$

Now, consider the steel stress-strain curve shown in figure 7-3a. It is noted that the strain energy U_{sf} is defined by the area under the stress-strain curve of reinforcing steel and can also be expressed in terms of $\bar{f}_s$. Thus,

$$U_{sf} = \bar{f}_s\,\varepsilon_{sf} = \int_0^{\varepsilon_{su}} f_s\,d\varepsilon + 0.7f_y\,\varepsilon_{su} \tag{7-17}$$

Using equation (7-17), the strain energy U_{sf} can also be calculated by the ultimate strain and yield stress of steel coupons. Based on the experimental results reported by Mander, et al. (1984), the average steel stress can be related to the yield stress, thus

$$\bar{f}_s \cong 1.4\,f_y \tag{7-18}$$

Then, substituting equations (7-17) and (7-18) into equation (7-16), the cumulative plastic column shear deformation capacity for concrete members with rectangular hoops becomes

93

$$\Sigma \Theta_{pS}(c) = 0.7 \frac{U_{sf}}{f_y} \tan\theta \qquad\qquad (7\text{-}19)$$

7.3.1.2 Members with Circular Hoops

Equating (7-11) and (7-14),

$$\left(A_{sh}f_T \frac{jd}{s} \cot\theta\right)\left(\Theta_{pS} jd \cot\theta \left[2N_c\right]\right) = U_{sf}A_b jd \, \pi \frac{jd}{s} \cot\theta \qquad\qquad (7\text{-}20)$$

where A_{sh} is as given by equation (7-12). Substituting equation (7-12) for A_{sh} into equation (7-20) and rearranging, the cumulative plastic column shear deformation capacity for concrete members with circular hoops is

$$\Sigma \Theta_{pS}(c) = \Theta_{pS}\left[2N_c\right] = 1.12 \frac{U_{sf}}{f_y} \frac{jd}{s} \frac{\sin\left(\dfrac{\pi/2}{1 + \dfrac{jd}{s}\cot\theta}\right)}{\sin\left(\dfrac{\pi/2}{1 + \dfrac{s}{jd}\tan\theta}\right)} \qquad\qquad (7\text{-}21)$$

7.3.2 Cumulative Plastic Shear Deformation at First Hoop Fracture

Using truss models as was done by Kim and Mander (1997), elongation in transverse hoops due to shear can be shown to be maximum at the middle of the unit shear length ($jd \cot\theta$). Therefore, it is considered that the transverse hoop located at the middle of the unit shear length is first subjected to fracture and, the ratio of the maximum tensile strain to the average can be calculated as

$$\frac{\varepsilon_{T\text{-max}}}{\varepsilon_{T\text{-avg}}} = 1.125 \qquad\qquad (7\text{-}22)$$

This denotes that the middle hoop is going to have the cumulative inelastic strain increased by 12.5% above the average. Therefore, the cumulative plastic deformation at first hoop fracture

94

can be obtained by modifying equations (7-9) and (7-21) to be proportionally smaller than the average. Thus, for rectangular hoops,

$$\Sigma \Theta_{pS1}(c) = 0.63 \frac{U_{sf}}{f_y} \tan \theta \qquad (7\text{-}23)$$

for circular hoops,

$$\Sigma \Theta_{pS1}(c) = \frac{U_{sf}}{f_y} \frac{jd}{s} \frac{\sin\left(\dfrac{\pi/2}{1 + \dfrac{jd}{s}\cot\theta}\right)}{\sin\left(\dfrac{\pi/2}{1 + \dfrac{s}{jd}\tan\theta}\right)} \qquad (7\text{-}24)$$

7.3.3 Cumulative Plastic Shear Deformation at Last Hoop Fracture

The strain ratio between maximum and minimum is $\varepsilon_{T\text{-max}}/\varepsilon_{T\text{-min}} = 1.25$ (see Kim, 1996). Thus the cumulative plastic column shear deformation at <u>last</u> hoop fracture becomes

$$\Sigma \Theta_{pS2}(c) = 1.25 \, \Sigma \Theta_{pS1}(c) \qquad (7\text{-}25)$$

The idealized energy-based damage model for structural members governed by transverse hoop steel fracture is depicted in figure 7-3b in which $\Theta_{pS1}(c)$ and $\Theta_{pS2}(c)$ are respectively the cumulative plastic column shear deformations at first and last hoop fracture.

7.3.4 Theoretical Crack Angle

The crack angle to be used in the above equations can also be derived from energy considerations. It was shown by Kim and Mander (1997) analytically, and later verified against experimental observations, that the theoretical crack angle is given by

$$\theta = \tan^{-1} \left[\frac{\rho_v n + \zeta \dfrac{\rho_v}{\rho_t} \dfrac{A_v}{A_g}}{1 + \rho_v n} \right]^{1/4} \qquad (7\text{-}26)$$

95

where n = modular ratio= E_s/E_c (ratio of elastic modulus of steel and concrete) and $\rho_v = A_{sh}/b_{ws}$ for a rectangular section (refer figure 7-2) and $\rho_v = \rho_s/2 = 2A_b/D''s$ for a circular section in which A_b = sectional area of a single leg of a transverse hoop and D'' = center-to-center diameter of the transverse reinforcement in a circular column. The parameter ζ = 0.5704 for fixed -fixed columns and 1.5704 for fixed-pinned columns. The remaining symbols are explained previously.
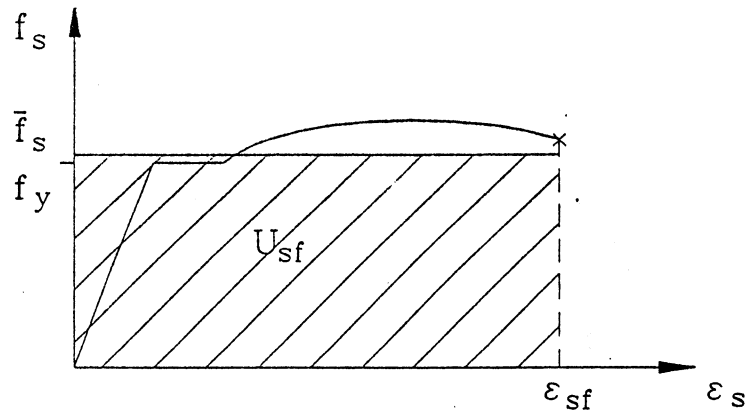
(a) Strain energy of reinforcing steel
    in terms of average stress
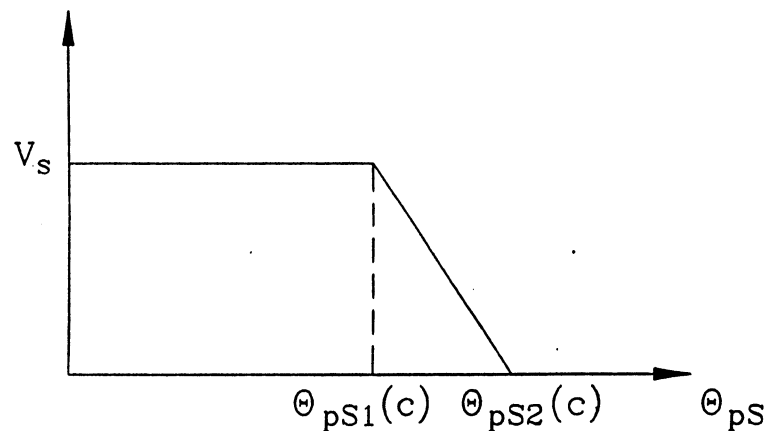
(b) Energy-based damage model due to
    transverse hoop steel fracture

Figure 7-3 Energy-Based Damage Model for Structural Members governed by Transverse Hoop Fracture.

7.3.5 Summary of Damage Evaluation Procedure

Step 1.   Determine the neutral axis depth ratio c/D.   For rectangular sections use equation (2-23):

$$\left(\frac{c}{D}\right) = \frac{\left(\dfrac{P_e}{f_c' A_g}\right) + \left(\dfrac{\gamma\, \rho_t f_y / f_c'}{1 - 2d'/D}\right)}{\left(\alpha\beta + \dfrac{2\gamma\, \rho_t f_y / f_c'}{1 - 2d'/D}\right)} \tag{SF-1a}$$

and for circular sections use equation (2-31):

$$\frac{c}{D} = \frac{1}{\beta}\left[\frac{\dfrac{P_e}{f_c' A_g} + 0.5\,\rho_t\, \dfrac{f_y}{f_c'}\left(\dfrac{1 - 2c/D}{1 - 2d'/D}\right)}{1.32\,\alpha}\right]^{0.725} \tag{SF-1b}$$

Step 2.   Determine the concrete compression force ratio $C_c / f_c' A_g$.   For rectangular sections use equation (2-16):

$$\left(\frac{C_c}{f_c' A_g}\right) = \alpha\beta\left(\frac{c}{D}\right) \tag{SF-2a}$$

and for circular sections use equation (2-28):

$$\frac{C_c}{f_c' A_g} = 1.32\,\alpha\left(\beta\ \frac{c}{D}\right)^{1.38} \tag{SF-2b}$$

Step 3.   Determine the equivalent plastic hinge length L_p using equation (2-9):

$$L_p = 0.08L + 4400\,\varepsilon_y d_b \tag{SF-3}$$

Step 4.   Determine the cumulative plastic drift capacity $\Sigma\theta_{pc}$ using equation (2-10):

$$\Sigma \theta_{PC} = \frac{0.016 \, (L_p/D)}{\left(\dfrac{C_c}{f_c' A_g}\right)\left(\dfrac{c}{D}\right)}$$

(SF-4)

Step 5.

Determine the component of the moment contributed by the eccentric concrete stress block M_c. For rectangular sections use equation (2-13):

$$M_c = 0.5 C_c D \left(1 - \beta \, \frac{c}{D} \right)$$

(SF-5a)

and for circular sections use equation (2-14):

$$M_c = 0.5 C_c D \left(1 - 1.2 \beta \, \frac{c}{D} \right)$$

(SF-5b)

Step 6.

Determine the theoretical crack angle using equation (7-26):

$$\theta = \tan^{-1} \left[\frac{\rho_v n + \zeta \, \dfrac{\rho_v}{\rho_t} \, \dfrac{A_v}{A_g}}{1 + \rho_v n} \right]^{1/4}$$

(SF-6)

Step 7.

Determine the cumulative plastic shear deformation $\Sigma \Theta_{pS1}(c)$ at first hoop fracture. For rectangular hoops use equation (7-23):

$$\Sigma \Theta_{pS1}(c) = 0.63 \, \frac{U_{sf}}{f_y} \tan \theta$$

(SF-7a)

for circular hoops use equation (7-24):

$$\Sigma \Theta_{pS1}(c) = \frac{U_{sf}}{f_y} \frac{jd}{s} \frac{\sin\left(\dfrac{\pi/2}{1 + \dfrac{jd}{s}\cot\theta}\right)}{\sin\left(\dfrac{\pi/2}{1 + \dfrac{s}{jd}\tan\theta}\right)}$$

(SF-7b)

Step 8.

Determine the cumulative plastic shear deformation at last hoop fracture $\Sigma \Theta_{pS2}(c)$ using equation (7-25):

98

$$\Sigma \Theta_{pS2}(c) = 1.25 \, \Sigma \Theta_{pS1}(c) \tag{SF-8}$$

Step 9.   Determine relationship between nominal strength and cumulative plastic drift in the form

$$\frac{F_i}{F_n} = 1 - \frac{M_c}{M_n} \frac{\Sigma \theta_{pi}}{\Sigma \theta_{PC}} \tag{SF-9}$$

7.4 NUMERICAL EXAMPLE

As before, a numerical example is used to illustrate the use of the energy-based shear capacity evaluation discussed in the previous section.

Relevant details of the pier bent analyzed is shown in figure 7-4. Note that the height of the pier is deliberately chosen to be 2591 *mm* (102 *in.*) to make it shear critical. Analysis steps are illustrated below.
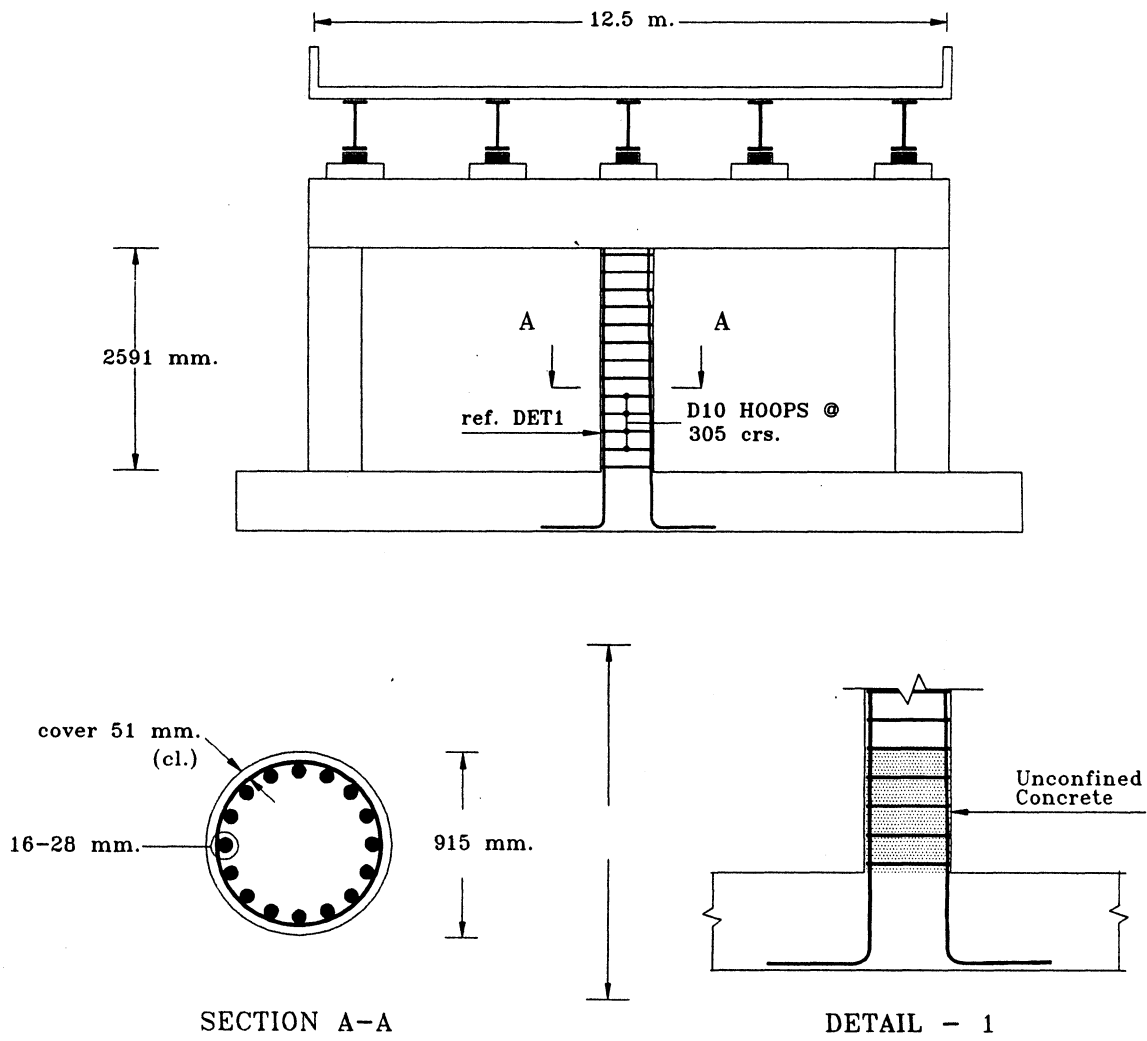
Figure 7-4 Illustrative Bridge Pier used in the Numerical Example.

<u>Given Data</u>

Diameter of the column $D = 915$ mm.

Height of the column $H = 2591$ mm.

Number of longitudinal bars $n = 16$ of diameter $d_b = 28$ mm.

Diameter of horizontal bars $d_{bh} = 10$ mm and spacing $s = 305$ mm.

Clear cover in the column $cov = 51$ mm.

Unconfined compression strength of concrete $f_c = 45$ MPa

Yield strength of longitudinal reinforcement $f_y = 330$ MPa

Yield strength of horizontal reinforcement $f_{yh} = 330$ MPa

Axial load ratio in the column ($P_e/f_c A_g$) denoted by $P_{rat} = 0.04$

1. <u>Neutral axis depth ratio:</u>

Longitudinal reinforcement ratio $\rho_t = \dfrac{n \cdot d_b{}^2}{D^2}$ -----> $\qquad \rho_t = 0.015$

Effective cover $d' = cov + d_{bh} + 0.5 \cdot d_b$ -----> $\qquad d' = 75$ mm.

Core diameter $D'' = D - 2 \cdot cov - d_{bh}$ -----> $\qquad D'' = 803$ mm.

Stress block parameters $\alpha = 0.66$ and $\beta = 1.3 - 0.01015 \cdot f_c$ ----> $\beta = 0.8433$

Let the c/D ratio be denoted by c_{rat}. As an initial value of this quadratic assume

$c_{rat} = 0.2$

$$cD_{rat} = root\left[\left[\dfrac{P_{rat} + 0.5 \cdot \rho_t \cdot \dfrac{f_y}{f_c} \cdot \dfrac{1 - 2 \cdot c_{rat}}{1 - 2 \cdot \dfrac{d'}{D}}}{1.32 \cdot \alpha \cdot \beta^{1.38}}\right]^{0.725} - c_{rat}, c_{rat}\right]$$

$cD_{rat} = 0.2071$

101

2. Concrete compression force ratio

Gross cross sectional area $\quad A_g := 0.25 \cdot \pi \cdot D^2 \quad \text{-----> } A_g = 6.5755 \cdot 10^5 \quad mm^2$

Core cross sectional area $\quad A_{cc} := 0.25 \cdot \pi \cdot D"^2 \quad \text{-----> } A_{cc} = 5.0643 \cdot 10^5 \quad mm^2$

Concrete compression force $\quad C_c := 1.32 \cdot \alpha \cdot \left(\beta \cdot cD_{rat} \right)^{1.38} \cdot f_c \cdot A_g$

Concrete compression force ratio $\quad \dfrac{C_c}{f_c \cdot A_g} = 0.0784$

3. Equivalent plastic hinge length

Young's Modulus of longitudinal steel $\quad E_s := 200000 \quad MPa$

Yield strain of longitudinal steel $\quad \varepsilon_y := \dfrac{f_y}{E_s} \quad \text{------> } \quad \varepsilon_y = 0.0017$

Equivalent plastic hinge length

$$L_p := 0.08 \cdot \dfrac{H}{2} + 4400 \cdot \varepsilon_y \cdot d_b \quad \text{-------> } \quad L_p = 306.92 \quad mm.$$

4. Cumulative plastic drift assuming concrete damage alone

$$\Sigma\theta_{PC} := \dfrac{0.016 \cdot \dfrac{L_p}{D}}{\left(\dfrac{C_c}{f_c \cdot A_g} \right) \cdot cD_{rat}} \quad \text{-------> } \quad \Sigma\theta_{PC} = 0.3305$$

5. Moment capacity generated by the eccentric concrete stress block

$$M_c := 0.5 \cdot C_c \cdot D \cdot \left(1 - 1.2 \cdot \beta \cdot cD_{rat} \right) \quad \text{------> } \quad \dfrac{M_c}{f_c \cdot A_g \cdot D} = 0.031$$

From ACI type analysis, nominal moment $\quad M_n := 1.65 \cdot 10^9 \quad N\text{-}mm.$

Therefore, $\quad \dfrac{M_c}{M_n} = 0.5084$

6. Theoretical crack angle

$$A_{bh} := 0.25 \cdot \pi \cdot d_{bh}^{2} \qquad \text{-----> } \qquad A_{bh} = 78.5398 \qquad mm^2$$

$$\rho_{v} := \frac{2 \cdot A_{bh}}{s \cdot D''} \qquad \text{-----> } \qquad \rho_{v} = 6.4136 \cdot 10^{-4}$$

Modulus of elasticity of concrete $\quad E_{c} := 4700 \cdot \sqrt{f'_{c}} \quad \text{-----> } \quad E_{c} = 3.1529 \cdot 10^{4} \qquad MPa$

Modular ratio $\quad n := \dfrac{E_{s}}{E_{c}} \qquad \text{-----> } \quad n = 6.3435$

Shear area $\quad A_{v} := 0.8 \cdot A_{g} \qquad$ and $\qquad \zeta := 0.5704 \quad$ (for fixed-fixed end condition)

Therefore, the theoretical crack angle

$$\theta := atan\left[\frac{\rho_{v} \cdot n + \zeta \cdot \dfrac{\rho_{v}}{\rho_{t}} \cdot \dfrac{A_{v}}{A_{g}}}{1 + \rho_{v} \cdot n}\right]^{0.25} \qquad \text{-----> } \qquad \theta = 0.3915 \quad rad.$$

7. Cumulative plastic shear deformation at first hoop fracture

Pitch circle diameter $\qquad D' := D - 2 \cdot d' \quad \text{-----> } \qquad D' = 765 \qquad mm.$

Assume $\quad jD := D' \qquad$ and $\qquad U_{sf} := 110 \quad MJ/m^3$

$$\Sigma\Theta_{pS1c} := \frac{U_{sf}}{f_{y}} \cdot \frac{jD}{s} \cdot \frac{\sin\left(\dfrac{0.5 \cdot \pi}{1 + \dfrac{jD}{s} \cdot cot(\theta)}\right)}{\sin\left(\dfrac{0.5 \cdot \pi}{1 + \dfrac{s}{jD} \cdot tan(\theta)}\right)} \qquad \text{-----> } \qquad \Sigma\Theta_{pS1c} = 0.1887 \quad rad.$$

8. Cumulative plastic shear deformation at last hoop fracture

$$\Sigma\Theta_{pS2c} := 1.25 \cdot \Sigma\Theta_{pS1c} \qquad \text{------> } \qquad \Sigma\Theta_{pS2c} = 0.2359 \qquad rad.$$

9. Application of damage model

The damage model is plotted in figure 7-5. Note that beyond $\Sigma\Theta_{pS1c} = 0.1887$ rad. the lateral force capacity drops rapidly and becomes zero after the last hoop fracture at $\Sigma\Theta_{pS2c} = 0.2359$ rad.
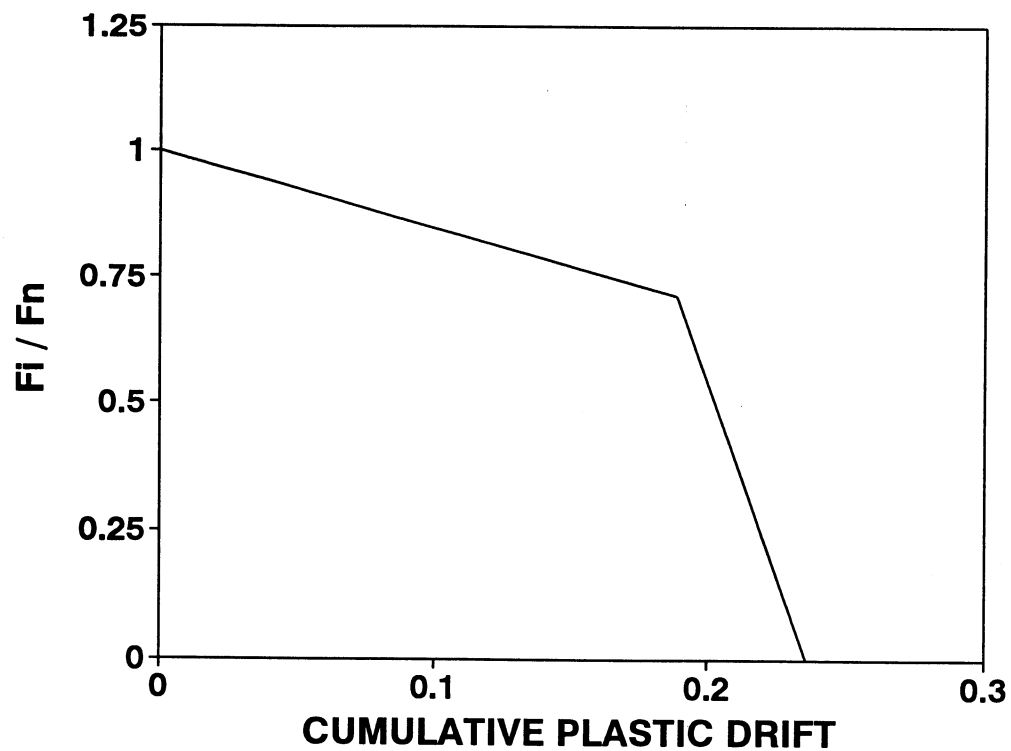
Figure 7-5 Energy Based Shear Model applied to the Illustrative Bridge Pier Example.

SECTION 8

ANALYSIS OF FATIGUE LIFE

8.1 INTRODUCTION

In the preceding section an attempt was made to look into the various fundamental modes of fatigue failure for bridge columns subjected to seismic attack. These included failure of longitudinal reinforcement through low cycle fatigue; loss of bond in anchorages and splices; shear failure due to buckling failure or even failure of the unconfined concrete due to crushing. However the best way to test the viability of a theory is to compare the predictions of the theoretical analysis with actual test results. This section examines experimental results obtained by previous investigators and tries to come up with a meaningful way of interpreting these results for the purpose of validating the present fatigue theory.

8.2 DETERMINATION OF EFFECTIVE NUMBER CYCLES TO FAILURE

8.2.1 Background

Since most experiments are conducted on specimens with different displacement amplitudes, it is necessary to use an appropriate method of cycle counting. Furthermore, this is also necessary for determining the effective number of cycles of loading in an earthquake time-history. The former and latter cases requiring cycle counting are needed for determining cyclic demand and cyclic capacity, respectively.

8.2.2 Miner's Linear Accumulation Rule

The effective number of cycles (N_{eff}) to failure can be obtained using Miner's linear damage accumulation rule which states that the damage accumulated up to the i-th loading cycle is given by

$$D_T = \Sigma D_i \tag{8-1}$$

where D_T is total damage and D_i = damage fraction for the i-th cycle of loading given by

$$D_i = \frac{n_i}{(N_f)_i} \tag{8-2}$$

where n_i = total number of cycles at the current rotational amplitude Θ_{ji} and $(N_f)_i$ = fatigue life at the rotational amplitude Θ_{ji}.

8.2.3 Effective Number of Cycles

By employing Miner's rule, an effective (or equivalent) number of cycles can be derived for a variable cycle history. The linear log-log relationship of plastic rotation to number of cycles of reversals $(2N_f)$ was first obtained by Coffin (1954) and Manson (1953). Later Koh and Stephens (1991) suggested that even total rotation can be used instead of plastic rotation as follows:

$$(N_f)_i = Q \, \Theta_{ji}^{1/c} \tag{8-3}$$

where Q = fatigue ductility coefficient and c = fatigue ductility exponent. Thus combining equations (8-1), (8-2) and (8-3) the <u>total</u> damage due to a random loading history can be obtained as

$$D_{random} = \sum \left(\frac{n_i}{Q \, \Theta_{ji}^{1/c}} \right) = \sum \frac{n_i}{Q} (\Theta_{ji})^{-1/c} \tag{8-4}$$

Damage at incipient failure for N_{eff} cycles at an assumed effective rotational amplitude $\Theta_{j\,eff}$ is given by

$$D_{constant} = \frac{N_{eff}}{Q \, \Theta_{j\,eff}^{1/c}} = \frac{N_{eff}}{Q} (\Theta_{j\,eff}^{-1/c}) = 1 \tag{8-5}$$

The effective number of cycles (N_{eff}) can be determined by equating the total damage due to random loading and that due to constant equivalent amplitude (equation (8-5)). Hence,

$$\frac{D_{random}}{D_{constant}} = \frac{\sum n_i (\Theta_{ji})^{-1/c}}{\sum N_{eff} (\Theta_{jeff})^{-1/c}} = 1 \qquad (8\text{-}6)$$

from which

$$N_{eff} = \sum n_i \left(\frac{\Theta_{ji}}{\Theta_{jeff}}\right)^{-1/c} \qquad (8\text{-}7)$$

Mander et al. (1994) showed that for concrete fatigue the coefficient c has a value of -0.5.

Effective Number of Cycles to Failure for Steel and Concrete Fatigue For specimens governed by failure due to low cycle fatigue of longitudinal reinforcement, the effective number of cycles to failure can be obtained using equation (8-7). Mander (1994) showed that for steel fatigue, $c = -0.333$, thus $-1/c = 3$.

Regarding cycle counting of experimental displacement history to determine the effective number of cycles N_{eff}, it should be noted that the procedure must be modified for concrete failure. This is because for steel fatigue the plastic curvature is given by

$$\phi_p D = C_{SP} N_f^{-1/2} \qquad (8\text{-}8)$$

and the total curvature (or displacement)

$$\phi D = C_{ST} N_f^{-1/3} \qquad (8\text{-}9)$$

whereas for concrete failure equation (8-7) suggests <u>plastic</u> curvature

$$\phi_p D = C_{CP} N_f^{-1.0} \qquad (8\text{-}10)$$

Thus it will be assumed that in terms of <u>total</u> displacement

$$\phi D = C_{CT} N_f^{-1/2} \qquad (8\text{-}11)$$

where C_{SP}, C_{ST}, C_{CP}, C_{CT} are fatigue constraints. Therefore, for concrete failure equation (8-7) may be written as

$$N_{eff}^c = \sum_i^n \left(\frac{\Theta_{ji}}{\Theta_{jeff}}\right)^2 \qquad\qquad\qquad (8\text{-}125)$$

and for steel failure

$$N_{eff}^s = \sum_i^n \left(\frac{\Theta_{ji}}{\Theta_{jeff}}\right)^3 \qquad\qquad\qquad (8\text{-}12)$$

An explanatory example of the damage accumulation analysis is given using a typical laboratory deformation history. To illustrative this concept, consider the accumulated damage that results from the small amplitude cycles in a typical laboratory test. For example, the testing protocol used in much of the current NCEER experimental research uses _two_ completely reversed cycles of lateral loading at increasing drift amplitudes of Θ = $\pm 0.25\%$, $\pm 0.5\%$, $\pm 1\%$, $\pm 2\%$, ± 3, ± 4 +... until failure occurs or when the actuator runs out of stroke capacity. Now suppose if the maximum experimental drift is Θ_{max} = $\pm 5\%$, then the effective number of cycles _prior_ to the $\pm 5\%$ drift amplitude is:

For steel fatigue failure

$$N_{eff}^C = \sum \left(\frac{\Theta_{ji}}{\Theta_{jeff}}\right)^3 = \frac{2}{5^3}\left(0.25^3 + 0.5^3 + 1^3 + 2^3 + 3^3 + 4^3\right) = 1.60$$

For concrete fatigue failure

$$N_{eff}^C = \sum \left(\frac{\Theta_{ji}}{\Theta_{jeff}}\right)^2 = \frac{2}{5^2}\left(0.25^2 + 0.5^2 + 1^2 + 2^2 + 3^2 + 4^2\right) = 2.27$$

Note that the results imply that the damage done prior to the two cycles of loading at the $\pm 5\%$ drift amplitude is equivalent to 1.6 cycles that leads to steel failure, and 2.27 cycles that leads to concrete failure if cycled entirely at the $\pm 5\%$ drift amplitude.

8.3 DETERMINATION OF EXPERIMENTAL PLASTIC CURVATURE

Experimental values of plastic curvature $(\phi_p D)$ can be obtained either directly from experimental results (if measured), otherwise inferred values must be computed as follows. The

experimental displacement ductility factor μ_Δ is given by

$$\mu_\Delta = \frac{\Delta_u}{\Delta_y} \qquad (8\text{-}14)$$

where Δ_u = ultimate displacement and Δ_y = yield displacement. Now the ultimate displacement is the sum of plastic and yield displacements where the plastic displacement (Δ_p) is given by

$$\Delta_p = \Delta_u - \Delta_y = \phi_p L_p(L-0.5L_p) \qquad (8\text{-}15)$$

where L = length of the column and L_p = plastic hinge length.

Combining equation (8-14) and (8-15) one obtains

$$\mu_\Delta = \frac{\Delta_p + \Delta_y}{\Delta_y} = \left(\frac{\Delta_p}{\Delta_y}\right) + 1 \qquad (8\text{-}16)$$

that is :

$$\mu_\Delta = \frac{\phi_p L_p(L-0.5L_p)}{\Delta_y} + 1 \qquad (8\text{-}17)$$

from which the non-dimensional plastic curvature $\phi_p D$ can be expressed as

$$\phi_p D = \frac{2(\mu_\Delta - 1)\Delta_y}{\left(\dfrac{L_p}{D}\right)^2\left[\left(\dfrac{2L}{L_p/D}\right) - D\right]} \qquad (8\text{-}18)$$

where the plastic hinge length is given by equation (2-9).

8.4 CLOSURE

In this section an appropriate method of counting the number of cycles for a specimen that had failed either by low cycle fatigue of the longitudinal reinforcement or fatigue of the unconfined concrete is proposed. This method is based on Miner's linear damage accumulation rule and uses the concept of relating the total number of reversals to failure ($2N_f$) to the

dimensionless plastic curvature ($\phi_p D$) according to Koh and Stephens (1991). In order to be able to compare the results of experiments conducted by previous researchers with the theoritical predictions it was necessary to obtain the maximum plastic curvature obtained before failure occured due to any one of the causes mentioned. An expression was also obtained from first principles that would predict the maximum plastic curvature obtainable from the section before failure occurs.

SECTION 9
EXPERIMENTAL VALIDATION

9.1 INTRODUCTION

To verify the authenticity of the theoretical models discussed so far, a comparison with experimental results is carried out in this section. However, before proceeding any further, it is important to lay down the fact that the fatigue-based models discussed so far assume that the individual failure models occur independent of each other. This means that any particular mode is not the outcome of another preceding failure more. In reality such well defined failure modes are very hard to find. All efforts have been made to identify such failure modes and present herein.

9.2 FATIGUE FAILURE CAPACITY OF UNCONFINED CONCRETE

This subsection compares the predictions of the unconfined concrete failure theory with actual experimental specimens. A short description of the experimental specimens are provided below.

(i) *Bridge Piers with Square Column*: Mander et al. (1993) conducted tests on an actual bridge pier as part of their study to assess the seismic vulnerability of bridge piers in eastern United States which were predominantly designed for gravity loading. The square specimen tested had a base width of 1118 *mm* that gradually tapered to 889 *mm* at the pier cap level. Test cylinders core drilled from the specimen showed an unconfined compression strength of $f_c' = 51$ *MPa*. Longitudinal reinforcement consisted of $16 - \#7$ (22 *mm*) bars enclosed by #3 (10 *mm*) hoops at 305 *mm* centers. The yield strengths of the longitudinal bars and hoop steel were 276 *MPa* and 262 *MPa*, respectively. The pier was provided with a clear cover of 51 *mm*. Loading on the bridge pier consisted of one cycle with ±0.25% drift amplitude which was followed by two cycles each with ±0.5% , ±0.75% , ±1.0% , ±1.5% and ±2% drift amplitudes. This was followed by a quasi-dynamic loading which consisted of 5 and 17 loading cycles with ±3.0% and 4% drift amplitudes when the column ultimately failed due to hoop fracture and buckling

of longitudinal reinforcement. The yield drift was recorded at $\pm 0.15\%$. All through the tests a vertical load of 1197 *kN* (269 *kips*) was sustained by the column.

(ii) *Square Building Columns*: Aycardi, Mander and Reinhorn (1992, 1994) tested four one third scale model columns which were designed primarily for gravity loadings. Each column specimen was 711 *mm* (28 *in.*) tall and had a 102 *mm* (4 *in*) square cross-section containing 4 #D4 bars (5.73 *mm* diameter) with a measured yield strength of 448 *MPa*. Steel used for transverse reinforcement was #11 gauge (3 *mm* diameter) smooth round wire with a yield strength of 386 *MPa*. Clear cover provided was 11 *mm*. Loading on the specimen consisted of two complete displacement controlled cycles of each drift level of $\pm 0.25\%$, $\pm 0.5\%$, $\pm 1\%$, $\pm 2\%$ and $\pm 5\%$. Specimen 2 considered for this study failed in the third cycle of $\pm 5\%$ due to buckling of longitudinal reinforcement and crushing the core concrete. The ultimate and the yield curvatures were recorded at 0.5 *rad/m* (0.0127 *rad/in.*) and 0.4 *rad/m* (0.001 *rad/in.*), respectively. At all times the specimen sustained a constant axial load of $0.3 f_c' A_g$.

Discussion of Unconfined Concrete Fatigue Capacity

An energy based fatigue theory that predicts incipient failure of unconfined concrete sections is compared with experimental specimens reported in the literature where failure in the unconfined concrete was observed. As can be seen in figures 9-1 to 9-2, the theory yields conservative results. The reason for this probably lies in the fact that failure in unconfined concrete is very hard to define. From figure 9-1b in which the normalized force level is plotted against the cumulative plastic drift it can be observed that the degradation of unconfined concrete is gradual. Theoretically speaking the final strength should be the level of lateral load after the concrete has failed just prior to the commencement of rocking. However, the experiments reported in the literature are not always continued to the final rocking stage. Considering these limitations, the theory seems to predict the behavior of the specimen reasonably well.
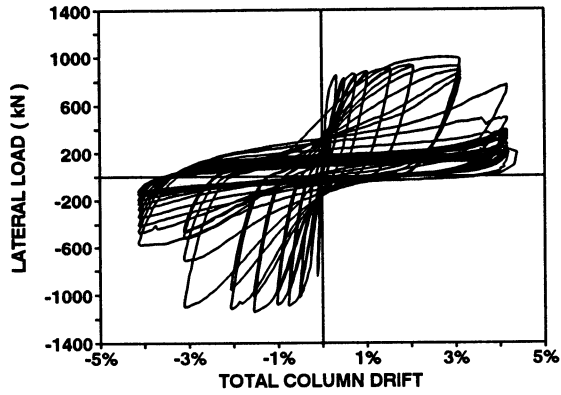
(a) Experimental Lateral Load - Column Drift Relationship.
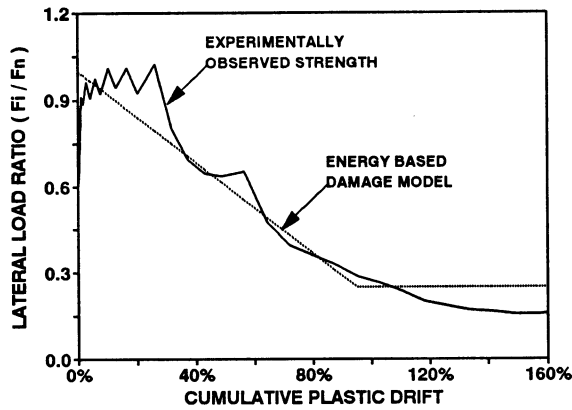
(b) Energy Based Damage Analysis Model.
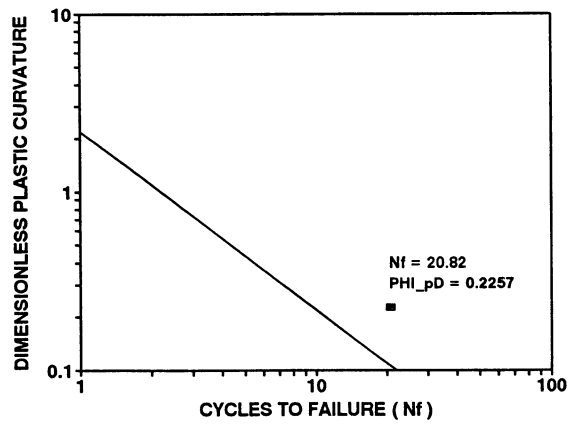
(c) Dimensionless Plastic Curvature - Cycles to Failure Relationship

Figure 9-1 Comparison of Analytical Expression with Test Results of Mander et al.
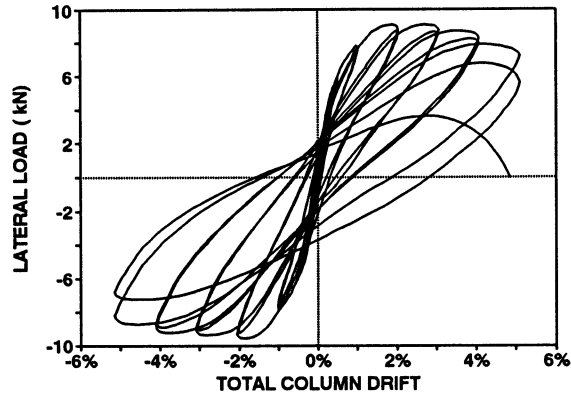
113

(a) Experimental Lateral Load - Column Drift Relationship.
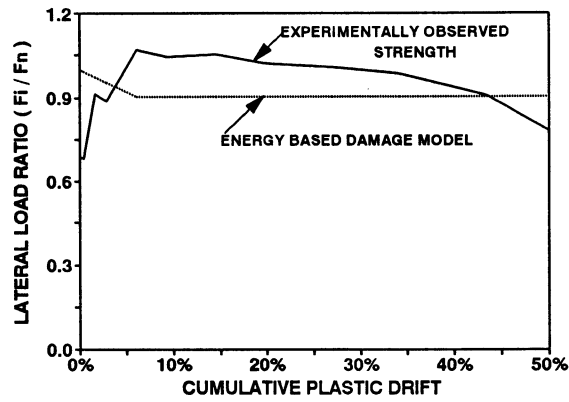
(b) Energy Based Damage Analysis Model.
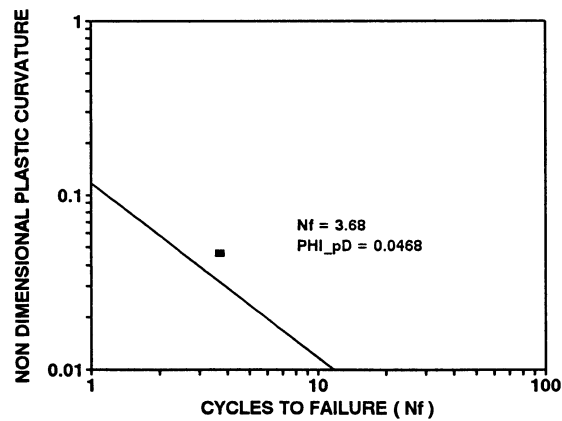
(c) Dimensionless Plastic Curvature - Cycles to Failure Relationship.

Figure 9-2 Comparison of Analytical Expression with Test Results of Aycardi et al.

114

9.3 FAILURE DUE TO LOSS OF BOND IN ANCHORAGES

The energy based model proposed in section 3 can be compared with actual experimental specimen where there had been an instances of anchorage failure. A brief history of the specimen is given below.

(i) *Circular Column*: Mander et al. (1996a) tested a cap beam column assemblage as part of the ongoing research on seismic vulnerability of bridge piers in eastern U.S. The subassemblage which was a part of the Niagara Parkway Bridge pier was 838 *mm* (33 *in.*) in diameter and reinforced with 16 #9 bars (d_b = 28.6 *mm*) with a clear cover of 50.8 *mm* (2 *in.*). The concrete core drilled out from the test specimen yielded compressive strengths of 45 *MPa* (6.5 *ksi*) in the column and 41 *MPa* (6 *ksi*) in the cap beam, respectively. The shear reinforcement in the column consisted of #5 bars (d_b = 15.9 *mm*) with a spacing of 229 *mm* (9 *in.*). Both the longitudinal and transverse reinforcements had a nominal yield strength of 40 *ksi*. The axial load applied on the column was 342.5 *kN* (77 *kips*) and the lever arm for the lateral load was 1933 *mm* (76.1 *in.*).

The results of the energy based analysis (figure 9-3) show that the theoretical predictions are in good agreement with the experimental data and is able to predict the failure mechanism as well as the cumulative displacement ductility failure limit state with reasonable accuracy.

9.4 FAILURE DUE TO LOSS OF BOND IN SPLICES

This section compares the energy based strength deterioration model proposed previously with experimental cases of lapped splice failure. The following cases are studied

(i) *Circular and Rectangular Columns*: As part of his research to investigate the performance of columns subjected to steel jacketing, Chai et al. (1991a) tested one set each of a circular and rectangular column that were provided with a lapped splice length of 381 *mm* (15 *in.*). The circular column had a diameter of 610 *mm* (24 *in.*) and reinforced with 26 #6 (d_b = 19.05 *mm*) Grade 40 f_y = 315 *MPa*) reinforcing bars with a cover of 20.32 *mm* (0.8 *in.*).
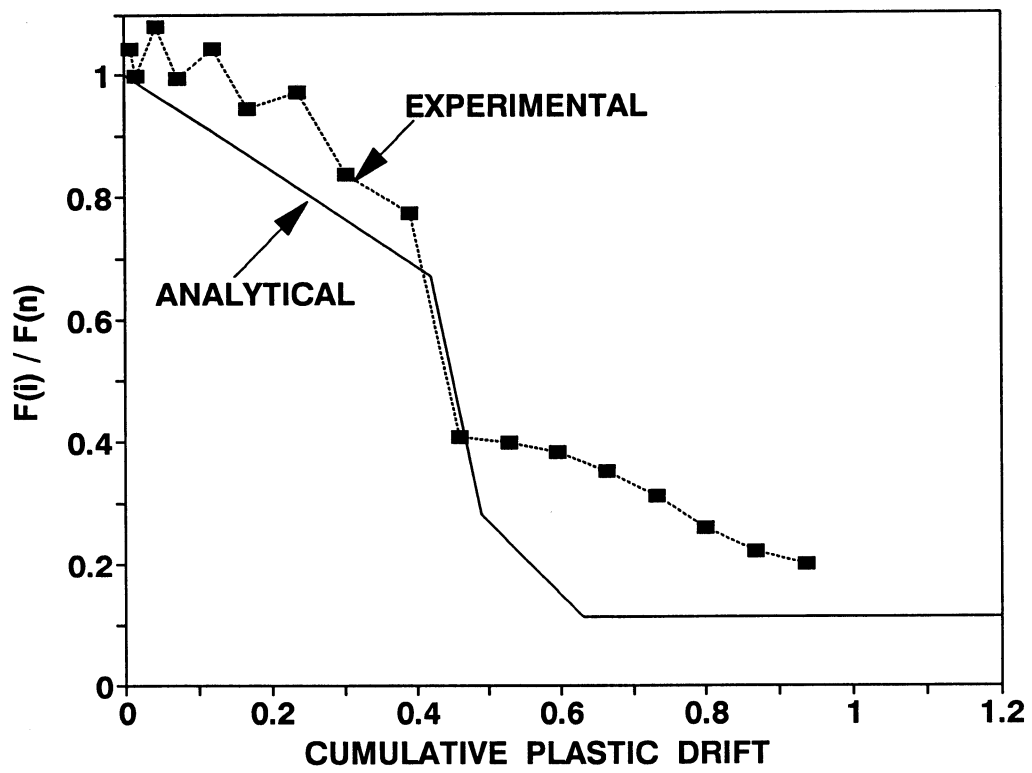
Figure 9-3 Comparison of Analytical Model with Test Results of Mander et al.

The concrete used had an unconfined compression strength (f_c') of 38.2 MPa (5.94 ksi) up to the rebar. The transverse steel consisted of #2 nominal Grade 40 $(f_y = 352\ MPa)$ rebars with a spacing of 127 mm (5 $in.$). The column carried an axial load of 1780 kN (400 $kips$) and had a lever arm of 3658 mm (144 $in.$).

The rectangular column tested by Chai et al. measured 730 mm (28 $\frac{3}{4}$ $in.$) × 489 mm (19 $\frac{1}{4}$ $in.$) and were reinforced with 32 #6 $(d_b = 19\ mm)$ Grade 50 $(f_y = 276\ MPa)$ rebars with a cover of 20 mm (0.8 $in.$) to the main bar. The transverse steel and axial load were exactly similar to the circular column. Relevant calculations for plotting the theoretical envelope are also provided.

(ii) *Circular Columns:* Cheng (1997), while investigating the effect of lapped splices in the flexural behavior of columns, tested three circular column specimens of varying concrete strengths and lapped splice lengths. The columns had an outer diameter of 603.25 mm (23.75 $in.$) and were provided with a clear cover of 48 mm (1.875 $in.$). Longitudinal reinforcement in the column consisted of 12 #6 $d_b = 19\ mm$) rebars with a nominal yield strength of 438 MPa (63.4 ksi). The crushing strength (f_c') of column CON-RO was 41.37 MPa (6 ksi) while for the columns CON-R1 and CON-R2 it was 31 MPa (4.5 ksi) and 45 MPa (6.5 ksi), respectively. Lateral reinforcement in the columns consisted of #3 $(d_b = 9.5\ mm)$ rebars spaced at 105 mm (4.125 $in.$) and having a nominal yield strength of 482 MPa (69.9 ksi). Column CON-R2 was provided with extra spiral reinforcement in the form of 11 mm (7/16 $in.$) cable of nominal yield strength of 690 MPa (100 ksi) at a spacing of 74 mm (2.9 $in.$). Lapped splice lengths in column CON-R0 and CON-R1 was 381 mm (15 $in.$) while for CON-R2 it was 191 mm (7.5 $in.$). All the columns had an axial load of 716 kN (161 $kips$) and a lever arm of 2743 mm (108 $in.$)

The results of the analytical predictions plotted against the experimental observations in figure 9-4 show that the results are in good conformity with the proposed theory.

117
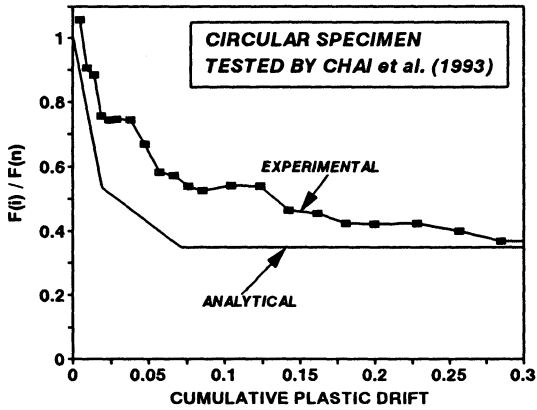
(a) *Circular Column Tested by Chai et al.*
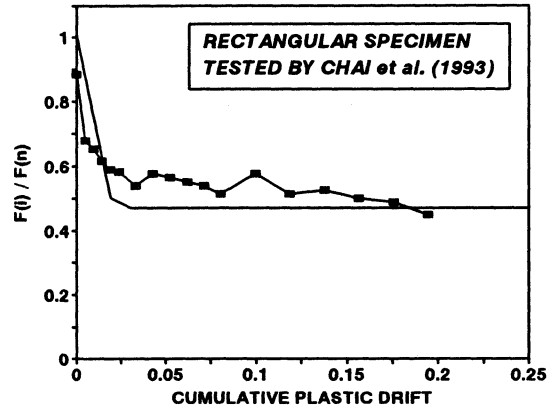
(b) *Rectangular Column Tested by Chai et al.*
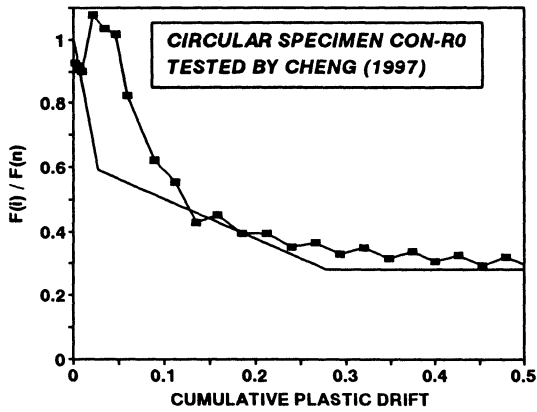
(c) *Circular Column Tested by Cheng et al.*
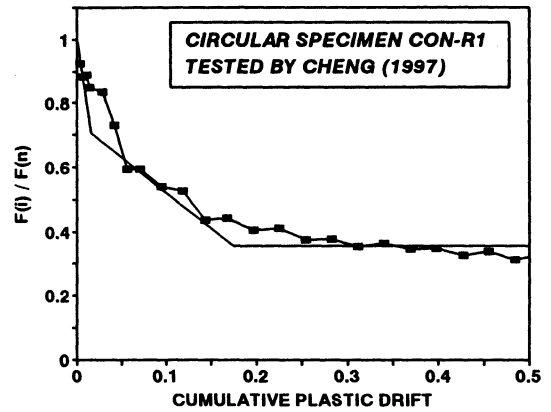
(d) *Circular Column Tested by Cheng et al.*
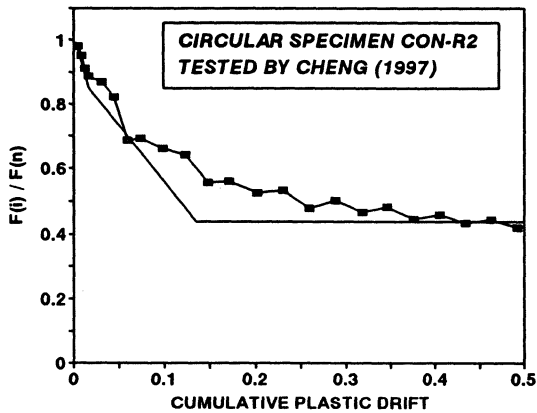
(e) *Circular Column Tested by Cheng et al.*

Figure 9-4   Comparison of Analytical Model with Experimental Cases of Lapped Splice Failure.

118

9.5   FAILURE OF LONGITUDINAL REINFORCEMENT DUE TO LOW CYCLE FATIGUE

This subsection compares the predictions of the low cycle fatigue theory in terms of plastic strain amplitude (ε_{ap}) of reinforcing bars given by equation (6-1) with test results where there had been instances of failure due to fracture of the steel. Since the most easily available test data is the plastic drift (θ_p^{expt}) at failure, the experimental plastic strain amplitude (ε_{ap}^{expt}) is obtained from the same using geometry in conjunction with the moment area theorem as

$$\varepsilon_{ap}^{expt} = \theta_p^{expt} \frac{D'}{2 L_p} \tag{9-1}$$

where D' = pitch circle diameter of the longitudinal reinforcement and L_p = plastic hinge length to be obtained from experimental data. Note that in case it is unavailable, equation (2-9) can be used instead. The relevant parameters used for the evaluation of the experimental plastic strain amplitude are listed in Table 9.1 for the specimens discussed in the following.

(i) *Non-Ductile Square columns*: Aycardi et al. (1992,1994) evaluated the seismic performance for square reinforced concrete columns $102\ mm \times 102\ mm$ cross section and $533\ mm$ tall designed primarily for gravity load. The loading history of the column specimen consisted of two cycles, each at drift amplitudes of $\pm 0.25\%$, $\pm 0.5\%$, $\pm 1\%$, $\pm 2\%$, $\pm 3\%$, $\pm 4\%$ and $\pm 5\%$ initially. Specimen 4, which suffered a low cycle fatigue failure, sustained an additional 14 cycles at a drift of $\pm 5\%$ that caused the first longitudinal bar fracture near the base of the column. Reinforcement in the columns consisted of $4 - D4$ bars ($d_b = 5.72\ mm$ $(0.225\ in)$, $A_b = 25.8\ mm^2$ $(0.04\ in^2)$) having a yield strength of $469\ MPa$ $(68\ ksi)$. Steel used for transverse reinforcement was smooth round wire ($\#11$ gauge) $3.1\ mm$ $(0.12\ in)$ in diameter with a clear cover of $11.2\ mm$ $(0.44\ in)$. The test unit 4 considered for this study sustained ultimate and yield curvatures of $0.988\ rad/m$ $(0.0251\ rad/in)$ and $0.079\ rad/m$ $(0.002\ rad/in)$, respectively.

(ii) *Square Hollow Column*: Mander et al. (1984) tested four hollow concrete box-type column sections which were typical scale models for railroad bridge piers used in New Zealand. Each hollow column specimen was $3200\ mm$ tall and had a $750\ mm$ square cross-section with $120\ mm$ thick walls containing $60 - D10$ ($10\ mm$ deformed bars) with a yield strength of $335\ MPa$.

Transverse reinforcement consisted of R6 (6 *mm* round bars) bars with a yield strength of 320 *MPa*. The column sections were provided with a clear cover of 20 *mm*. The loading history of Specimen A which suffered a low cycle fatigue failure, consisted of two complete reversed cycles at each displacement ductility factors of $\mu = \pm 2$, ± 4, ± 5, ± 8. This was followed by a full-scale dynamic loading where the longitudinal rebars sustained 40 cycles at displacement ductility factor of ± 4 before the test was terminated. At about cycle 35, the bars commenced fracturing due to low cycle fatigue. The non dimensional parameter $(\phi_p D)$ is obtained using equation (8-18). The yield displacement (Δ_y) was measured at 14 *mm*.

(iii) *Square Columns*: Watson and Park (1994) tested eleven reinforced concrete columns each having an overall height of 3900 *mm* and a shear span $L = 1600$ *mm*. The columns either had 400 *mm* square or octagonal sections. The longitudinal reinforcement in the column consisted of $12 - 16$ *mm* diameter bars with a yield strength of 446 *MPa* for units 1 to 4 and 474 *MPa* for units 5 to 11. The clear cover provided was 13 *mm* (0.5 *in*) for all the columns. The square column Units 1 and 2 chosen for this study were provided with 7 *mm* and 8 *mm* diameter transverse reinforcement. The loading history on the column units consisted of two cycles to nominal displacement ductility factors $\mu = \pm 2$, $\pm 4 < \pm 6$, ± 8. First fracture of a longitudinal rebar was observed at about 60% of the second cycle and 80% of the first cycle to the displacement ductility factor of ± 10 for Units 1 and 2, respectively. The ultimate and the yield curvatures sustained by the specimen were 0.201 *rad/m* and 0.01 *rad/m* for Unit 1 and 0.1981 *rad/m* and 0.011 *rad/m* for Unit 2, respectively.

(iv) *Circular Columns*: Chai, Priestley and Seible (1991b) tested six circular columns to study the retrofit measures in a bid to enhance the flexural strength and ductility of circular bridge columns. The columns tested with a height of 3657 *mm* (144 *in.*) an external diameter of 610 *mm* (24 *in.*) were 0.4 scale prototypes of actual CALTRANS bridge columns with a 1524 *mm* (60 *in.*) diameter. The longitudinal reinforcement in the columns consisted of 26 — ($d_b = 19.05$ *mm*) bars giving a percentage of steel = 2.53%. The transverse spiral steel consisted of ($d_b = 6.35$ *mm*) bars at a 127 *mm* (5 *in*) pitch. The cover to the main bar was 20 *mm* (0.8 *in*). These columns were tested with and without retrofit. The retrofitted columns were provided with steel jackets fabricated from 4.75 *mm* (3/16 *in*) thick A36 hot-rolled steel providing a

volumetric confinement ratio of 0.031.

It is of interest to note that low cycle fatigue failure was only observed in the retrofitted columns. This is because the effective plastic hinge length is very small leading to a much higher strain demand on the longitudinal reinforcement. Thus the column specimen of interest in this analysis are Units #6 and #4 since they failed by low cycle fatigue. Loading history for column consisted of three cycles, each at ductility factors of $\mu = \pm1, \pm1.5, \pm2, \pm3, \pm5, \pm6$ and ±7 with the longitudinal bars fracturing at the first cycle to the displacement ductility factor of 8. The retrofitted column 4 behaved essentially same as column 6 with excellent stable response up to the third cycle to a ductility factor of 8 was observed. The plastic hinge length (L_p) for retrofitted columns were obtained using a slightly modified version of the formula suggested by Chai, Priestley and Seible

$$L_p = 8800\, \varepsilon_y\, d_b + v_g \qquad (9\text{-}2)$$

where ε_y and d_b denote the yield strain and diameter of the longitudinal bar and v_g = the vertical gap provided between the toe of the steel jacket and top of the footing and was 25 mm for columns 4 and 6. Note that the above formula implicitly assumes that yield penetration occurs on either side of the vertical gap both into the jacketed column and in the foundation. The yield displacement Δ_y = 28 mm was observed.

(v) *Octagonal Columns*: Zahn et al. (1986) tested two spirally reinforced octagonal columns having a maximum dimension of 400 mm during the course of his doctoral studies at the University of Canterbury at Christchurch. Unit 5 chosen for this study was reinforced with 16 - 16 mm diameter reinforcing bars $(f_y = 337\, MPa)$ and circular Grade 380 spiral of diameter 10 mm. The cover up to the hoop steel was 13 mm. The test unit was subjected to two completely reversed cyclic loading or displacement ductilities of 2, 4 and 6 before failing at about 70% of the first cycle to the ductility factor of 8. The clear length of the column was 1600 mm and the yield displacement was recorded at 10 mm.

(vi) *Circular and Rectangular Columns*:   Priestley et al. (1994) tested twelve circular and rectangular column specimens during their studies on shear failure of bridge columns. Circular columns C6R and C8R with an outer diameter of 632 *mm* (25 *in*) were retrofitted with steel jacket of thickness 3.2 *mm* (1/8 *in*) and had 24 – #6 deformed bars with a yield strength of 469 *MPa* (68 *ksi*) as longitudinal reinforcement. The *M/VD* ratio for the two were 2 and 1.5, respectively. The retrofitted rectangular column R2R was provided with a steel jacket of thickness 0.5 *mm* (3/16 *in*) and had 22 – #6 bars with a yield strength of 324 *MPa* (47 *ksi*). The dimensions of column R2R was 406 *mm* × 610 *mm* (16 *in* × 24 *in*), with a *M/VD* ratio of 2.0. The transverse reinforcement for the columns consisted of #2 *GRADE*40 (6 *mm* diameter with nominal strength of 276 *MPa*) rebars with a clear cover of 203 *mm* (8 *in*). Column C6R sustained three cycles at each displacement ductility factors of $\mu = \pm1, \pm1.5, 2, \pm3, \pm4, \pm5, \pm6$ and ±8 before losing its capacity shortly after the third cycle to $\mu = 8$ due to the fracture of longitudinal reinforcement. Column C8R similar to C6R also failed due to low cycle fatigue, but could easily sustain slightly more than the second cycle (2.25 *cycles*) to $\mu = 8$. Rectangular column R2R was stable up to $\mu = 10$ but lost its capacity after the 3rd cycle to $\mu = 10$. Failure as before was attributed to low cycle fatigue of longitudinal reinforcement. The plastic hinge length L_p was obtained using equation (9-2). Yield displacements of $\Delta_y = 13.5$ *mm* (0.53 *in.*) and 11.5 *mm* (0.45 *in.*) were observed for the circular and rectangular columns respectively.

Table 9.1 Observed ε_{ap}^{expt} and Cycles to Fatigue Failure

Experiments Conducted by	Units	N_{eff}	D'/L_p	θ_p^{expt}	ε_{ap}^{expt}	Symbols in Figure 9-5a
Aycardi et al.	4	17.6	0.67	0.042	0.014	A
Mander et al.	A	7.5	2.11	0.031	0.032	M
Watson et al.	1	3.2	1.21	0.055	0.033	W1
Watson et al.	2	2.4	1.20	0.048	0.029	W2
Chai et al.	4	7.6	2.12	0.053	0.056	C4
Chai et al.	6	5.6	2.12	0.053	0.056	C6
Zahn et al.	5	1.8	1.37	0.044	0.030	Z
Priestley et al.	C6R	5.6	1.48	0.045	0.033	P6
Priestley et al.	C8R	4.8	1.48	0.049	0.036	P8
Priestley et al.	R2R	5.9	2.14	0.033	0.035	P2

(vii) *Circular Columns*: Mander and Cheng (1995) tested three one-third scale model pier specimens to illustrate the concept of replaceable plastic hinge. These columns were of the same size (279 *mm diameter*, 1452 *mm in height*) and were reinforced with W2 (4.05 *mm diameter*) circular hoop (f_y = 317 *MPa*) at 50.8 *mm* spacing outside the plastic hinge zone with a clear cover of 20 *mm*. The longitudinal reinforcement of the conventionally designed column consisted of 12 — D13 Grade 414 *MPa* rebars, while the other two columns were provided with twelve 12.7 *mm* diameter high strength threadbars (f_{su} = 841 *MPa*). Subsequently they also tested a near full size octagonal column specimen 610 *mm*. diameter and 3048 *mm*. high. The main part of the column was reinforced with twelve 25 *mm*. high strength threadbars. Within the replaceable hinge zone the longitudinal bars consisted of twelve fuse-bars that were machined down to about 70% of their original diameter and connected via couplers to the foundation starter bars. Within the replaceable hinge was also a central core (279 *mm* in diameter and 1016 *mm* in length) that consisted of highly confined high strength concrete. The test results can be compared with analytical predictions in the same way as before assuming that the fuse bars are uniformly strained over their entire length. Thus the same equation (9-1) can be used to evaluate the experimental plastic strain amplitude by replacing L_p with the fuse bar length L_f. Relevant

details of the experimental specimens are given in table 9.2 and the test results are compared in figure 9-5b.

Table 9.2 Observed ε_{ap}^{expt} and Cycles to Fatigue Failure for Specimens tested by Mander et al.

Series	Specimen	N_{eff}	D' / L_p	θ_p^{expt}	ε_{ap}^{expt}
Conventional	CO	19	0.74	0.042	0.016
Replaceable (Variable Amplitude)	R0	5.1	1.54	0.041	0.032
	R1	6.7	1.54	0.037	0.038
	R2	2.9	2.43	0.038	0.046
	R3	4.5	1.54	0.039	0.031
	R4	5.6	1.13	0.040	0.023
Precast (Variable Amplitude)	PC-R0	5.1	1.13	0.044	0.025
	PC-R1	6.2	1.13	0.043	0.025
	PC-R2	7.3	1.13	0.040	0.023
	SHEAR	6.7	1.13	0.040	0.023
Precast (Constant Amplitude)	FTG-6	3.0	1.13	0.052	0.030
	FTG-5	5.4	1.13	0.041	0.023
	FTG-4	7.8	1.13	0.029	0.017
	FTG-3.5	13	1.13	0.023	0.013
	FTG-3	25	1.13	0.018	0.011
	FTG-2.5	107	1.13	0.012	0.007
	FTG-2	440	1.13	0.005	0.003
Prestressed (Full Size)	PS-R1	5.7	0.53	0.017	0.017
	PS-R2	9.2	0.53	0.019	0.019

(a) EXPERIMENTS BY VARIOUS RESEARCHERS

## (b) EXPERIMENTS BY MANDER et al. (1995)
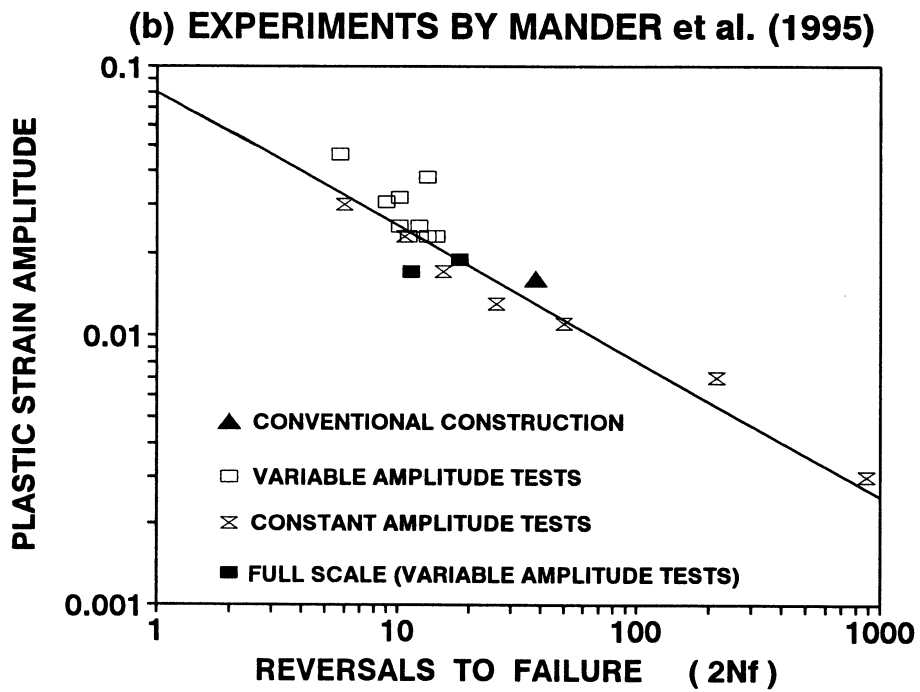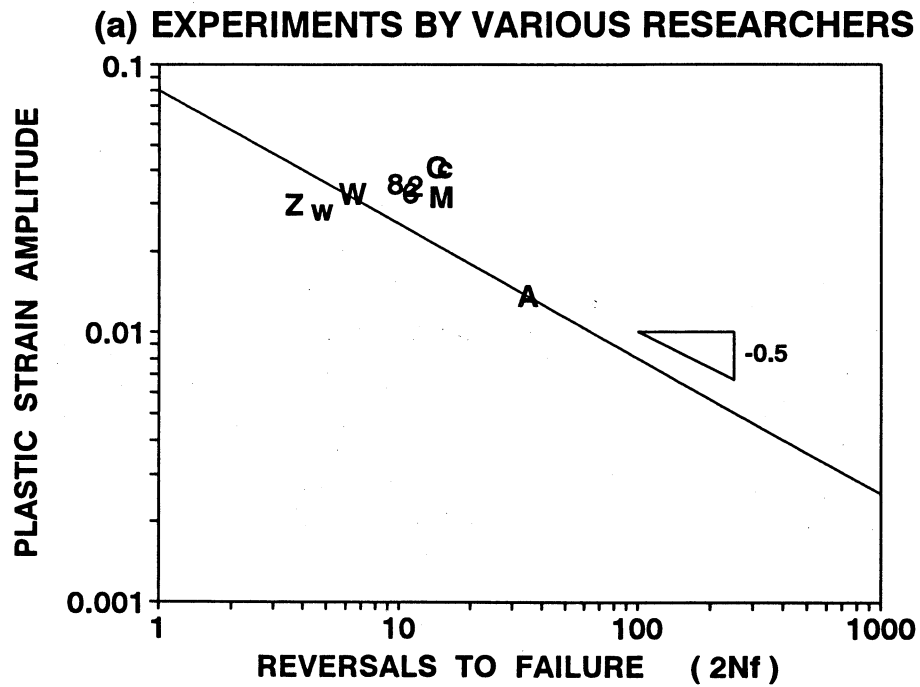
Figure 9-5 Comparison of Analytical Expression with Test Results of Low Cycle Fatigue.

9.6 Transverse Reinforcement Failure in Shear

This subsection compares the theoretical predictions of cumulative plastic drift at transverse reinforcement fracture in shear with experimental results. A brief history of the specimen used for this illustration is given below.

(i) *Retrofitted Model Pier tested by Mander et al. (1996b):* Mander et al. (1996b) while experimenting on the seismic vulnerability of non-ductile bridges tested a 1/3 scale model pier bent that was a typical representation of the ones commonly found in the eastern United States. The details of this pier bent are listed in section 10.2. In the second phase of the experimentation, the model bent was retrofitted by concrete jacketing the foundation and the cap beam so that the damage in these critical regions were prevented during retest. Due to the additional concrete layers added to these regions, the length of the column was reduced to $1321\,mm$. The circular columns in the three pier bent were $279\,mm$ in diameter and reinforced with $16 - \#3\,(9.5\,mm)$ longitudinal bars with a yield strength of $474\,MPa$. The transverse reinforcement was in the form of $4.8\,mm$ soft wire hoops with a measured $f_y = 268\,MPa$. The strain energy absorption at fracture (modulus of toughness) for these class of wire hoops was estimated at $78.9\,MJ/m^3$. The average axial load $(P_e/f_c'A_g)$ in the columns was 0.0169. The bent was quasistatically tested in drift control with three cycles at $\pm 1.6\%$ and two cycles each for remaining drift levels of $\pm 3.1\%$ and $\pm 4.7\%$. Shear cracks in the form of corner-to-corner diagonal X-cracks were first observed at a drift amplitude of 3.1%. As a result, failure of the transverse reinforcement in shear occured during the last two cycles at $\pm 4.7\%$ drift. The result of the experiment is compared with the theoretical prediction in figure 9-6. It is evident that the theory predicts the cumulative plastic drift at first hoop fracture with fair degree of accuracy.

9.7 Closure

In this section fatigue expressions for the various failure modes discussed so far have been compared with actual experimental results which had instances of identical failure modes. These included failure of unconfined concrete, failure due to loss of bond in anchorages, failure due to loss of bond in the lap splices, failure due to low cycle fatigue of the longitudinal

126
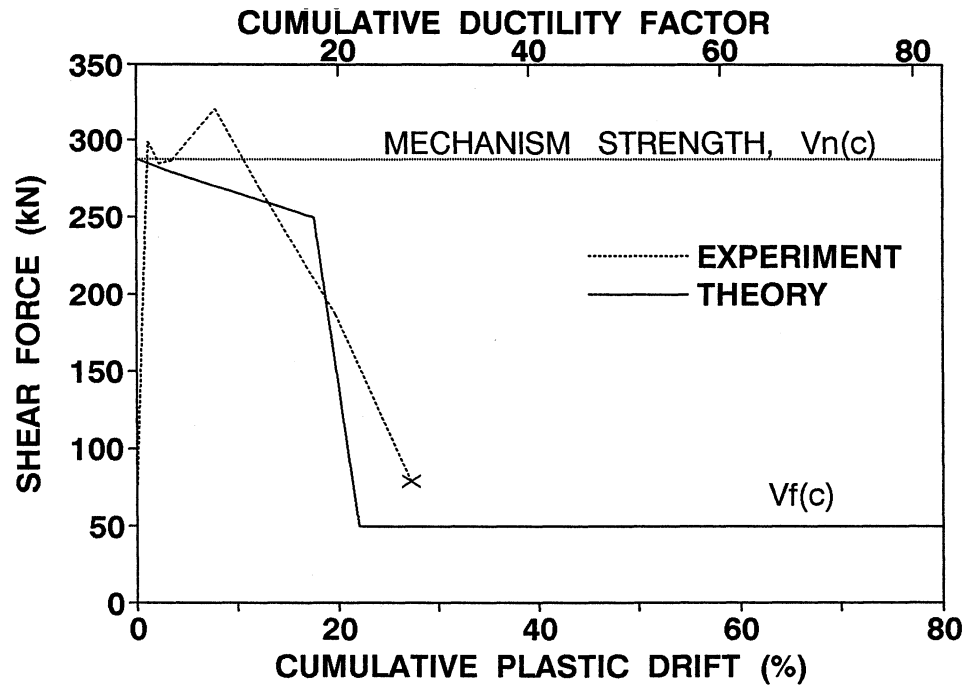
Figure 9-6 Comparison of Analytical Prediction with Test Result of Transverse Hoop Fracture in Shear.

reinforcement and transverse hoop fracture in shear. In the majority of the cases the analytical predictions are conservative in nature. Another point of extreme importance is the fact that the theory assumes that the different failure modes occur independently of each other. This implicitly means that one particular mode of failure does not in any way influence the outcome of another related/unrelated mode of failure. In reality such a scenario is indeed hard to find. However such an approach was adopted in formulating the theoretical expressions in order to better understand the various failure modes assuming them to be isolated. More often than not the failure of an actual structure is influenced by a number of modes that simultaneously follow each other. Such a case study has been performed in the next section where the complete failure analysis of a bridge pier bent is performed taking into account all the various failure modes discussed so far.

SECTION 10

APPLICATION OF ENERGY-BASED FATIGUE DAMAGE ANALYSIS
TO A BRIDGE PIER WITH MULTIPLE FAILURE MODES

10.1 INTRODUCTION

In the previous section, the proposed energy based strength deterioration models were compared with test results. Great care was taken in choosing experimental specimens with very well-defined failure models since it constituted one of the necessary conditions for applying the theoretical models. This meant that the individual models can only be compared to subassemblage or component testing rather than the complete structure itself. This is because more often than not, structure failures are an outcome of several different failure models occurring simultaneously or in conjunction with each other. Therefore, it is of interest to investigate whether these models are capable of predicting the overall behavior of a complete structure as it fails under the impact of lateral loading.

10.2 DESCRIPTION OF SPECIMEN

Mander et al. (1993, 1996a) demonstrated the analysis method using the prototype column-cap beam subassemblages for the flexural compressive concrete deterioration and combination with bond/anchorage failure, respectively. In this subsection the evolving energy-based analysis method will be employed for the evaluation of a whole reinforced concrete structure with multiple local failure mode.

The 1/3 scale model pier tested by Mander et al. (1996b) was a typical representation of the non-seismically designed ridge pier bents used in the eastern United States. The plan view and elevation of the same is shown in figure 10-1. The #3 (9.5 mm) longitudinal bar had a yield strength of 474 MPa while the Grade 1022 soft wire (4.8 mm dia) possessed a yield strength of 268 MPa. The 28 day compressive strength of the upper and lower columns were 59 and 68 MPa, respectively. The average axial load level of the column was $0.0145 f_c' A_g$.
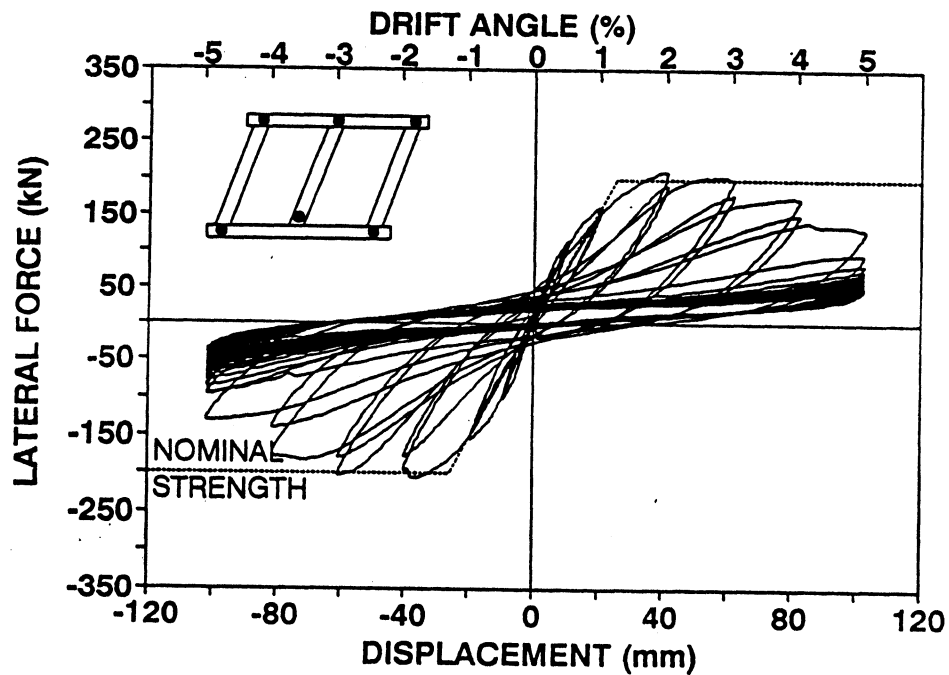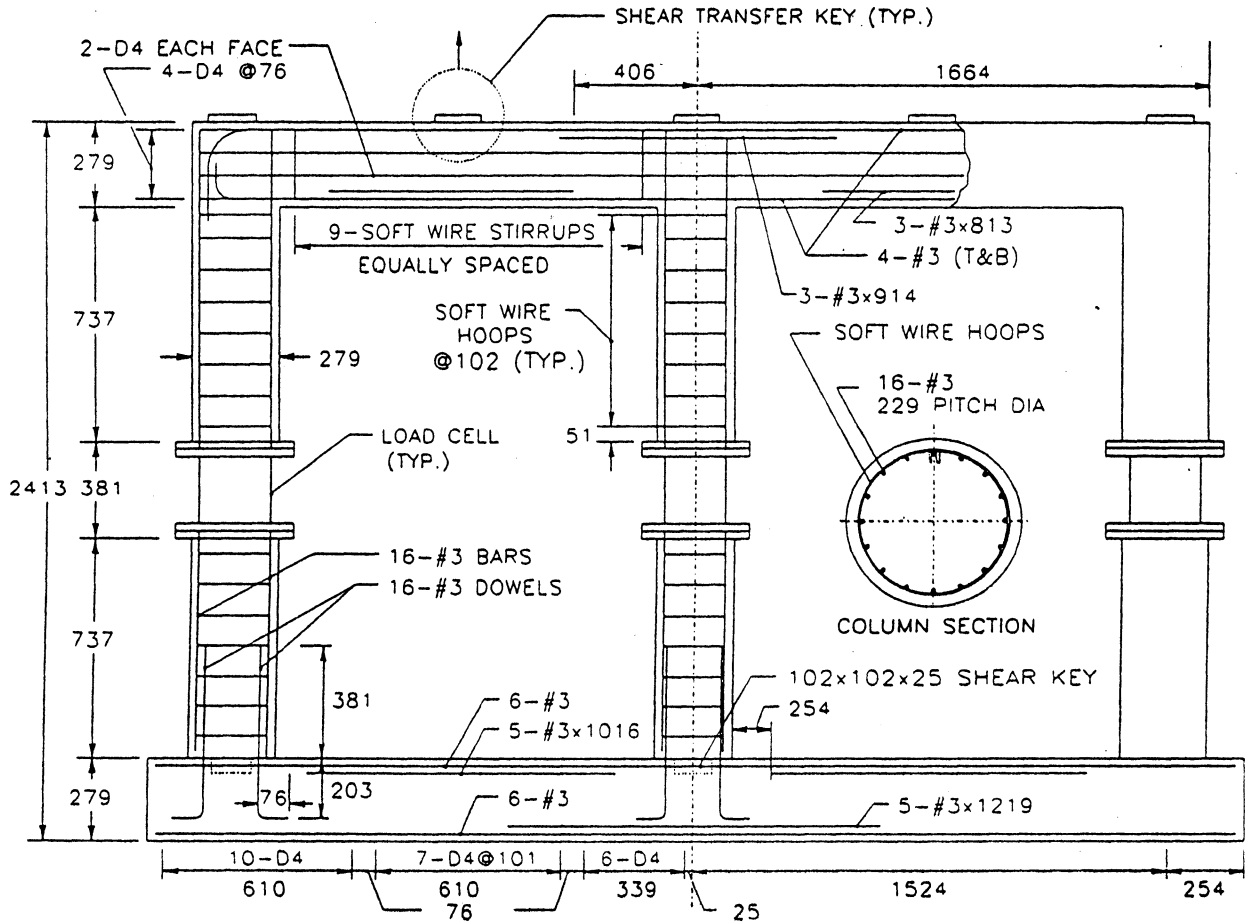
Figure 10-1 Model Pier Bent Construction Plan & Experimental Hysteresis Results.

The next step is to apply the energy based methodology for modeling the behavior of the pre retrofitted model pier. Nominal plastic mechanism strengths gave a more critical value for the initial strength, F_n = 200 kN for the pre-retrofitted model pier. The calculated residual strength due to the rocking mechanism was $F_{rocking}$ = 15.5 kN. The limiting displacement due to instability was calculated as Δ = 228 mm.

10.3 ANALYTICAL MODELING

A non-seismically designed multi-column bent pier under the inelastic cyclic loading is usually degraded by the combination of several local failure modes such as flexure, bond/anchorage, column shear, joint shear, and/or low-cycle fatigue of longitudinal rebar. However, not all the local failure modes participate in the structural failure at the same time, but they emerge mode by mode at various locations depending on the applied displacement history. It was observed from the laboratory experiment that this was true for the original (pre-retrofitted) model pier bent. This sequential degradation in the present energy-based damage analysis will now be demonstrated.

The expected failure mode for each critical section should firstly be determined for the postulated structural failure mechanism. For the pre-retrofitted model pier, the column sidesway mechanism is assumed and perfect strength in lap-splices, column shear and joint shear are also assumed. Based on the model construction plan in figure 10-1, it was determined that four different column end types should be considered for local failure modes as shown in figure 10-2.

Column end type 1 ; The top of the external columns belongs to this type. The expected local failure mode is the bond/anchorage failure of straightly anchored column longitudinal steel. However, there is some level of confinement provided by the well-anchored cap beam "U" bars.

Column end type 2 ; The top of the middle column is classified in this type. In this column end, the bond/anchorage failure of straightly anchored column longitudinal steel is expected. No confinement is assumed, since the cap beam side bars just pass through the beam-column joint.

131

Column end type 3 ; The bottom of the external columns is in this category. Column dowel bars are anchored with 90° hook into the foundation beam. However, no confinement is provided for the hook-anchored portion of the bars. Therefore, bond/anchorage failure of the straight portion of the anchored dowel bars is considered.

Column end type 4 ; The bottom of the middle column belongs to this type. Since the beam-column joint is T-shaped with the massive concrete footing pad, the 90° anchored column dowel bars are considered to have sufficient confinement so that bond/anchorage failure can be prevented. Therefore, fracture in the column longitudinal steel due to low-cycle fatigue is expected.

Although the external columns under inelastic cyclic loading may respond differently in between push and pull due to frame action, the dissipated energy in the external columns for any cycle should be the same. Therefore, an average column is used for the analysis. Energy-based concrete damage analysis for the average column of the model pier is summarized in table 10-1 with parameter values.

The next step is to consider the effect of concrete deterioration with bond/anchorage failure on the column end types 1, 2 and 3 as per the procedure given in subsections 2.2.3 and 3.2. The calculated parameter values of an average column for each column end type are summarized in table 10-2.

The damage model analysis due to concrete deterioration with steel fracture due to low-cycle fatigue was also performed for the column end type 4 as per the procedure given in subsection 6.2.1.

The underlying assumption in modelling the composite behavior is that the four locations at which inelastic actions are considered to be concentrated will act as four individual springs in parallel. Hence the overall stiffness (or more appropriately the overall force displacement behavior) can be presumed to be the sum of all the individual contributions.

132
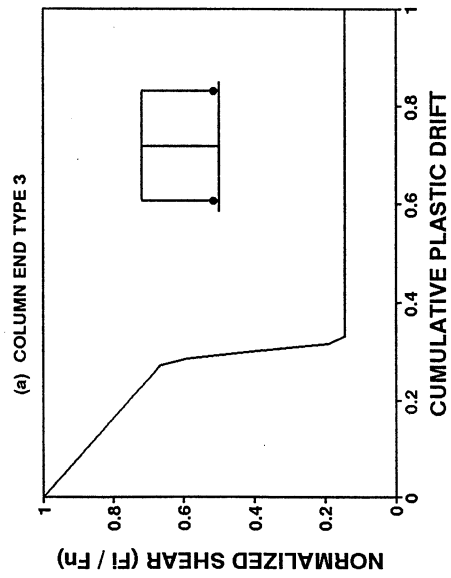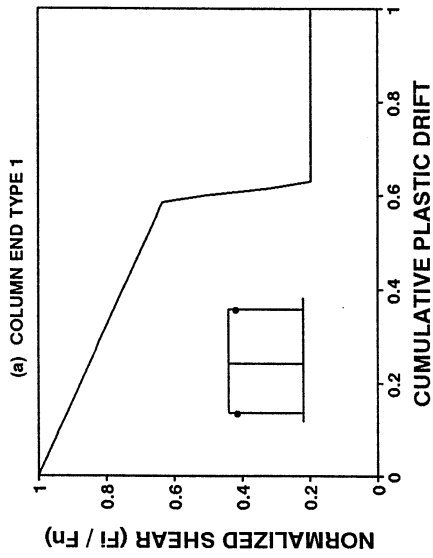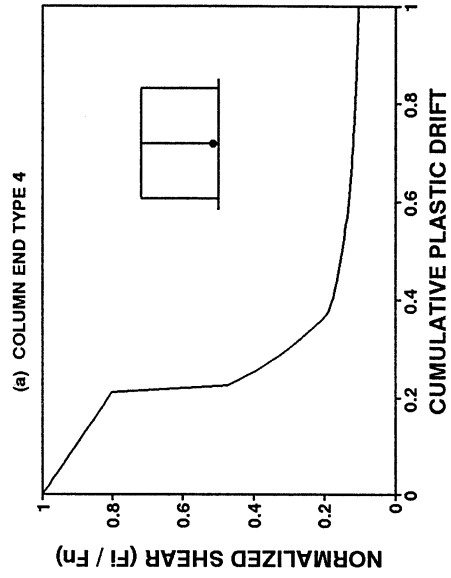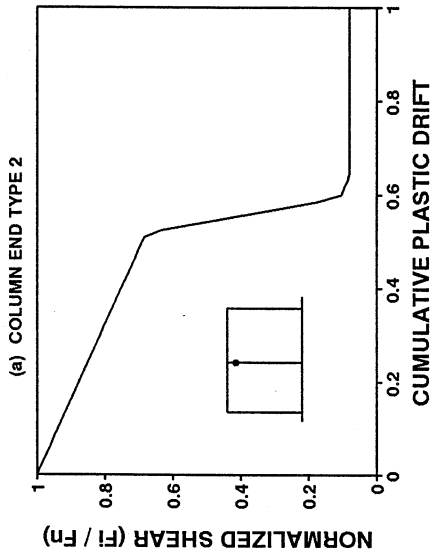
Figure 10-2 Expected Local Failure Modes and Corresponding Responses for Pre-retrofited Model Pier.

Table 10-1. Energy-based concrete damage analysis for the average column of the pre-retrofitted model pier.

Drift in Test (rad.)	Number of Cycles	Total Cumulative Drift (rad.)	Plastic Drift θ_{pi} (rad.)	Cumulative Plastic Drift $\Sigma\,\theta_{pi}$	Cumulative Damage Index D_{ci}	$\dfrac{M_i}{M_n}$
0.0025	3	0.015	0	0	0	1.0
0.005	2	0.035	0	0	0	1.0
0.01	2	0.075	0	0	0	1.0
0.02	2	0.155	0.0075	0.03	0.043	0.98
0.03	2	0.275	0.0175	0.1	0.142	0.94
0.04	2	0.435	0.0275	0.21	0.299	0.87
0.05	6.5*	1.085	0.0375	0.703	1.0	0.56

*Number of cycles chosen for D_{ci} = 1.0.

Note:

1. Refer to subsection 2.2.3 for damage analysis procedure.
2. Relevant parameter values are

$P_e/f_c'A_g$ = 0.0136; c/D = 0.21; $C_c/f_c'A_g$ = 0.068; L_p/D = 0.62;

M_c = 26.7 kN-m; M_n = 62 kN-m; M_c/M_n = 0.43; F_n = 66.9 kN; θ_y = 0.0125 rad.

Finally, the evaluated local damage models should be combined together for the response of the whole pre-retrofitted model pier. The weight factors (number of probable plastic hinge locations susceptible to a particular failure mode to the total number of probable plastic hinge locations) readily come out of the number of the corresponding column end type in the pre-retrofitted model pier. Figure 10-2 presents the individual response for the local damage models for the model pier. The combined response of energy-based damage model for the pier is compared to the experimental observation in figure 10-3. The strength deterioration limit is defined as the limit of usefulness in terms of strength. In this limit the cumulative plastic drift capacity $\Sigma\,\theta_{PC}$ may be taken as the drift in which the strength drops to $0.8F_n$, in which F_n is the nominal flexural strength (Park and Paulay, 1975). For the model pier, the theoretical and experimental useful limits are respectively $\Sigma\,\theta_{PC}$ = 0.211 rad. and $\Sigma\,\theta_{PC}$ = 0.211 rad.. The experimentally observed limit for residual strength was 1.86 rad.

Table 10-2. Energy-based concrete damage analysis combined with bond/anchorage failure for individual column end types of the model pier.

Parameters	Column End Type		
	Type 1	Type 2	Type 3
Weight Factor	1/3	1/6	1/3
ρ_s *at joint*	0.0055	0	0.003
f_{yh} *(MPa)*	455	N.A.	N.A.
l_{em} *(mm)*	228	228	200[a]
d_b *(mm)*	9.5	9.5	9.5
f_{rb} *(MPa)*	60	0	0
f_y *(MPa)*	474	474	474
$\Delta M_s / M_n$	0.50	0.57	0.531
n *(number of bars)*	16	16	16
f'_c *(MPa)*	56.6	56.6	56.6
U_{ab} *(N/mm²-mm)*	96.3	96.3	96.3
ε_y	0.0024	0.0024	0.0024
L_p *(mm)*	174	174	86[b]
ξ	0.578	0.578	1.17
$\Sigma \theta_{PB}$ *(rad.)*	0.59	0.519	0.28
F_1/F_n	0.63	0.678	0.654
$F_{rocking}/F_n$	0.196	0.081	0.144
F_2/F_n	0.134	0.108	0.124
$\Sigma \theta_{PR}$ *(rad.)*	0.63	0.638	0.33

[a]Straight anchored portion of column dowel bars with a 90° hook is used.

[b]For assumed perfect lap-splices, $L_p = 9d_b$ is used.

Note:

1. Parameter values for the average column in table 3-3 are used.

2. Notations are explained in subsection 2.2.3 and 3.2.

3. Weight factor is determined by the portion of number of column end types

Table 10-3. Energy-based damage analysis due to concrete deterioration combined with longitudinal bar fracture due to low-cycle fatigue for column end type 4 of pre-retrofitted model pier.

Drift (θ_i) (radians)	Plastic Drift (θ_π) (radians)	Number of Cycles ((n_i))	Cumulative Plastic Drift ($\Sigma\,\theta_{pi}$)	$\Delta\,D'/D'$	$\dfrac{\Delta\,M_s}{M_n}$	$\dfrac{M_c}{M_n}$	$\dfrac{F_i}{F_n}$
0	-	-	-	-	-	0.43	1.0
0.05	0.0375	0.2[a]	0.225	0.068	0.317	0.213	0.472
0.05	0.0375	22	1.86	0.349	0.562	0.087	0.1

Note: Notations are explained in subsection 6.2.
[a]Number of cycles chosen arbitrarily to illustrate the working procedure

10.4 CLOSURE

In this section the energy damage models for various modes of failure were combined together to predict the behavior of a bridge pier bent. This was compared to the experimental results of a real bent which was tested at the SUNY seismic testing facility. It can be inferred that results predicted were reasonably accurate and hence the methodology can be used for other bridge piers that have identical failure modes.
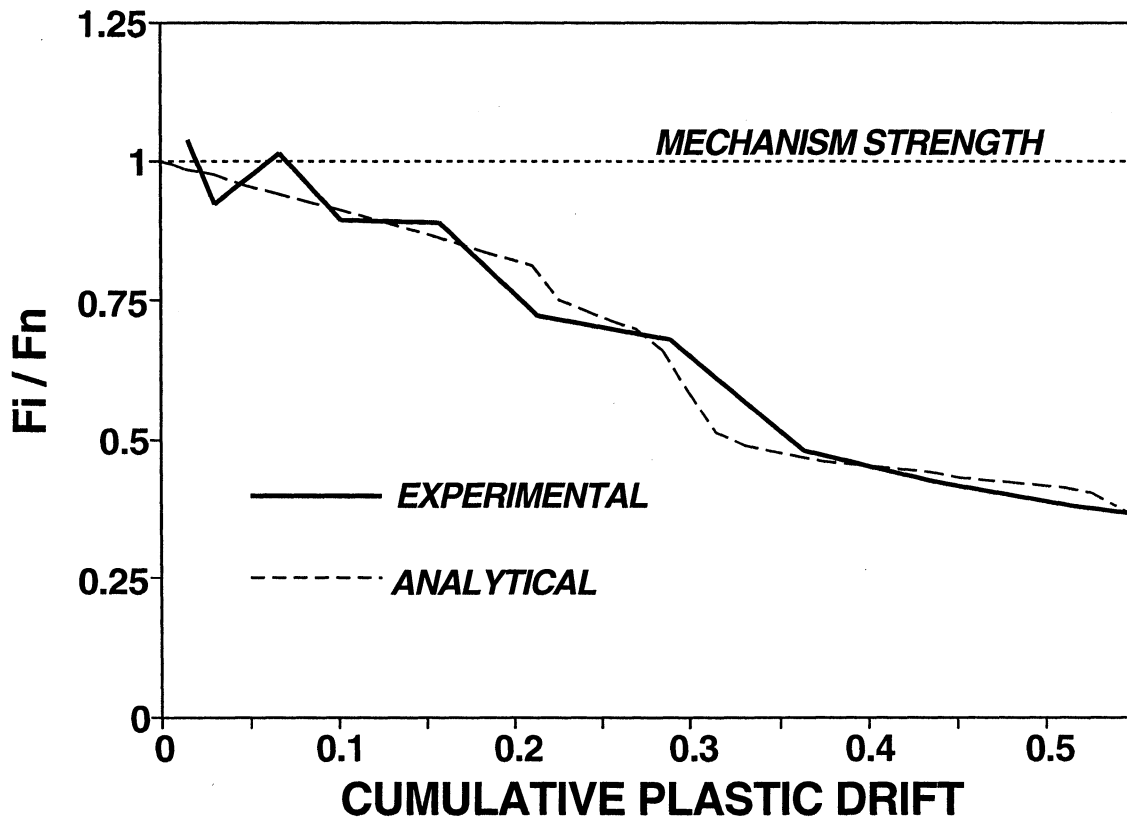
Figure 10-3 Results of Energy-Based Damage Model Analysis for the Model Pier.

SECTION 11
SUMMARY AND CONCLUSIONS

11.1 SUMMARY

Modern seismic design codes which came into existence after the devastating consequences of the 1971 San Fernando Valley earthquake have revolutionized in many ways that lifeline structures are designed. This put those structures which preceded the modern codes potentially at risk since their desired capacity (both strength and displacement) were not up to the envisaged level. Since it is economically not feasible to demolish the deficient structures, much of the current effort is directed towards alleviating their performance level. Although there is a plethora of techniques by which such performance objectives can be attained, it is critical to have a fair idea of the inherent deficiencies of the structure to reach a workable solution. This is an extremely important topic which has not been addressed in sufficient detail in any codal provisions. The consequences can be either be a semi-retrofitted structure whose weaknesses have not been ameliorated completely or one which has been an overkill-both of which are unacceptable.

It is now well known that confinement of the concrete in the potential plastic hinge zones is the key to achieving ductility and improved performance under strong ground shaking. However, most of the older bridge columns are generally not equipped with sufficient confining reinforcement which makes them vulnerable to earthquakes. More often than not such hazard zones are also locations of lap splices of the main vertical reinforcement. Another serious deficiency found in older structures was the unavailability of sufficient anchorage length of the column reinforcement both at the foundation and at the cap beam level. All these potential failure modes have been studied in great detail in the current work and simple easy to use expressions are derived to estimate the strength of the structure governed by such failure modes. Although the theoretical development assumes that the individual failure modes are independent of each other, in reality there can be a considerable overlap and the outcome of one particular

mode can have a strong influence on the other. However, such interaction has not been considered for simplicity in the current work though it is verified that the theory yields dependable results even for structures where there had been more than one type of failure mode.

11.2 CONCLUSIONS

Lifeline structures which precede the modern seismic codes are potentially at risk due to detailing deficiencies in the potential plastic hinge zones. Unavailability of sufficient lateral reinforcement either for confinement or for buckling restraint can be considered to be one of the major reasons for such poor performance. In most cases the problem is even aggravated by the presence of lap splices in the plastic hinge zones or inadequate length of anchorage at the foundation or at the cap beam level. All these failure modes need to be identified before the designer attempts any rehabilitating operation to assess the inherent strength of the structural component. Although modern seismic codes are explicit in the design of new structures there is a paucity of reliable analytical methods specifically for existing non-ductile structures. The current work looks into this problem from a new perspective to give a reliable estimate of the strength and deformation characteristic of the structure using principles of energy balance. Simple expressions which are easy to use are derived that can capture the behavior of the structure governed by all the above failure modes. Worked out examples are provided at the end of each section to illustrate the analysis steps. However, no analytical development is complete without comparison with actual test data. A section is devoted to testing the analytical expressions against carefully chosen test results where there had been actual instances of specific failure modes.

SECTION 12
REFERENCES

Allahabadi, R. and Powell, G.H. (1988) "DRAIN-2DX User Guide," Report UCB/EERC-88/06, Earthquake Engineering Research Center, University of California, Berkeley.

Ang, B.G., Priestley, M.J.N. and Paulay, T. (1989) "Seismic Shear Strength of Circular Reinforced Concrete Columns," *ACI Structural Journal*, pp. 45-59.

ATC 6-2 (1983) Seismic Retrofitting Guidelines for Highway Bridges, Applied Technology Council.

Aycardi, L.E., Mander, J.B. and Reinhorn, A.M. (1992) "Seismic Resistance of Reinforced Concrete Frame Structures Designed Only for Gravity Loads: Part II-Experimental Performance of Subassemblages," Technical Report NCEER-92-0028, National Center for Earthquake Engineering Research, State University of New York at Buffalo.

Aycardi, L.E., Mander, J.B. and Reinhorn, A.M. (1994) "Seismic Resistance of Reinforced Concrete Frame Structures Designed Only for Gravity Loads: Experimental Performance of Subassemblages," *ACI Structural Journal,* V. 91, No. 5, pp. 552-563.

Bang, M.S. and Meyer, C. (1989) "Damage of Plain Concrete As a Low-Cycle Fatigue Phenomenon," Technical Report, Department of Civil Engineering and Engineering Mechanics, Columbia University in the City of New York, New York.

Banon, H., Biggs, J.M. and Irvine, H.M. (1981) "Seismic Damage in Reinforced Concrete Frames", *Journal of Structural Engineering, ASCE,* V. 114, No. 7, pp. 1588-1605.

Bazant, Z.P., and Oh, B.H. (1993) "Crack Band Theory for Fracture of Concrete," *Materiaux et Constructions,* Paris, France, 16(93), pp. 155-177.

Bhadra, S. (1994) "An Experimental Investigation of the Seismic Performance of a Retrofitted Bridge Pier Designed Only for Gravity Loads," M.S. Thesis, Department of Civil Engineering, State University of New York, Buffalo.

Buckle, I.G., Friedland, I.M. (1995), Sesimic Retrofitting Manual for Highway Bridges, National Center for Earthquake Engineering Research, State University of New York at Buffalo.

Chai, Y.H., (1991a), "Steel Jacketing of Circular Reinforced Concrete Bridge Columns for Enhanced Performance," Ph.D. Dissertation, University of California, San Diego, California.

Chai, Y.H., Priestley, M.J.N. and Seible, F. (1991b) "Seismic Retrofit of Circular Bridge Columns for Enhanced Bridge Performance," *ACI Structural Journal*, V. 88, No. 5, pp. 572-584.

Chai, Y.H., Priestley, M.J.N. and Seible, F. (1994) "Analytical Model for Steel Jacketed R.C. Circular Bridge Columns," *Journal of Structural Engineering, ASCE*, V. 120, No. 8, pp. 2358-2376.

Chang, G.A. and Mander, J.B. (1994a) "Seismic Energy Based Fatigue Damage Analysis of Bridge Columns: Part I — Evaluation of Seismic Capacity," Technical Report NCEER-94-0006, National Center for Earthquake Engineering Research, State University of New York at Buffalo.

Chang, G.A. and Mander, J.B. (1994b) "Seismic Energy Based Fatigue Damage Analysis of Bridge Columns: Part II — Evaluation of Seismic Demand," Technical Report NCEER-94-0013, National Center for Earthquake Engineering Research, State University of New York at Buffalo.

Cheng, C.T. (1997) "New Paradigms for the Seismic Design and Retrofit of Bridge Piers", Ph.D. Dissertation, Department of Civil Engineering, State Univerity of New York at Buffalo.

Chung, Y.S., Meyer, C. and Shinozuka, M. (1987) "Seismic Damage Assessment of RC Members," Technical Report NCEER-87-0022, National Center for Earthquake Engineering Research, State University of New York at Buffalo.

Chung, Y.S., Meyer, C. and Shinozuka, M. (1989a) "Modelling of Concrete Damage," *ACI Structural Journal*, V. 86, No. 3, pp. 259-271.

Chung, Y.S., Meyer, C. and Shinozuka, M. (1989b) "Automated Damage-Controlled Design of RC Buildings," *Proceedings* of the Fifth Annual Conference on Structural Safety and Reliability (ICOSSAR 89), San Francisco CA, V. I, pp. 383-390.

Chung, Y.S., Meyer, C. and Shinozuka, M. (1990) "Automated Seismic Design of Reinforced Concrete Building Frames," *ACI Structural Journal*, V. 87, No. 3, pp. 326-340.

Collins, M.P. and Mitchell, D. (1991), <u>Prestressed Concrete Structures</u>, Prentice-Hall, Englewood-Cliffs, New Jersey.

Darwin, D. and Nmai, C.K. (1986) "Energy Dissipation in RC Beams Under Cyclic Loading," *Journal of Structural Engineering, ASCE,* V. 112, No. 8, pp. 1829-1846.

DiPasquale, E. and Cakmak, A.S. (1987) "Detection and Assessment of Seismic Structural Damage," Technical Report NCEER-87-0015, National Center for Earthquake Engineering Research, State University of New York at Buffalo.

DiPasquale, E. and Cakmak, A.S. (1988) "Identification of the Serviceability Limit State and Detection of Seismic Structural Damage," Technical Report NCEER-88-0022, National Center for Earthquake Engineering Research, State University of New York at Buffalo.

Dutta, A., (1995), "Fatigue Analysis of Non-Ductile Concrete Columns," M.S. Thesis, Department of Civil Engineering, State University of New York at Buffalo, Buffalo, New York.

Dutta, A. and Mander, J.B.,(1998) "Capacity Design and Fatigue Analysis of Confined Concrete Columns", Technical Report MCEER-98-0007, Multidisciplinary Center for Earthquake Engineering Research, State University of New York At Buffalo.

Gosain, N.K., Brown, R.H. and Jirsa, J.O. (1977) "Shear Requirements for Load Reversals on RC Members," *Journal of Structural Engineering, ASCE,* V. 103, No. 7, pp. 1461-1476.

Hsu, T.T.C. (1993), *Unified Theory of Reinforced Concrete*, CRC Press Inc.

Kannan, A.E. and Powell, G.H. (1973) "DRAIN-2D: A General Purpose Computer Program for Dynamic Analysis of Inelastic Plane Structures," Report Nos. EERC 73-6 and EERC 73-22, University of California, Berkeley.

Kasalanti, A. (1993) "Variable Amplitude Low Cycle Fatigue Behavior of Reinforcing Steel," M.S. Thesis, Department of Civil Engineering, State University of New York at Buffalo.

Kim, J.H. (1996) "Seismic Evaluation of Shear Critical Reinforced Concrete Columns and their Connections", Ph.D. Dissertation, Department of Civil Engineering, State Univerity of New York at Buffalo.

Kim, J.H. and Mander, J.B.,(1997) "A Deformation Model for Shear and Flexure in Structural Concrete Members", Technical Report NCEER-97-XXXX, (to be published), National Center for Earthquake Engineering Research, State University of New York At Buffalo.

Koh, S.K., Stephen, R.I., (1991), "Mean Stress Effects on Low-Cycle Fatigue for a High Strength Steel," *Fatigue Fracture of Engineering Materials and Structure*, vol 14.

Krawinkler, H. and Zohrei, M. (1983) "Cumulative Damage in Steel Structures Subjected to Earthquake Ground Motions," *Journal on Computers and Structures,* V. 16, No. 1-4, pp.

531-541.

Kunnath, S.K., Reinhorn, A.M. and Lobo, R.F. (1992) "IDARC Version 3.0: A program for the Inelastic Damage Analysis of RC Structures," Technical Report NCEER-92-0022, National Center for Earthquake Engineering Research, State University of New York at Buffalo.

Kunnath, S.K., Reinhorn, A.M. and Park, Y.J. (1990) "Analytical Modelling of Inelastic Seismic Response of RC Structures," *Journal of Structural Engineering, ASCE*, V. 116, No. 4, pp. 996-1012.

Mahmoodzadegan, B. (1995) "Experimental Evaluation of the Seismic Resistance of a Slab-On-Girder Highway Bridge," Ph.D. Thesis, Department of Civil Engineering, State University of New York at Buffalo.

Mander, J.B. and Cheng, C.T., (1995) "Renewable Hinge Detailing for Bridge Columns," Pacific Conference on Earthquake Engineering, Australia.

Mander, J.B., Kim, J.H. and Ligozio, C.A. (1996b) "Seismic Performance of a Model Reinforced Concrete Bridge Pier Before and After Retrofit," Technical Report NCEER-96-0009, National Center for Earthquake Engineering Research, State University of New York at Buffalo.

Mander, J.B., Mahmoodzadegan, B., Bhadra, S. and Chen, S.S. (1996a) "Seismic Evaluation of a 30 Year Old Non-Ductile Highway Bridge Pier and its Retrofit," Technical Report NCEER-96-0008, National Center for Earthquake Engineering Research, State University of New York at Buffalo.

Mander, J.B., Panthaki, F.D., and Kasalanati, A., (1994), "Low Cycle Fatigue Behavior of Reinforcing Steel," *Journal of Materials in Civil Engineering, ASCE*, vol 6, number 4.

Mander, J.B., Pekcan, G., and Chen, S.S., (1995a), "Low-Cycle Variable Amplitude Fatigue Modeling of Top-and-Seat Angle Connections," *Engineering Journal, AISC*, vol 32, number 2.

Mander, J.B., Priestley, M.J.N., and Park, R., (1984), "Seismic Design of Bridge Piers," Research Report 84-2, Department of Civil Engineering, University of Canterbury, Christchurch, New Zealand.

Mander, J.B., Priestley, M.J.N., and Park, R., (1988a), "Theoretical Stress Strain Model for Confined Concrete," *Journal of Structural Engineering*, ASCE, vol 114, number 8.

Mander, J.B., Priestley, M.J.N., and Park, R., (1988b), "Observed Stress Strain Behavior of Confined Concrete," *Journal of Structural Engineering*, ASCE, 1988b, vol 114, number

8.

Mander, J.B., Waheed, S.M. and Chaudhary, M.T.A. and Chen, S.S. (1993) "Seismic Performance of Shear Critical Reinforced Concrete Bridge Piers," Technical Report NCEER-93-0010, National Center for Earthquake Engineering Research, State University of New York At Buffalo.

Manson, S.S, "Behavior of Materials under Conditions of Thermal Stress," (1953), *Heat Transfer Symposium*, University of Michigan Engineering Research Institute.

Morcos, S.S. and Bjorhovde, R. (1995) "Fracture Modelling of Concrete and Steel", *Journal of Structural Engineering, ASCE,* V. 121, No. 7, pp. 1125-1133.

Panthaki, F.D. (1992) "Low Cycle Fatigue Behavior of High Strength and Ordinary Reinforcing Steels," M.S. Thesis, Department of Civil Engineering, State Univerity of New York at Buffalo.

Park, Y.J, and Ang, A.H-S. (1985) "Mechanistic Damage Model for Reinforced Concrete," *Journal of Structural Engineering, ASCE,* V. 111, No. ST4, pp. 722-739.

Park, Y.J., Ang, A.H-S. and Wen, Y.K. (1985) "Seismic Damage Analysis of Reinforced Buildings," *Journal of Structural Engineering, ASCE,* V. 111, No. ST4, pp. 740-757.

Park, Y.J., Ang, A.H-S. and Wen, Y.K. (1987) "Damage Limiting Aseismic Design Of Buildings," *Earthquake Spectra,* V. 3, No. 1, pp. 1-26.

Park, Y.J., Reinhorn, A.M. and Kunnath, S.K. (1987) "IDARC: Inelastic Damage Analysis of RC Frame-Shear Wall Structures," Technical Report NCEER-87-0008, National Center for Earthquake Engineering Research, State University of New York at Buffalo.

Paulay, T. and Priestley, M.J.N. (1992) Seismic Design of Reinforced Concrete and Masonry Structures, John Wiley and Sons, Inc., New york.

Priestley, M.J.N., Seible, F., Xiao, Y. and Verma, R. (1994a) "Steel Jacketted Retrofitting of Reinforced Concrete Bridge Columns for Enhanced Shear Strength - Part 1: Theoritical Considerations and Test Design," *ACI Structural Journal,* V. 91, No. 4, pp. 394-405.

Priestley, M.J.N., Seible, F., Xiao, Y. and Verma, R. (1994b) "Steel Jacketted Retrofitting of Reinforced Concrete Bridge Columns for Enhanced Shear Strength - Part 2: Test Results and Comparison with Theory," *ACI Structural Journal,* V. 91, No. 5, pp. 537-551.

Priestley, M.J.N., Verma, R. and Xiao, Y.(1994c) "Seismic Shear Strength of Reinforced Concrete Columns", Journal of Structural Engineering, Vol. 120, No. 8, ASCE, August, pp. 2310-2329.

Raghavendrachar, M. and Aktan, A.E. (1992) "Flexibility by Multireference Impact Testing for Bridge Diagonistics," *Journal of Structural Engineering, ASCE*, V. 118, No. 8, pp. 2186-2203.

Schlaich, J., Schafer, K. and Jennewein, M. (1987), "Toward a Consistent Design of Structural Concrete", *PCI Journal*, Vol. 32,, No. 3, May-June, pp. 74-150.

Watson, S., Zahn F.A., and Park, R. (1994) "Simulated Seismic Load Tests on Reinforced Concrete Columns," *Journal of Structural Engineering, ASCE*, V. 120, No. 6, pp. 1825-1849.

Williams, M.S., Sexsmith, R.G. (1994) "Review of Methods of Assessing Seismic Damage in Concrete Structures," Technical Report 94-02, Earthquake Engineering Research Facility, University of British Columbia, Vancouver, Canada.

Zahn, F.A., (1986), "Design of Reinforced Concrete Bridge Columns for Strength and Ductility," Research Report 86-7, Department of Civil Engineering, University of Canterbury, Christchurch, New Zealand.